General Disclaimer

One or more of the Following Statements may affect this Document

- This document has been reproduced from the best copy furnished by the organizational source. It is being released in the interest of making available as much information as possible.

- This document may contain data, which exceeds the sheet parameters. It was furnished in this condition by the organizational source and is the best copy available.

- This document may contain tone-on-tone or color graphs, charts and/or pictures, which have been reproduced in black and white.

- This document is paginated as submitted by the original source.

- Portions of this document are not fully legible due to the historical nature of some of the material. However, it is the best reproduction available from the original submission.

INTERNAL LOW REYNOLDS NUMBER
TURBULENT HEAT TRANSFER

by

Harold C. Reynolds, Jr.
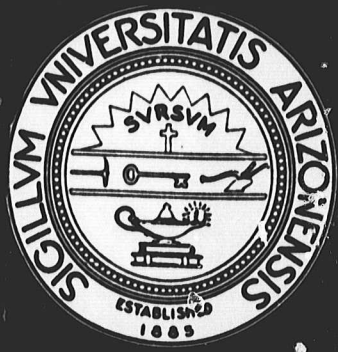
ENGINEERING EXPERIMENT STATION
COLLEGE OF ENGINEERING
THE UNIVERSITY OF ARIZONA
TUCSON, ARIZONA

INTERNAL LOW REYNOLDS NUMBER

TURBULENT HEAT TRANSFER

by

Harold C. Reynolds, Jr.

January 1968

D. M. McEligot, Principal Investigator

Energy, Mass and Momentum Transfer Laboratory

Aerospace and Mechanical Engineering Department

The University of Arizona

Tucson, Arizona

ACKNOWLEDGMENTS

TABLE OF CONTENTS

TABLE OF CONTENTS--Continued

TABLE OF CONTENTS--<u>Continued</u>

LIST OF ILLUSTRATIONS

LIST OF ILLUSTRATIONS--<u>Continued</u>

LIST OF TABLES

ABSTRACT

The results of a semi-analytical and experimental study of adiabatic tube flow and an analytical and experimental investigation of the thermal entrance region for gas flowing through electrically heated circular tubes are presented. Emphasis is placed on the low Reynolds number turbulent flow regime--defined as fully turbulent flow at bulk Reynolds numbers from 3,000 to about 15,000. Adiabatic air velocity and friction data and localized heat transfer measurements for air and helium, at low heating rates, are presented for this range.

The adiabatic data were obtained in a 1.61 inch ID tube for flow at bulk Reynolds numbers from 3,000 to 15,000. A continuous, Reynolds number-dependent, profile is developed from the data by using a modification of Reichardts' wall and middle law eddy diffusivity expressions. The velocity profile satisfies continuity. It is valid for all Reynolds numbers in excess of 3,000 for which the flow is fully turbulent and the Blasius friction factor expression is valid.

The thermal entrance problem for a fully developed velocity profile is solved analytically by the method of Sparrow, Hallman, and Siegel. The solution is based on the profile developed from the velocity study. Tabular values

of the eigenvalues and normalized Nusselt numbers for gases are presented for a range of Reynolds numbers from 3,000 to 50,000. The axial variation of Nusselt number is found to be correlated by

$$\frac{Nu}{Nu_{\infty}} = 1 + 0.8(1 + 70,000 \ Re^{-\frac{3}{2}})(\frac{x}{D})^{-1}$$

to within ± 5 per cent for $x/D \geq 2$. The fully developed value agrees with the Dittus-Boelter correlation,

$$Nu_{\infty} = 0.021 \ Re^{0.8} \ Pr^{0.4}$$

For the eigenvalues, λ_n^2, and the associated constants, A_n, correlations of the form

$$\lambda_n^2 = A_{1,n} Re^{-b_{1,n}} + C_{1,n} Re^{-d_{1,n}}$$

$$A_n = -A_{2,n} Re^{-b_{2,n}} + C_{2,n} Re^{-d_{2,n}}$$

are obtained. The coefficients and powers are presented in tabular form.

Heat transfer data are presented, primarily for helium, for the low Reynolds number turbulent range. A one-quarter inch, resistively heated, vertical, circular tube was used for the study. The data cover an axial range from 1.2 to 96 diameters; wall-to-bulk temperature ratios vary from 1 to 1.4. In the low Reynolds number turbulent

regime, these data clearly support the present analytical solution rather than the prediction obtained by applying the eddy diffusivity distribution used by Sparrow, Hallman, and Siegel.

CHAPTER I

INTRODUCTION

At present, the treatment of turbulent flow in circular tubes has been adequately developed for high Reynolds number flow only. When these treatments are extended, the predicted velocity profiles do not agree with data in the low Reynolds number range. Resulting friction factor predictions are compared to experimental correlations in Figure 1. Discrepancies exceed twenty per cent. Further, when heat transfer predictions for the downstream Nusselt number are based on these adiabatic velocity profiles, they overpredict the available data by as much as fifty per cent as the Reynolds number is reduced.

In this work the term "low Reynolds number turbulent flow" will refer to fully turbulent flow for the tube Reynolds number range from 3000 to 30,000, i.e., the region of the discrepancies just mentioned. The criterion for "fully turbulent flow" is an intermittency factor--the ratio of the time the velocity is fluctuating to the total time of measurement--equal to unity at the location of interest. An "asymptotic" or "universal" profile refers to a non-dimensional, Reynolds number-invariant profile which is valid for large Reynolds numbers. For the flow of
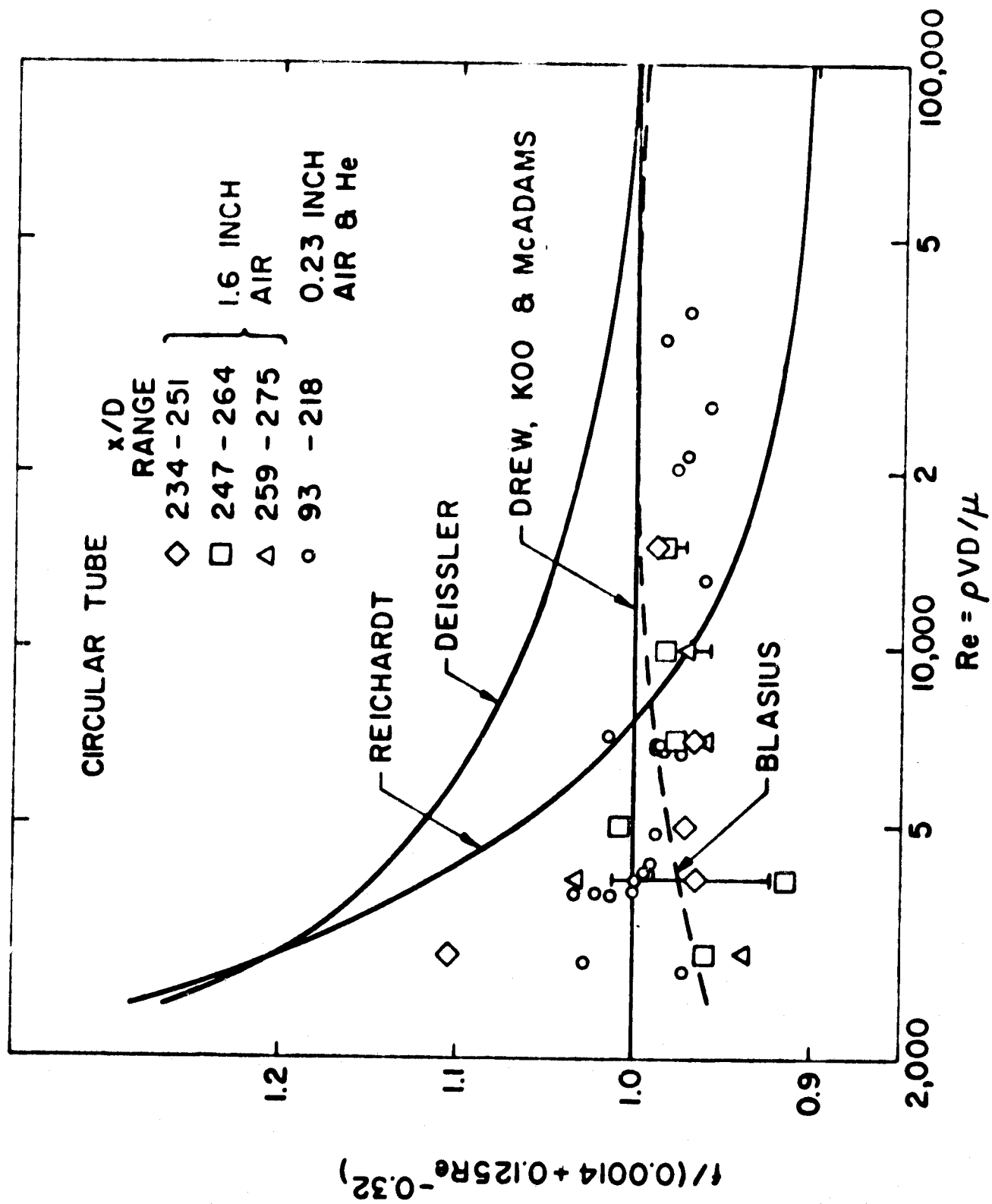
Figure 1. Adiabatic Friction Factors. Semi-empirical predictions of Reichardt (24) and Deissler (61) compared to correlations by Drew, Koo and McAdams (1) and Blasius (1) and to present data.

an incompressible fluid with constant viscosity, thermal conductivity and specific heat, it can be shown that ideally the velocity profile and normalized temperature profile approach invariant distributions as the flow progresses down a channel under constant wall heat flux. Fully developed conditions are reached when the invariant axial profiles are approached. For turbulent flow, this condition usually may be considered to be attained within fifty diameters or less after the start of heating. Thereafter, changes in the friction and heat transfer coefficients are indiscernible for practical purposes, and the fluid bulk temperature and the tube wall temperature then both increase linearly. The section of the channel wherein the temperature profile adjusts to the fully established value from the uniform value prior to heating is called the thermal entry region, or the thermal entrance.

With a solution for a boundary condition of constant wall heat flux from the start of heating, problems involving any axial variation of wall heat flux can be handled by the method of superposition, provided that the governing energy equation remains linear. This equation will be linear in temperature in the limiting case of low heat transfer rates because fluid properties can then be considered constant. To date, no thermal entry solution is available for low Reynolds number turbulent flow.

Currently there is an increasing interest in the problem of relaminarization of a gas which is being heated strongly. Such conditions may exist in solid core nuclear rockets and in the fuel ducts of engines designed for hypersonic flight. But no basis will exist for determination of the difference between behavior with the strong fluid property variation, accompanying the high heating rates, and "normal" behavior--unless a thermal entry solution is made available for the same Reynolds number range for the low heating rate conditions.

To overcome the foregoing discrepancies, this study was undertaken to provide accurate predictions for (a) adiabatic tube flow emphasizing the low Reynolds number, turbulent flow regime, and (b) local heat transfer characteristics in the thermal entrance and downstream regions (based on the results of the flow study). The flow regime of interest is the bulk Reynolds number range from 3000 to 30,000, with the main emphasis placed on the 3000 to 15,000 interval. The adiabatic velocity profile data presented cover the latter flow range and confirm earlier trends indicated by isolated data in this particular regime. Through inclusion of the Reynolds number as an additional parameter, an adiabatic velocity profile has been developed that adequately correlates the data in this regime, as well as for Reynolds numbers in excess of 30,000.

Based on the improved description of the adiabatic velocity profile, the energy equation, a second order partial differential equation, was solved. Under the idealizations of constant wall heat flux, fully developed velocity profile, and constant fluid properties, an eigenvalue thermal entrance solution was obtained. It yielded temperature profiles and local Nusselt numbers as functions of axial distance and bulk Reynolds number. Experimental data, for low and moderate heating rates for gas flow in smooth, circular, electrically heated tubes, are presented for comparison with the analysis. These data are extrapolated to zero heating rate results to correspond with the idealizations of the analysis.

This study is expected to be directly applicable to the heat transfer problems of resistojets, nuclear powered space vehicles utilizing gaseous propellents, proposed central station and marine gas cooled nuclear reactors, and to heated duct flow, in general. It may find use in the treatment of gas cooled nuclear reactor start up, shut down and partial loss of flow accidents. The results can also be used in electrical heating applications and for circular tube heat exchanger analysis.

CHAPTER II

PREVIOUS ADIABATIC STUDIES

An adequate representation of the velocity profile is a necessity in the treatment of internal heat transfer problems. As the first step in the development of such a representation, the pertinent literature is reviewed. Emphasis is on the low Reynolds number turbulent range and deviations from asymptotic generalizations.

For circular tubes, the shear stress can be expressed as

$$\tau = \mu\frac{du}{dy} + \rho\overline{u'v'} \qquad (2-1)$$

Two essentially equivalent approaches have been used in trying to express the Reynolds stress, $\overline{u'v'}$, in terms of mean fluid properties: the eddy diffusivity approach, and the mixing length approach postulated by Prandtl (2). The literature abounds with velocity profile formulations, based on innumerable variations of the two approaches, for the high Reynolds number, or asymptotic, regime. Semi-empirical models have been employed for the eddy diffusivity. Integration of the momentum equation, containing the resulting diffusivity expressions with a constant or linear variation employed for the shear stress, yields a universal

6

velocity profile. The constants of the profile are determined from experimental high Reynolds number u^+ versus y^+ velocity profile data. The unfamiliar reader is referred to the texts by Knudson and Katz (1), or Kays (2), or the critical literature survey on internal turbulent flow by Cess (3) for more complete details of existing treatments for high Reynolds number turbulent flow.

For high Reynolds number flow, the experimental data can be represented to within ten per cent by any of a number of u^+ versus y^+ velocity correlations, each independent of bulk Reynolds number. However, data by Senecal (4), Rothfus and Monrad (5), and Page and his co-workers (6) show the normalized velocity profile is not invariant below Reynolds numbers of about 30,000.

To date, only five studies have attempted to include the low Reynolds number dependency. Rothfus and Monrad (5) indicate that a unique correlation is obtained if $u^+ V_b/u_\xi$ versus $y^+ u_\xi/V_b$ is plotted rather than u^+ versus y^+. However, the lack of an adequate prediction for u_ξ reduces the usefulness of this correlation. Gill and Scher (7), extending the reasoning of Van Driest (8), considered the mixing length as dependent upon the Reynolds number. Their eddy diffusivity expression was phrased to yield a velocity profile that varies smoothly from a parabolic shape at Re = 1,800 to agreement with Nikuradse's data at Re = 100,000. Pai (10) approximated the velocity profile

with a second order polynomial, with coefficients also chosen to yield a step-wise continuous variation from the parabolic laminar profile to the asymptotic high Reynolds number universal profile. However, Rotta's (17) experimental observation of a continuous axial variation from laminar to fully developed turbulent flow, while the diameter Reynolds number remains constant during transition, invalidates any single curve extrapolation to the laminar profile as in the last two formulations. For an entrance region analysis Hanratty and Johnk (11) used Deissler's (12) high Reynolds number velocity expression for $y^+ \leq 26$ and a power law of the form $Cy^{+ \ 1/M}$, in the turbulent core, with C and M as functions of Reynolds number. The lowest Reynolds number employed in their investigation was 18,000.

McEligot, Ormand, and Perkins (9) applied a two layer treatment with a variable laminar sublayer thickness as a basis for a downstream heat transfer analysis. Their continuous, Reynolds number dependent velocity profile was based on Senecal's data (4) at Reynolds numbers of 3,000 to 4,000 (which they believed met the requirements of fully developed turbulent flow). The profile was extrapolated to a universal profile at higher Reynolds numbers in an arbitrary manner due to lack of additional useable data. The chosen profile was required to satisfy continuity and the Blasius friction factor. In the laminar sublayer the eddy diffusivity was taken as zero. In the turbulent core

a modified form of the mixing length expression presented by Schlichting (13) was employed, with the coefficients determined as functions of the bulk Reynolds number. The resulting expression for the velocity was quite complex and required numerical solution. Their predictions of fully developed Nusselt numbers for the low Reynolds number turbulent range showed a substantial improvement over the existing analyses since the latter had been based on the asymptotic velocity profile.

Boelter, Martinelli, and Jonassen (14) have also indicated that, for low Reynolds number turbulent flow, the distance to the edge of the laminar sublayer, y_1^+, is not constant. This conclusion is further supported by the trend of the data obtained by Rothfus and Prengle (15) with a dye tracing technique to show the breakup of laminar flow. For the flow regime presently under consideration, the foregoing information invalidates the approximation that the laminar sublayer extends to a constant value of y^+ (commonly taken as 5) as utilized by some investigators (14, 16) for high Reynolds number flow.

Adiabatic tube flow studies by Rotta (17) have shown intermittent laminar and turbulent flow can exist in the transition flow regime. As the axial distance increases, the percentage of the time during which smooth flow is observed diminishes. Flow of this transitory nature, indicated by an intermittency factor (the fraction

of time during which the flow at a given position remains turbulent) of less than one, can persist for large axial distances before the development of a continuous fully developed turbulent flow (defined by $\gamma = 1$). Or the transition may be completed in a very short distance. The apparent distance required shows a strong variation with Reynolds number in the range $2000 \lesssim Re \lesssim 3000$. Extrapolation of Rotta's results by McEligot, Ormand, and Perkins (9) yielded an intermittency factor of 0.95 at about twenty-five diameters for Re = 3000, indicating fully turbulent flow can be achieved at this Reynolds number for tubes with reasonably short hydrodynamic entry lengths. On the other hand, Preston (18) examined Nikuradse's 1932 and 1933 friction data and noted that data for all roughnesses tended to a smooth tube friction curve, from which a transition to the laminar curve began to occur at a bulk Reynolds number of 4470. He concluded that this was the lowest possible Reynolds number for fully developed flow. However, Knudson and Katz (1), Senecal (4), and Schlichting (13) are a few of numerous authors who present data that are in agreement with the Blasius smooth tube friction curve for Reynolds numbers as low as 3000. The apparent disagreement is probably explained by the observation that Nikuradse's friction data for $Re \lesssim 5000$ involved total pressure differences with magnitudes of order of the experimental uncertainty (19). To avoid such conceptual

difficulties in the present paper, fully developed flow
will be defined in the terms of the intermittency factor,
i.e., $\gamma = 1$.

Sources of velocity traverse data in the Reynolds
number range of interest, 3000 to 15,000, are presented in
Table 1. It is seen that data are scarce. Except for the
data of Senecal (4) and Nikuradse (19), data are untabu-
lated and are thus not available in a form of sufficient
accuracy for development of a velocity profile.
Nikuradse's data (19) were collected in the exit plane of a
circular tube where excessive free turbulence probably was
being generated and transverse mean flow was not inhibited
by the tube wall. It is concluded that only the work of
Senecal--for the narrow range, $3000 \leq Re \leq 4000$--are useful
for the present purposes. Additional data are necessary to
describe the approach from Re = 4000 to the asymptotic
profile.

Table 1. Available Adiabatic Low Turbulent Reynolds Number
Circular Tube Velocity Data for Re < 15,000

Investigators	Re	Data tabulated	Tube ID, inches	Location of measuring station, diameters
Nikuradse (19)	4,000 6,100 9,200	Yes	0.3937	0.001 to 0.002 behind exit plane of tube, i.e., outside tube
Rothfus, Monrad, and Senecal (20)	6,210	No	3.0	≈ 100
Seban and Shimazaki (21)	6,200	No	1.49	90
Deissler (22)	8,000 11,000 14,000	No	0.87	100
Senecal (4)*	3,002 3,464 4,108	Yes	0.50	360
	3,062 4,085		0.75	240
Bakewell (23)	8,700	No	11.2	≈ 27

*Senecal presents additional profiles at Re < 3000, but for these data it is not clear that γ would be approximately unity at the measuring station.

CHAPTER III

VELOCITY DISTRIBUTION

A continuous, Reynolds number-dependent, velocity profile is developed. It is based on a modification of Reichardt's wall and middle law eddy diffusivity expressions (24) and additional adiabatic velocity measurements for fully developed turbulent flow.

Experimental Apparatus

The facility employed for the measurement of the velocity and wall friction data was located at Texas Technological College. It has been described in detail elsewhere (25).[1] Important details of the apparatus, and the modifications performed for the present study are included herein. The basic test section was horizontal and unheated. It was fabricated from a twenty foot section of 1.61 inch i.d. Inconel pipe. Twenty-seven static pressure taps (with 1/16 inch diameter holes) were axially spaced at 2.720 inch intervals upstream and downstream from a probe traversing mechanism. The traversing mechanism was relocated to 255 diameters from the inlet by adding another

---

1. Copies available upon request from the Department of Mechanical Engineering, Texas Technological College, Lubbock, Texas.

twenty foot section of Inconel pipe, with identical dimensions, upstream from the basic test section. Mating ends of the two pieces of tubing were machined square and steel collars were used to assure alignment at the joints. Joints were made air tight by applying U. S. Royal industrial adhesive (epoxy) at the ends of the collars. Alignment of the two sections was achieved with a six foot carpenter's floor level. An exit length of 62 diameters followed the probe. Details are presented in Appendix A, Figure A-1.

All velocity measurements were obtained with a square ended impact probe constructed from 0.0355 inch o.d. stainless steel hypodermic tubing. The particular probe used had an impact tube coefficient of one since calibration showed that viscous corrections were unnecessary for local probe Reynolds numbers greater than 20 (see Appendix A). The particular probe design used is also the least sensitive to pitch and yaw (25).

The probe traversing mechanism consisted of a micrometer drive, graduated in 0.001 inch increments, with an Inconel spindle. A 0.036 inch hole had been drilled along the axis of the spindle and the velocity probe was silver soldered to the end. The probe traversing mechanism was housed within a 1/2 inch diameter thin wall tube, which was welded to the test section at a right angle to the wall static taps. A similar arrangement, use to obtain

temperature profiles, was located diametrically opposite
the velocity traversing mechanism. A small horizontal slit
was milled through the test section wall for each mechanism
to allow the probe to be completely withdrawn into its
housing when not in use (see Appendix A, Figure A-2). In
this construction the velocity probe tip was constrained to
travel along the radius located at 90° from the probe
reference wall static tap. The temperature probe was not
utilized during the present investigation.

A Flow Corporation Model MM3 Micromanometer, with a
resolution of $\pm$0.0001 inches and a stated accuracy of
$\pm$0.0002 inches of butyl alcohol, was employed to measure
the impact (velocity) pressure drop and the axial wall
pressure drops. The velocity was calculated from the
expression

$$u = \sqrt{\frac{2g_c \, \Delta P}{\rho}}$$

(3-1)

The practice of neglecting the contribution of the
fluctuating turbulent velocity components, which are of
importance only in the immediate vicinity of the wall, is
incorporated into the above equation (26, 27). Extrapola-
tion of Sandborn's (28) fluctuating velocity component data
to the low Reynolds number range, suggests the error
created by this omission is probably negligible beyond one
probe diameter ($y/r_w = 0.0441$) from the wall. For the

present investigation this distance corresponds to a $y^+ \approx$ 4.5 to 12 corresponding to the lowest and highest Reynolds number runs, respectively. In his work, $y/r_w = 0.01$ was the largest value at which a probe correction was utilized. Hanratty and Johnk (11) and Daily and Hardison (27) indicate that disagreement and uncertainty exist in the literature concerning probe corrections. Although the work of Daily and Hardison contained an extensive and comprehensive literature survey on impact probes and corrections, neither group used a correction for their data. The main justification in both cases was the inability to formulate meaningful, accurate correlations from the available literature.

In the present work, the corrections suggested by Daily and Hardison, including Fage's correction for the effective center displacement of a probe in a circular tube (29), have been considered with the uncertainty analysis. This analysis revealed the uncertainty in measuring the probe pressure drop always predominated over the possible error in neglecting the fluctuating velocity correction. At y/r_w values of 0.0472 and 0.1093 and a Reynolds number of 4080, the difference in the predicted uncertainties with and without consideration of the corrections are 3.64 versus 3.45 and 2.64 versus 2.58 per cent respectively. The corrections and uncertainty analysis are discussed in Appendix A.

A 0-125 psig compressor supplied air through a large storage tank. Three pressure regulators connected in series controlled the flow. The last regulator was capable of controlling with 0.01 psig sensitivity and 0.013 psi drift in 15 hours for upstream pressures of 0 to 25 psig. For flow at Reynolds numbers of 7000 and above. the last two regulators were bypassed. During the collection of the friction data, the probe was completely withdrawn into its housing.

Experimental Results

Adiabatic velocity profile and friction data were collected for Reynolds numbers of 3020, 4080, 5010, 7030, 10,100, and 15,000. Fully turbulent flow, as defined via the intermittency factor, was checked with hot wire measurements of the fluctuating axial velocity component at the probe station (255 diameters) and at approximately 307 diameters (7.5 diameters from exit). The intermittently smooth and jagged output, observed at lower Reynolds numbers, was completely undetectable above a Reynolds number of 2700.

Wall friction data are presented in Figure 1 for the 1.6 inch tube used in the velocity study and the 1/4 inch tube used in the heat transfer study. For the 1.6 inch tube, good agreement is seen between the Blasius friction factor expression (1) and the experimental data,

except for the lowest Reynolds number run where the uncertainty is largest.

The velocity data are presented in standard non-dimensional coordinates (u^+, y^+) in Figures 2 and 3. Shown, for comparative purposes, are Senecal's data for a bulk Reynolds number of 3002, as well as the semi-theoretical profiles to be discussed later. Uncertainty intervals for selected data points, predicted after the manner of Kline and McClintock (30), are also presented.[2] In forming u^+ and y^+ the experimental friction data were employed. Dew point measurements showed that dry air properties were applicable. The test section temperature and pressure were considered invariant across any given cross section. A maximum Mach number of 0.023 was observed for the 15,000 Reynolds number run.

As a check on the experimental velocity profiles, the bulk velocity was obtained by graphical integration (with a planimeter). The maximum percentage difference between the integrated and measured mass flow rates was +3.6 per cent at a bulk Reynolds number of 3017. For this Reynolds number, Fage (29) indicates an error of approximately +1.4 per cent can exist in the integrated bulk velocity due to the effective center displacement effect.

----

2.   Details of the data collection and reduction are presented in Appendix A. Tabulated values are available in Appendix B.
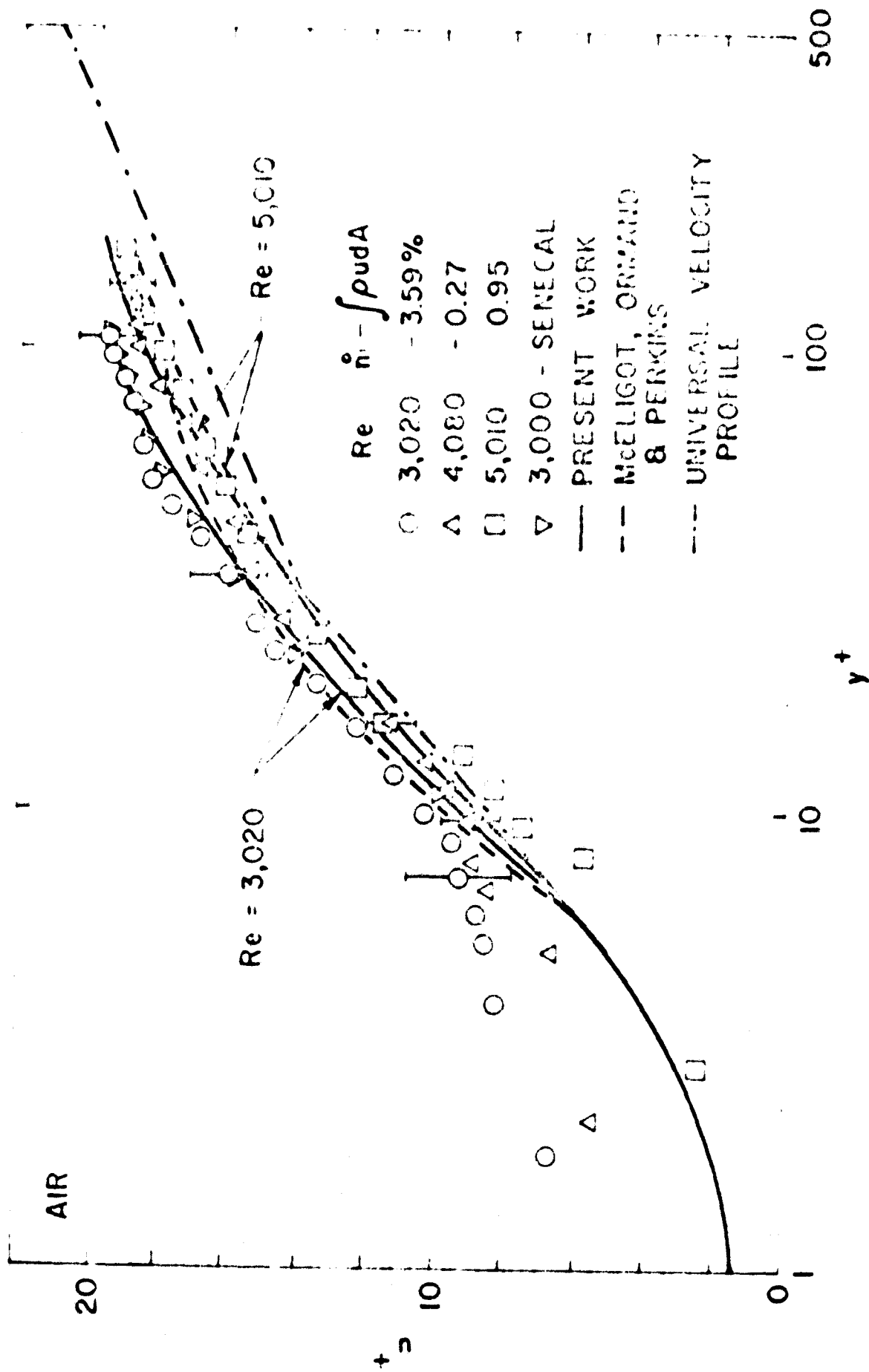
Figure 2. Turbulent Velocity Profiles: Semi-Empirical Prediction Compared with Data. Re = 3020 to 5010

AIR

Re = 7,030

Re = 15,000

Re	m-∫ρudA	
○ 7,030	1.00%	
△ 10,100	1.45	
□ 15,000	2.13	

——— PRESENT WORK

– – – McELIGOT, ORMAND & PERKINS

— - — UNIVERSAL VELOCITY PROFILE
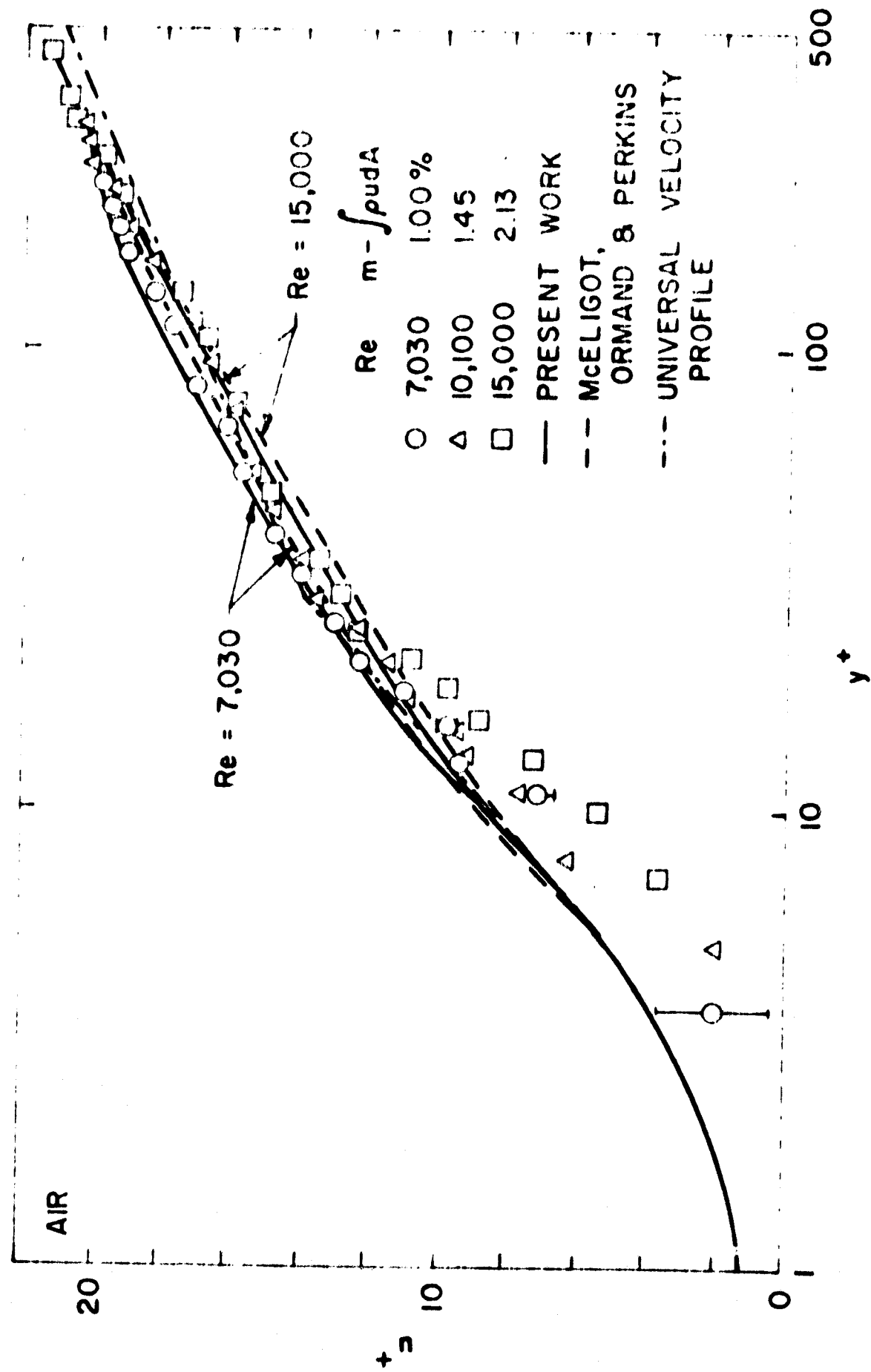
Figure 3. Turbulent Velocity Profiles: Semi-Empirical Predictions Compared with Data, Re - 7030 to 15,000

An additional error is present due to the flow area reduction that occurs when the probe is inserted into the tube. With the probe fully extended a maximum reduction of 1.4 per cent occurs in the flow area. The width of the milled slot in the wall is approximately 1 per cent of the circumference.

A large deviation from accepted viscous sublayer magnitudes is observed in the immediate vicinity of the wall ($y^+ \leq 15$). The deviation can be attributed to the presence of the small milled slot in the tube wall. This disturbance in the wall could cause the generation of additional turbulence in the proximity of the slot resulting in values of the impact pressure drop differing from the pressure drop which would exist if the slot was not present. This deviation eliminated the possibility of using these data to determine effective laminar sublayer thicknesses and laminar sublayer velocities accurately. From a qualitative examination of the data, it appears the slot effect is no longer felt beyond y/r_w ranging from approximately 0.09 to 0.05 ($y^+ = 9.7$ to 21.3), corresponding to the lowest and highest flow rates, respectively. Experimental velocity profiles, presented by Haugen and Dhanak (31) for plane flow over rectangular slots, show that such slots may be expected to have a negligible effect at $y^+ = 40$. Unfortunately, their results were presented graphically and could not be used to establish

the lower bound for whic.. the present data would be valid. For further details the reader is referred to Appendix A.

Semi-Empirical Profile

Theoretical objections to the earlier McEligot, Ormand, and Perkins (9) velocity formulation exist, even though substantial improvement in the low Reynolds number heat transfer predictions was obtained with its use. Their development produces zero values for the eddy diffusivity in the laminar sublayer and at the tube centerline. Current thinking supports the concept of a smooth eddy diffusivity distribution which varies as the fourth power of y on approaching the wall (2, 3). Moreover, their profile is based on the extrapolation of data in the narrow Reynolds number range between 3000 and 4000. The present development was undertaken to resolve these objections.

Using his data as a basis, Reichardt (24) has shown that for high Reynolds number, fully turbulent, tube flow, the eddy diffusivity in the turbulent core can be represented by a middle law which has a non zero value at the centerline

$$\frac{\epsilon_m}{\nu} = \frac{\mathcal{K} r_w^+}{6} \left[1 - (\frac{r}{r_w})^2 \right] \left[1 + 2(\frac{r}{r_w})^2 \right] \tag{3-2}$$

Near the wall he suggests the form

$$\frac{\epsilon_m}{\upsilon} = \mathcal{K}(y^+ - y_1^+ \tanh y^+/y_1^+) \qquad (3\text{-}3)$$

as reasonable, with the values $\mathcal{K} = 0.4$ and $y_1^+ = 11$. In the present study a continuous expression was developed by expressing equation 3-2 in the equivalent form,

$$\frac{\epsilon_m}{\upsilon} = \frac{\mathcal{K}y^+}{6}\left[2 - \frac{y^+}{y_{\mathcal{C}}^+}\right]\left[1 + 2(1 - \frac{y^+}{y_{\mathcal{C}}^+})^2\right] \qquad (3\text{-}4)$$

and by replacing $\mathcal{K}y^+$ by the right side of equation 3-3, which closely approaches $\mathcal{K}y^+$ in the core. For the resulting expression,

$$\frac{\epsilon_m}{\upsilon} = \frac{\mathcal{K}}{6}(y^+ - y_1^+ \tanh \frac{y^+}{y_1^+})\left[2 - \frac{y^+}{y_{\mathcal{C}}^+}\right]\left[1 + 2(1 - \frac{y^+}{y_{\mathcal{C}}^+})^2\right] \qquad (3\text{-}5)$$

$\mathcal{K}$ and y_1^+ were determined as functions of bulk Reynolds number, as described below.

For fully developed flow in a circular tube, a force balance shows the shear stress distribution to vary linearly with the radius. Introduction of the defining equation for shear stress (equation 2-1) yields

$$(1 - \frac{y^+}{y_{\mathcal{C}}^+}) = (1 + \frac{\epsilon_m}{\upsilon})\frac{du^+}{dy^+} \qquad (3\text{-}6)$$

where $y_{\mathcal{C}}^+ = \frac{Re}{2}\sqrt{f(Re)/2}$

The velocity is obtained directly by integration of this relation, with ϵ_m/ν described by equation 3-5. Numerical results cannot be obtained without assigning values to $\mathcal{K}$ and y_1^+. The bulk velocity may be defined as the one-dimensional velocity equivalent to the mass flow rate, i.e., for incompressible flow

$$V_b^+ = \frac{2}{y_\mathcal{C}^{+2}} \int_0^{y_\mathcal{C}^+} u^+(y_\mathcal{C}^+ - y^+) \, dy^+ \tag{3-7}$$

The Blasius friction factor

$$f = f(Re) = 0.0791 \, Re^{-1/4} \tag{3-8}$$

was chosen to evaluate the friction factor for the present study.

From the definition of the friction factor it can be shown that the dimensionless bulk velocity and the friction factor are related by

$$V_b^+ = \sqrt{\frac{2}{f(Re)}} \tag{3-9}$$

For a given friction factor (Reynolds number), only a discrete number of combinations of $\mathcal{K}$ and y_1^+ exist which will satisfy continuity, i.e., produce the same value for the bulk velocity from both equations 3-7 and 3-9. At various Reynolds numbers, a trial and error solution was performed on the University of Arizona IBM 7072 digital

computer to obtain possible combinations which would satisfy continuity. Simpson's Rule was employed in all integrations performed.

For each experimental Reynolds number, the most acceptable combination of y_1^+ and $\mathcal{K}$, along with a limiting band of combinations, was determined; this band was plotted against bulk Reynolds number. The criterion employed for an acceptable combination was close agreement between the data and the velocity profiles predicted by numerically integrating equation 3-6 (with the given combination of $\mathcal{K}$ and y_1^+). As further guide in the selection, eddy diffusivities predicted by equation 3-5 for the same combinations were compared with eddy diffusivities derived from the experimental data via equation 3-6. The non-dimensional velocity derivative was evaluated by graphically determining the slopes of several plots of a given profile and averaging the results. The plot of the acceptable combinations revealed that a constant value of $\mathcal{K} = 0.4225$ would suffice. Values of y_1^+ corresponding to the value of $\mathcal{K}$ chosen were then plotted on logarithmic coordinates, and an equation was developed to fit the data.

It was found that the results for y_1^+ and $\mathcal{K}$, as functions of bulk Reynolds number could be represented by

$$y_1^+ = 11 + 9.1116 \ \exp(-0.27249 \ Re \ x \ 10^{-3})$$

$$+ \left[15.83 \ \exp(-0.9498 \ Re \ x \ 10^{-3}) \right]^4 \tag{3-10}$$

$$\mathcal{K} = 0.4225$$

The second exponential term in the expression for y_1^+ is negligible for Reynolds numbers above 4000. The expressions for y_1^+ and $\mathcal{K}$ are valid for Reynolds numbers to approximately 10^5. The limiting upper Reynolds number may be determined by the user as the point at which he is no longer willing to accept the Blasius correlation for the friction factor. For high Reynolds number flow the profile converges to Reichardt's form with $y_1^+ = 11$ and $\mathcal{K} = 0.4225$. The use of a value of $\mathcal{K}$ larger than used by Reichardt has been indicated by Hinze (32), and more recently has been employed by Spalding. Spalding suggests that a value of $\mathcal{K}$ as large as 0.43 is not unreasonable (33).

The velocity predictions are compared with the experimental data for Reynolds numbers of 3020, 4080, and 5010 in Figure 2, and 7030, 10,100, and 15,000 in Figure 3. For comparative purposes, the McEligot, Ormand, and Perkins profile and the universal logarithmic profile (1, 9) are also included.

Due to the method of evaluating the Reynolds number-dependent coefficients of the present formulation,

the value of the predicted friction factor,

$$f = \frac{2}{(V_b^+)^2} \qquad\qquad (3\text{-}11)$$

must agree closely with the Blasius value when integration of the theoretical velocity profile is performed to obtain V_b^+. The same applies for the McEligot, Ormand, and Perkins profile (9) which was also forced to fit the Blasius friction factor expression. The extension of the asymptotic profiles predicts friction values differing by 30 to 7 per cent from the Blasius values for the low Reynolds number turbulent flow range of 3000 to 15,000. These results have been presented for comparison with the experimental friction factors in Figure 1.

CHAPTER IV

DISCUSSION OF ADIABATIC VELOCITY PROFILE

As illustrated in Figures 2 and 3, the present formulation is seen to correlate the valid experimental data to within 7.5 per cent. For Reynolds numbers below 4080 the formulation of McEligot, Ormand, and Perkins (9) predicts higher velocities in the so-called buffer layer than the present formulation and appears to give a slightly better correlation of the buffer layer data at Reynolds numbers of 3020 and 4080. The present treatment predicts higher values in the turbulent core than the former formulation; substantial improvement in the prediction is noted at 3020. Both formulations predict the overall trends of the data, and both satisfy continuity (i.e., realistic friction factor) due to the method of determining the Reynolds number dependent coefficients of the velocity profile. The present velocity data do not clearly discriminate between the two semi-empirical predictions. Since both formulations were forced to satisfy the Blasius friction factor, the friction factor measurements cannot be used to discriminate. The question as to which best describes low Reynolds number turbulent flow remains to be tested by the heat transfer studies.

From a theoretical standpoint the present profile is more desirable. The eddy diffusivity is finite to the wall, while the McEligot, Ormand, and Perkins (9) development assumes a zero value in a laminar sublayer. Moreover, in the vicinity of the wall the present analysis approaches zero as y^3, which Reichardt has shown from continuity considerations to be the limiting behavior for isotropic turbulence (Elrod (34) has shown the power should be ≥ 4 for random turbulence). Both the eddy diffusivity and velocity profiles are continuous over the entire tube and are seen to have zero derivatives at the center line. The present analysis also predicts a positive finite, value of eddy diffusivity at the center line, which Reichardt (24) and Hinze (32) have verified as correct, rather than the zero or minus one value predicted by many of the other existing formulations. Although the center line behavior of the eddy diffusivity has little effect on the results of heat transfer analyses, where the velocity-eddy diffusivity formulations have found their main application, it is desirable for the formulation to satisfy as many of the known conditions as possible.

It is not altogether surprising that y_1^+ was found to be Reynolds number dependent, whereas a constant value of $\mathcal{K}$ was sufficient to correlate the data in the low Reynolds number range. In his original paper, Reichardt indicated that y_1^+ was a measure of the thickness of the

viscous sub layers, which references (9, 14, 15, 32) have shown to vary with the Reynolds number. Conversely, $\mathcal{K}$ characterizes an eddy diffusivity expression valid primarily in the turbulent core of the flow, where the effect of the wall decays rapidly with distance. It is reasonable to expect that the value of $\mathcal{K}$ would be equally valid at low Reynolds numbers as long as the flow was fully turbulent in the core and not effected by the proximity of another surface. As discussed earlier, the use of a value of $\mathcal{K}$ larger than Reichardt's value of 0.4 is not a complete innovation. Reichardt, in his original paper, noted that the accuracy of the available measurements were not sufficient for a close determination of $\mathcal{K}$. The main dis-advantage of the present formulation is that it involves a numerical integration for the velocity profile. This is true of most of the more recent eddy diffusivity and mixing length models for both high and low Reynolds number turbulent flow. A closed form solution for the velocity cannot be obtained without additional simplifying assump-tions and relaxation of boundary conditions above and beyond those employed in the more recent works.

CHAPTER V

PREVIOUS DIABATIC STUDIES

As a background to the low Reynolds number turbulent thermal entrance region study, the present state of the art will now be considered. Experimental and analytical investigations of local heat transfer characteristics for turbulent flow in circular tubes, specifically directed at the Reynolds number regime from 3,000 to 30,000, are almost nonexistent. Modern advances in technology have made it increasingly important for the design engineer to accurately predict these characteristics for optimization within material limitations. Once thermal entrance region solutions are obtained for the constant wall heat flux boundary condition, it is possible to predict wall temperatures with axially varying wall heat flux by superposition (2). However, existing analytical formulations are inadequate for such predictions since they are based on high Reynolds number data and assumptions. This is especially true below bulk Reynolds numbers of 15,000.

Analyses for the prediction of turbulent heat transfer and friction characteristics for fully established conditions and constant fluid properties are well established for Reynolds numbers in excess of 50,000. The

analyses of Martinelli (16), Sparrow, Hallman, and Siegel (35), Deissler (36), and the Dittus-Boelter experimental correlation (2), with a 0.021 coefficient, all correlate the fully developed data to within 6 per cent. In light of entrance data collected in the last ten years (37), the thermal entrance region solution of Sparrow, Hallman, and Siegel has gained wide acceptance over the boundary layer integral analysis performed by Deissler (36) and later extended by Wolf (38). The Sparrow, Hallman, and Siegel solution is based on a slightly modified version of Deissler's velocity and eddy diffusivity expressions (12) and the assumed equivalence between the eddy diffusivities of heat and momentum. The form of the partial differential energy equation used was linear because fluid properties were taken to be constant. Since their treatment forms the basis for the present analysis it is described now in greater detail.

Sparrow and co-workers separate the temperature field into two parts which represent the entrance and fully developed regimes, respectively. An ordinary differential equation was obtained with the temperature in the fully established region as the dependent variable. This equation was integrated directly. For the remaining portion of the temperature field, a second separation of variables yielded (1) an ordinary differential equation which has an exponential solution for the axial variation,

and (2) a Sturm-Liouville equation for the radial dependency. For the solution of the Sturm-Liouville equation, the first five eigenvalues were obtained at Reynolds numbers of 50,000, 100,000, and 500,000 by employing a digital computer. The numerical method was not indicated, but the nature of the problem suggests a trial and error solution was probably used to obtain the eigenvalues.

In addition to the large number of constant property investigations, several recent variable property thermal entrance and downstream studies have been conducted (39, 40, 41). These studies have not been completely successful in predicting variable property data.

In the portion of the low Reynolds number range from 3,000 to 15,000 heat transfer data for gases are scarce and erratic. In the remaining range from 15,000 to 30,000 data are more plentiful, but still not abundant. The majority of the data are confined to fully developed conditions or to average values for the entire length of a test section. McEligot, Ormand, and Perkins (9) point out an increasing deviation between the fully developed data and previous analytical predictions with decreasing Reynolds number. The discrepancy approached fifty per cent. This trend was also present in the majority of the variable property data they examined. Malina and Sparrow (42) have presented variable and constant property entrance region data for water and oil (Pr = 3, 48, 75), with the

Reynolds number range between 12,000 and 30,000 included.
Their entrance region data show the dimensionless entrance
distance (defined as the axial distance for the local heat
transfer coefficient to reach ninety-five per cent of its
fully developed value) to decrease with increasing Reynolds
numbers. The same trend is indicated by the data of
Hanratty and Johnk (11). In contrast, the analysis of
Sparrow, Hallman, and Siegel (35) shows a very slight
increase in the entrance length for increasing Reynolds
numbers. The lowest Reynolds number considered in their
solution was 50,000.

The increase in velocity with respect to the value
predicted by a universal velocity profile (see Figure 2)
can explain the deviation between heat transfer analyses
and data for Reynolds numbers below 30,000. The observed
thickening of the viscous sublayer represents a reduction
in the turbulent component for momentum transfer. There-
fore, the turbulent transport of energy is reduced so that
the resulting Nusselt number decreases also. The available
analyses, with the exceptions to be discussed below, are
formulated using semi-empirical velocity and eddy dif-
fusivity, or mixing length, expressions based on universal
velocity profiles which do not vary with Reynolds number.
It should be expected that these analyses would be valid
only for high Reynolds numbers. It may be recalled that in
the wall friction problem the comparable analyses showed

agreement with friction factor measurements in the high Reynolds number range only.

Heat transfer analyses which treat the deviation from the universal velocity profile are scarce. McEligot, Ormand, and Perkins (9) predict Nusselt numbers, for fully established temperature fields in circular tubes, which are in agreement with available data. Their analysis utilized a varying velocity profile which was based on Senecal's data (4) at Reynolds numbers of 3,000 and 4,000 and was arbitrarily extrapolated to a universal velocity profile at higher Reynolds numbers. Equivalence between the eddy diffusivities of heat and momentum was employed. The energy equation was solved by numerical means. The Dittus-Boelter correlation with a coefficient of 0.021 correlated their data, and the data of others, to within five per cent of their predictions for Reynolds numbers above 4,000.

Gill and Lee (43) used the low Reynolds number velocity profile of Gill and Scher (7) to predict heat transfer results for parallel plates with constant wall temperatures. McEligot, Ormand, and Perkins (9) point out that the results show a sharper approach to the laminar Nusselt number than is noted in circular tube experiments. Haberstroh and Baldwin (44) adopted Pai's low Reynolds number profile (10) to predict temperature profiles and Nusselt numbers for fully developed tube flow with constant wall heat flux. For low turbulent Reynolds numbers, the

validity of this analysis, as well as the formulation of Gill and Lee (43), is questionable. Both studies were based on velocity profiles with monotonic variation from high Reynolds number results to parabolic laminar profiles. Such a procedure is in disagreement with Rotta's (17) experimental observations of intermittent laminar and turbulent flow at values of Reynolds numbers in the transition range.

Temperature profile measurements by Hanratty and Johnk (11) indicate the eddy diffusivity of heat varies with axial position in the thermal entry. These changes are confined to the centerline region of the tube after the first three to four diameters. But, they conclude the calculation method of Sparrow, Hallman, and Siegel (35), coupled with Reynolds analogy, $\epsilon_H = \epsilon_m$, is adequate for the prediction of heat transfer results in the thermal entry region. Deissler (45) had shown earlier that extension of adiabatic profiles was valid for moderate heating rates. The lowest Reynolds number employed in the work of Hanratty and Johnk was 18,000, but only the data collected for Reynolds numbers of 24,000 and 35,000 were sufficiently accurate to analyze the variation of eddy diffusivity in the entrance region.

Of the limited number of low Reynolds number adiabatic velocity profiles, only the formulation due to McEligot, Ormand, and Perkins (9), and the present profile

developed in Chapter III appear to be without serious objections. Though the present formulation is theoretically more rigorous, both apparently correlate the low Reynolds number velocity data reasonably well. A substantial improvement in the prediction of fully developed Nusselt numbers has been obtained by McEligot, Ormand, and Perkins (9) employing their profile.

As noted, no thermal entry solution is available for low Reynolds number turbulent flow. The method of Sparrow, Hallman, and Siegel (35) will be applied in the following study, with both of the above formulations, (a) to provide a usable low Reynolds number thermal entrance solution and (b) to resolve, if possible, which formulation provides the best description of the velocity profile.

CHAPTER VI

HEAT TRANSFER ANALYSIS

For steady, low Mach number, hydrodynamically fully developed flow of an incompressible fluid, with constant properties, negligible viscous dissipation and negligible natural convection effects, the energy equation for circular tubes can be written as

$$\frac{\mathcal{V}}{r_w - y} \frac{\partial}{\partial y} \left[(r_w - y) \beta(\overline{y}) \frac{\partial T}{\partial y} \right] = u \frac{\partial T}{\partial x} \qquad (6-1)$$

where

$$\beta(\overline{y}) = \frac{\epsilon_H}{\mathcal{V}} + \frac{1}{Pr}$$

For the nondimensional form of equation 6-1,

$$\frac{1}{y_{\mathcal{C}}^+ (1 - \overline{y})} \frac{\partial}{\partial \overline{y}} \left[(1 - \overline{y}) \beta(\overline{y}) \frac{\partial \Theta}{\partial \overline{y}} \right] = u^+ (\overline{y}) \frac{\partial \Theta}{\partial x^+} \qquad (6-2)$$

a solution for the temperature profile and Nusselt number was obtained at Pr = 0.71 for all axial positions. The boundary conditions were constant wall heat flux and uniform initial temperature. The method used by Sparrow, Hallman, and Siegel (35) was employed to solve equation 6-2 with the following important changes:

38

1. The eddy diffusivity and velocity profiles for adiabatic low Reynolds number flow were used in place of the profile used by Sparrow, Hallman, and Siegel. The use of Reynolds analogy, $\epsilon_H = \epsilon_m$, was retained. It leads to

$$\frac{\epsilon_H}{\upsilon} = \frac{\epsilon_m}{\upsilon} = \frac{\kappa}{6} \left[y^+ - y_1^+ \tanh \frac{y^+}{y_1^+} \right] \left[2 - \overline{y} \right]$$

$$\cdot \left[1 + 2(1 - \overline{y})^2 \right]$$

(6-3)

with $\kappa = 0.4225$

and $y_1^+ = 11 + 9.1116 \exp(-0.27249 \ \text{Re} \times 10^{-3})$

$$+ \left[15.83 \exp(-0.9498 \ \text{Re} \times 10^{-3}) \right]^4$$

for the eddy diffusivity of heat. The velocity is obtained by integration of the defining equation for $\frac{\epsilon_m}{\upsilon}$,

$$u^+(\overline{y}) = \int_0^{\overline{y}} \frac{(1 - \zeta)}{1 + \frac{\epsilon_m}{\upsilon}} \ y_\zeta^+ \ d\zeta$$

(6-4)

These profiles were shown to be valid for all fully turbulent Reynolds numbers greater than, or equal to 3000, whereas the profiles used by Sparrow, Hallman, and Siegel are valid only above 30,000.

2. The distance from the tube wall, y, was used in place of the radial coordinate as the independent variable.

3. A different nondimensionalization was employed.
    This leads to different numerical magnitudes for
    the eigenvalues than would be obtained using the
    nondimensionalization of reference (35).

Results were obtained numerically on an IBM 7072; a
fifth order Predictor-Corrector, with a Runge-Kutta proce-
dure for starting, was employed in the eigenvalue solution.
Since the series solution was truncated, results are not
available at $x/D = 0$. Details of the numerical work are
available in Appendix G.

For later comparison, the same numerical program
was used to solve the energy equation with the eddy dif-
fusivity and velocity profile expressions used by Sparrow,
Hallman, and Siegel (35), and the low Reynolds number
expression developed by McEligot, Ormand, and Perkins (9).
A solution employing the latter profile was deemed desirable
since the velocity data presented in Chapter III did not
discriminate between their profile and the present one.
Both low Reynolds number profiles predict the deviation of
the nondimensionalized velocity, u^+, from the universal
velocity profiles for Reynolds numbers below 30,000. This
is not true of the profile used by Sparrow, Hallman, and
Siegel.

Due to the wide spread knowledge and availability
of the method of Sparrow, Hallman, and Siegel (35) (see

Kays (2) and summary in Chapter V), only the results
obtained using equations 6-3 and 6-4 for equation 6-2 are
presented. Details of the present solution may be found in
Appendix H. Comparisons with the solutions obtained using
the other two profiles and data are deferred to a later
section.

The local Nusselt number may be given in terms of
the fully developed value as

$$\frac{Nu}{Nu_\infty} = \frac{1}{1 + \sum_n A_n e^{-\lambda_n^2 x^+}} \qquad (6-5)$$

The first seven values of the eigenvalues, λ_n^2 and A_n, are
presented for gases in Tables 2 and 3 for a range of
Reynolds numbers. Since a searching method was employed in
their evaluation, the accuracy of any individual eigenvalue
is independent of previously calculated values. Eigen-
values and associated coefficients for laminar flow, as
calculated by the present numerical program, are also
compared with the Siegel, Sparrow, and Hallman (46) laminar
solution to establish confidence in the validity of the
present numerical method. For the laminar case, no
ambiguity in the calculation of the velocity profile is
possible. At the upper end of the range, Re = 50,000, the
Sparrow, Hallman, and Siegel solution (as generated by the

Table 2. Eigenvalues

Re	λ_0^2	λ_1^2	λ_2^2	λ_3^2	λ_4^2	λ_5^2	λ_6^2
			$Pr = 0.71$				
3,000	0	0.06237	0.18445	0.37272	0.62918	0.95341	1.34509
4,000	0	0.06414	0.18900	0.37796	0.63446	0.95916	1.35174
6,000	0	0.06364	0.18843	0.37448	0.62420	0.93958	1.32121
8,000	0	0.06282	0.18693	0.37157	0.61763	0.92695	1.30073
10,000	0	0.06185	0.18461	0.36739	0.61025	0.91443	1.28121
20,000	0	0.05749	0.17239	0.34431	0.57250	0.85683	1.19763
30,000	0	0.05479	0.16446	0.32895	0.54756	0.81991	1.14581
50,000	0	0.05176	0.15547	0.31138	0.51890	0.77745	1.08637
			Laminar Comparison Re = 1787, Pr = 0.7				
Present	0	0.02053	0.06705	0.13926	0.23710	0.36056	0.50962
Siegel, Sparrow, and Hallman	0	0.02053	0.06705	0.13926	0.23709	0.36056	0.50963

Table 3. Values of $-A_n$

Re	A_0	A_1	A_2	A_3	A_4	A_5	A_6
			Pr = 0.71				
3,000	0	0.33773	0.16694	0.09392	0.05958	0.04151	0.03045
4,000	0	0.30427	0.16409	0.09909	0.06423	0.04486	0.03330
6,000	0	0.26889	0.15281	0.10119	0.06959	0.04969	0.03705
8,000	0	0.24989	0.14279	0.09871	0.07130	0.05260	0.03981
10,000	0	0.23796	0.13545	0.09539	0.07109	0.05398	0.04164
20,000	0	0.21008	0.11765	0.08415	0.06598	0.05373	0.04446
30,000	0	0.19720	0.10971	0.07848	0.06235	0.05217	0.04486
50,000	0	0.18319	0.10113	0.07209	0.05766	0.04922	0.04367
		Laminar Comparison Re = 1787, Pr = 0.7					
Present	0	0.43358	0.15111	0.07965	0.05021	0.03497	0.02598
Siegel, Sparrow, and Hallman	0	0.43358	0.15111	0.07965	0.05021	0.03497	0.02598

present program) is a maximum of 1.1 per cent higher than the solution obtained from their published eigenvalues.

The Nusselt numbers for fully established conditions, used to normalize the thermal entry values, are represented within 4 per cent by a Dittus-Boelter equation of the form

$$Nu_{\infty} = 0.021 \ Re^{0.8} \ Pr^{0.4} \tag{6-6}$$

for the range of Reynolds numbers from 3000 to 50,000. The agreement could be improved to 3 per cent with the use of a coefficient of 0.0231 and a power of 0.79 for Re, but such reduction is probably not worthwhile for design.

The entry region solution is presented graphically in Figure 4 and is listed in Table 4. The analysis shows the dimensionless entrance distance to decrease slightly with increasing Reynolds number. For all Reynolds numbers the Nusselt number can conservatively be considered to reach its downstream value by $x/D = 30$. In the entrance region the Nusselt number increases markedly, at a fixed axial position, as the Reynolds number decreases. The main effect is confined to distances less than 10 diameters; at $x/D = 3$, a 16 per cent increase in the normalized Nusselt number is observed between Reynolds numbers of 50,000 and 3,000. The solution is approaching the laminar solution of Siegel, Sparrow, and Hallman (46), though a considerable
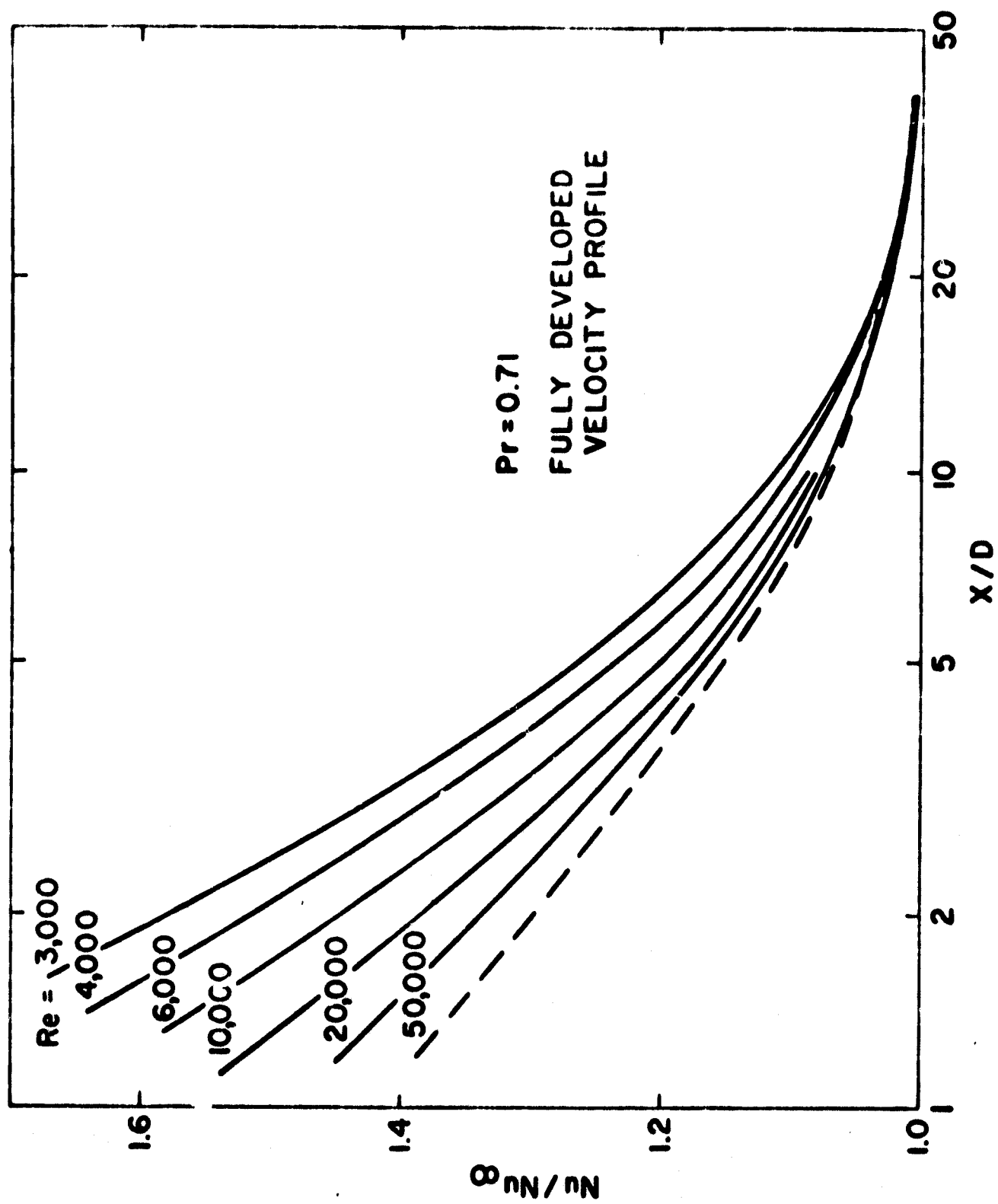
Figure 4. Thermal Entrance Solution for Turbulent Low Reynolds Number Flow

Table 4.   Entrance Region Nusselt Number

Re	3,000	4,000	6,000	10,000	20,000	50,000
Nu_∞	11.056	14.081	19.571	29.463	50.275	100.810
x/D	$\longleftarrow$		Nu/Nu_∞			$\longrightarrow$

$$Pr = 0.71$$

2.5	1.4951	1.434	1.3780	1.3292	1.2936	1.2638
5.0	1.2655	1.2306	1.2020	1.1795	1.1657	1.1550
7.5	1.1674	1.1445	1.1273	1.1148	1.1087	1.1049
10.0	1.1126	1.0967	1.0856	1.0782	1.0757	1.0751
12.5	1.0784	1.0669	1.0595	1.0549	1.0543	1.0553
15.0	1.0556	1.0471	1.0421	1.0392	1.0397	1.0415
17.5	1.0399	1.0335	1.0301	1.0783	1.0292	1.0314
20.0	1.0288	1.0240	1.0216	1.0205	1.0217	1.0240
22.5	1.0209	1.0173	1.0156	1.0150	1.0162	1.0184
25.0	1.0152	1.0125	1.0113	1.0109	1.0121	1.0141
27.5	1.0111	1.0090	1.0082	1.0080	1.0090	1.0109
30.0	1.0081	1.0065	1.0059	1.0059	1.0068	1.0084
32.5	1.0059	1.0047	1.0043	1.0043	1.0051	1.0065
35.0	1.0043	1.0034	1.0031	1.0031	1.0038	1.0050
37.5	1.0032	1.0025	1.0023	1.0023	1.0029	1.0039
40.0	1.0023				1.0022	1.0030

difference still exists in the normalized Nusselt number
between the turbulent values at 3000 and the laminar
results at 2000.   Both the Nusselt number and the entry
length variations are consistent with the trends of the
laminar solution, the oil and water data of Malina and
Sparrow (42), and the air data of Hanratty and Johnk (11).
At a Reynolds number of 50,000 the solution, which is based
on the present velocity profile, agrees within two per cent
with the solution of Sparrow, Hallman, and Siegel as
calculated by the present program.   Agreement to within one
per cent is obtained using their published eigenvalues.

To ease application by the engineer, the entrance
region results for the constant heat flux boundary have
been correlated by the equation

$$\frac{Nu}{Nu_{\infty}} = 1 + 0.8(1 + 70,000 \ Re^{-\frac{3}{2}})(\frac{x}{D})^{-1} \qquad (6-7)$$

Agreement is within 5 per cent for $x/D \geq 2$, with improve-
ment to 3 per cent or less for $x/D > 4$ over the range
$3000 < Re < 50,000$.   For $x/D > 12$ the prediction could be
improved by the use of a separate correlation for $\frac{Nu}{Nu_{\infty}}$
similar to the above expression.   The somewhat "poor"
disagreement (3 per cent) in the downstream region is
tolerated for the sake of simplicity in the correlation.
The analysis shows that the fully developed value is
reached for $x/D > 30$.

To treat problems with axially varying wall heat flux the local Nusselt numbers are not directly available. Instead, they must be derived for the heat flux variation of interest by employing the eigenvalues and constants. The eigenvalues and associated constants of the present study were found to be correlated by the expressions

$$\lambda_n^2 = A_{1,n} Re^{-b_{1,n}} + C_{1,n} Re^{-d_{1,n}} \tag{6-8}$$

and

$$An = -A_{2,n} Re^{-b_{2,n}} + C_{2,n} Re^{-d_{2,n}} \tag{6-9}$$

for Reynolds numbers from 4000 to 50,000. The above three correlations are equally valid for helium ($Pr = 0.664$) and air ($Pr = 0.71$). Numerical values for the coefficients and constants are presented in Table 5.

Table 5. Numerical Coefficients and Powers for Eigenvalue Correlation

n	$A_{1,n}$	$b_{1,n}$	$C_{1,n}$	$d_{1,n}$
1	0.170	0.1098	1.347×10^5	2.5
2	0.491	0.1064	1.466×10^5	2.34
3	0.945	0.1029	2.39×10^5	2.33
4	1.531	0.1001	2.65×10^5	2.30
5	2.29	0.1001	3.32×10^5	2.64
6	0.33	0.1033	0.059×10^5	1.662

n	$A_{2,n}$	$b_{2,n}$	$C_{2,n}$	$d_{2,n}$
1	1.25	0.179	-2.84×10^{-11}	3.64
2	0.650	0.172	-5.91×10^1	1.061
3	0.459	0.171	$2.82 \times 10^{+12}$	3.99
4	0.235	0.1299	9.86×10^4	1.885
5	0.1193	0.0817	1.25×10^5	1.91
6	0.0442	0	5.13×10^5	2.13

CHAPTER VII

EXPERIMENTAL HEAT TRANSFER INVESTIGATION

Apparatus

The apparatus used was a redesigned version of the heat transfer loops used by Perkins and Worsoe-Schmidt (40) and McEligot, Magee, and Leppert (41). Briefly, the test section consisted of a vertical, thin walled, one-quarter inch, circular Inconel 600 tube with a 100 diameter hydrodynamic entrance, 100 diameter heated length, and a 30 diameter exit. Two pressure taps were located just beyond the extremes of the 100 diameter heated length. The test section was enclosed in a six foot long, six inch diameter vacuum chamber to minimize heat loss effects and allow localized heat loss calibration. The vacuum environment also reduces the response time necessary to reach steady conditions with heating. A. C. power for electrical heating was provided by a line voltage stabilizer, a variable transformer and a 20-to-1 transformer in series. Above approximately 80 amperes, a Lincoln model TM-500 AC/DC welder was used as the power source. Variable area flow meters, with specified accuracy of one per cent of full scale, were used as the primary flow measurement devices. A Foxboro integral orifice, differential pressure

cell served as a secondary check. The gas was supplied by a four bottle gas manifold. Test gas passed through two pressure regulators connected in series and through the flow measuring equipment before entering the test section. Flow control was achieved by means of two regulating valves, located downstream of the test section.

Method of Testing

The method of testing closely parallels that of the above references (40, 41). In summary, the results presented herein were obtained for the flow of helium and air through a vertical, resistively heated tube. Premium grade Chromel-Alumel thermocouples were spot welded to the tube at various axial positions. Heat transfer data were obtained for a number of different low power settings at each of four different inlet Reynolds numbers in the desired range. Measurements of the tube wall temperatures were obtained for axial positions ranging from $x/D = 1.21$ to 95.68 with a maximum wall-to-bulk temperature of 1.41. Test section pressures of approximately 100 psia were employed to hold the entering Mach number below 0.033 to avoid compressibility and viscous dissipation effects. The modified Grashof/Reynolds quotient was kept below 20 to avoid natural convection effects (47). The reader will recall that these effects were neglected in the analysis to which the data are compared. To determine the thermocouple

conduction error of the wall thermocouples (48), internal test section temperatures were measured with a ceramic thermocouple probe when the system was at power but without flow; comparison to the outside wall thermocouples led to calibration of the error for each wall thermocouple. The test section emissivity, $e(x, T)$, was also determined locally from these calibration runs. This calibration provided a convenient method for evaluating the local external heat loss.

The local energy generation was evaluated from the i^2R' product. In the resistance calibration the assumption was made that the local resistance at a given temperature was equal to the average test section resistance at the same temperature. The variation of the average test section resistance with temperature was obtained from voltage and current measurements taken during a large number of runs without flow. For heating without flow the axial temperature remained essentially constant. These runs were spaced over a two year period and indicated a slight decrease in resistance with time. Consequently, for the resistance variation with temperature, the data reduction procedure used a straight line correlation which favored the resistance data obtained during the same time period as the heat transfer data. The wall heat flux was evaluated by subtracting the radial radiation and axial conduction heat losses from the local energy generation.

Data reduction was performed on an IBM 7072 digital computer employing a modification of the data reduction program used by McEligot (49). The reduced data are presented in Appendix II.

A method similar to that of Malina and Sparrow (42) was used to approach the constant property idealization of the analysis. For each of the fixed inlet Reynolds numbers, the data for the various power settings were normalized by a Dittus-Boelter correlation (with a 0.021 coefficient) and were plotted against the wall-to-bulk temperature ratio on logarithmic coordinates. This choice of normalization partially removes the effect of small variations in the inlet Reynolds number, even though these variations never exceeded 0.8 per cent for a given flow setting. For a given thermocouple, extrapolation of the data to a wall-to-bulk temperature ratio of one removes the temperature dependent variable properties effect. The extrapolation procedure is demonstrated in Figure 5 for several of the thermocouples.

For the helium data the uncertainty of the extrapolated constant property Nusselt numbers is estimated to range from a low of four per cent to a high of nine per cent for each of the inlet bulk Reynolds numbers of 4180, 6800, and 10,300. Typically, the uncertainty at first decreases with axial position and, then, begins to increase at large x/D due to increasing uncertainty in the bulk
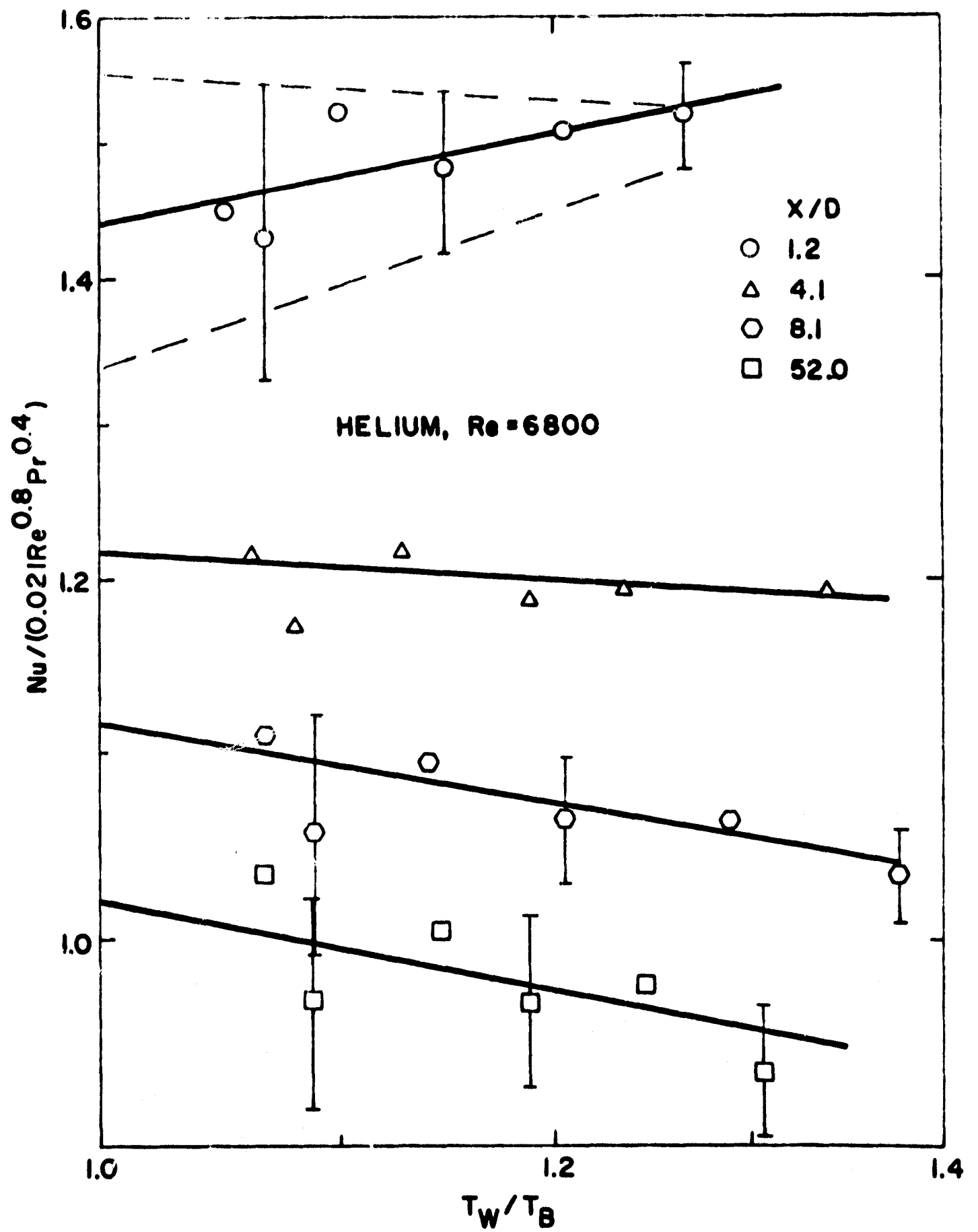
Figure 5. Constant Property Extrapolation at Re = 6800

temperature. A maximum difference of 0.8 per cent was observed between the mass flow rates measured with the primary and secondary flow meters. Adiabatic friction factor measurements, taken before and after the heating runs without changing the flow settings, showed a maximum deviation from the Blasius friction factor (1) of -2 per cent; it occurred for the 10,300 Reynolds number runs.

The uncertainty for the air data at a Reynolds number of 3860 was considerably larger than for the helium Nusselt numbers; it ranged from 8-1/2 to 13 per cent. This increase is predominantly due to the very small range of wall-to-bulk temperature ratios for which the air data were obtained (a maximum of 1.09 versus 1.4 for the helium data). The percentage uncertainties in Nu are high for small wall-to-bulk temperature differences. Without data at larger ratios, the estimated uncertainty bands obtained in the constant property extrapolation process become larger. In addition, an increased uncertainty in the mass flow rate (5.7 per cent versus a maximum of 3.2 per cent for the helium runs) also contributed to the higher uncertainties for the air runs. A difference of 3-3/4 per cent between the primary and secondary flow rates and a 3 per cent overprediction of the adiabatic friction factor were observed. This indicates the measured flow rate could be low, which would result in the calculation of an excessive value for the Nusselt number.

In summary, the dominant uncertainty in the Nusselt number was found to be due to the uncertainty in the wall-to-bulk temperature difference, which decreased in importance as the difference increased. However, most of the results can probably be considered conservatively to have uncertainties within 10 per cent. The reader should be careful not to be misled by the exaggerated expansion of the ordinate on some of the figures.

CHAPTER VIII

COMPARISONS OF HEAT TRANSFER RESULTS

Entrance Region

The constant wall heat flux analysis is compared with the extrapolated constant property data for air at a bulk Reynolds number of 3860, and for helium at Reynolds numbers of 4180, 6800, and 10,250 in Figures 6 through 9. The numerical solution was rerun for each set of experimental conditions to obtain the theoretical predictions shown. Solutions generated using the McEligot, Ormand, and Perkins (9), and the Sparrow, Hallman, and Siegel (35) velocity profiles are also included. The idealization of constant wall heat flux is satisfied for $x/D > 2$, with $\frac{q_w''}{q_{w_{max}}''}$ having reached 0.955 to 0.985 at $x/D = 1.2$ for all runs. The experimental heat flux distribution may be represented by an exponential variation in the immediate thermal entry,

$$q_w'' = q_{wmax}''(1 - e^{-mx^+})$$

For this axial distribution the method of superposition (2) yields

57
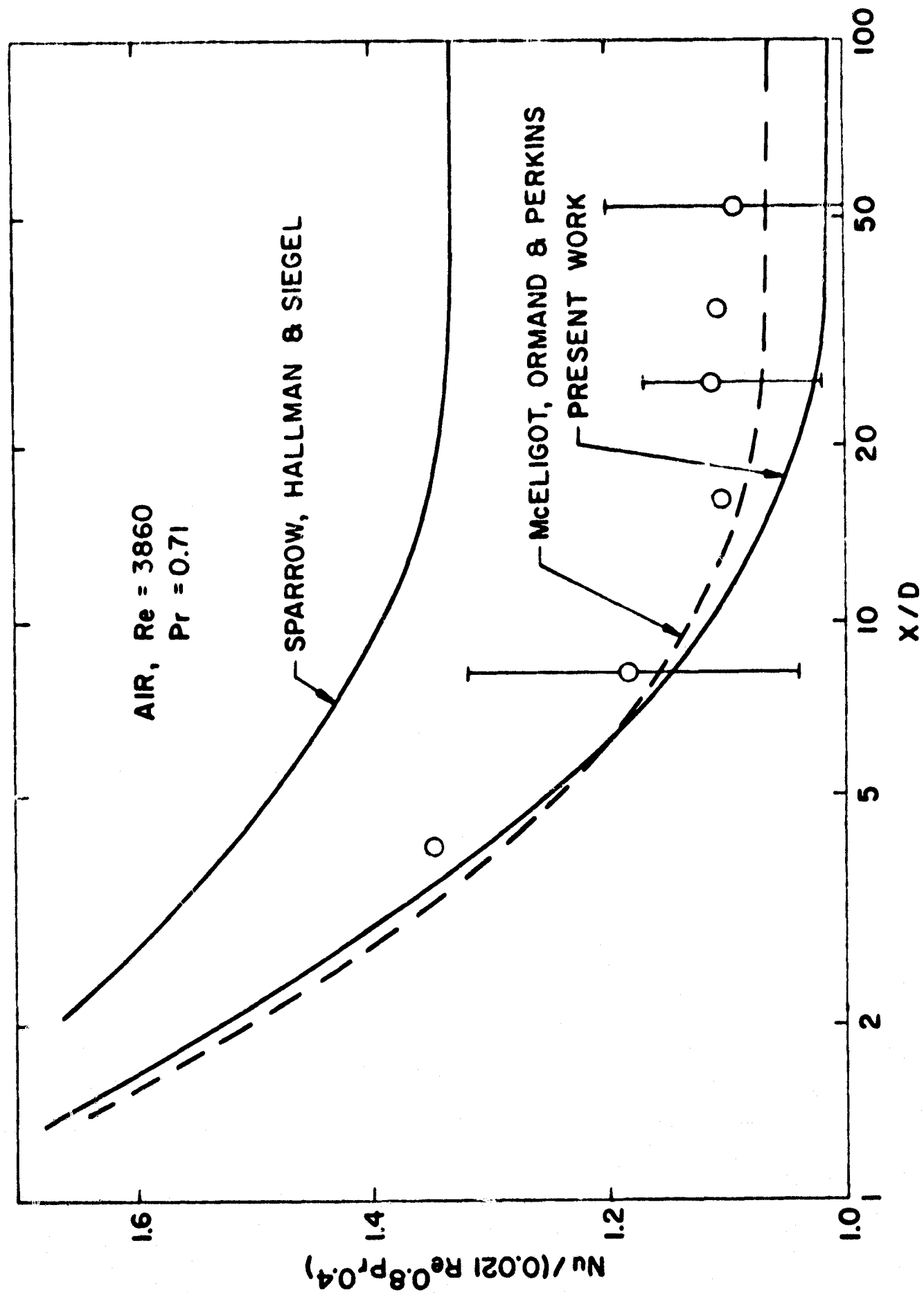
Figure 6. Thermal Entrance Solutions Compared with Experiment, Re = 3860

58
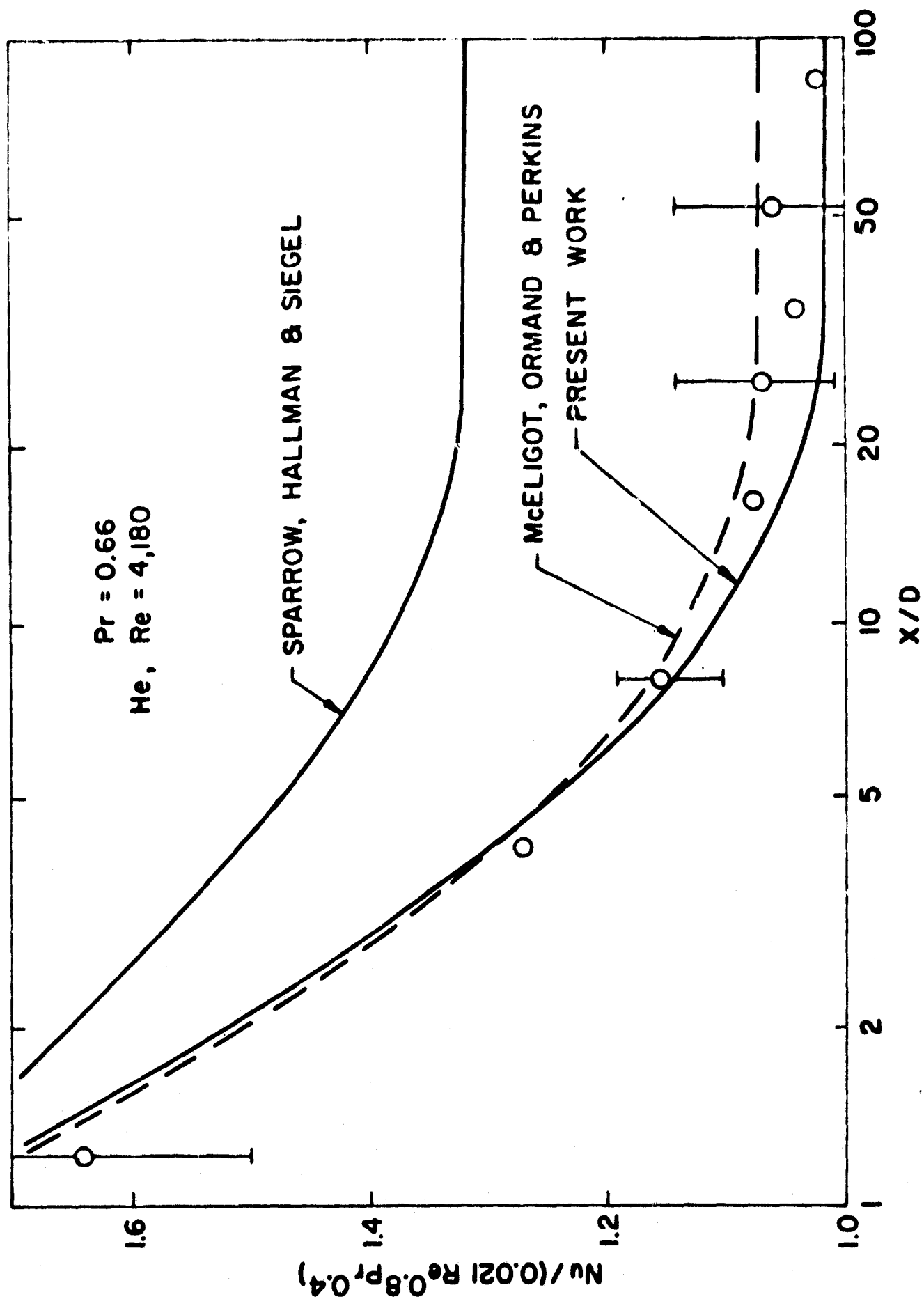
Figure 7. Thermal Entrance Solutions Compared with Experiment, Re = 4180

59
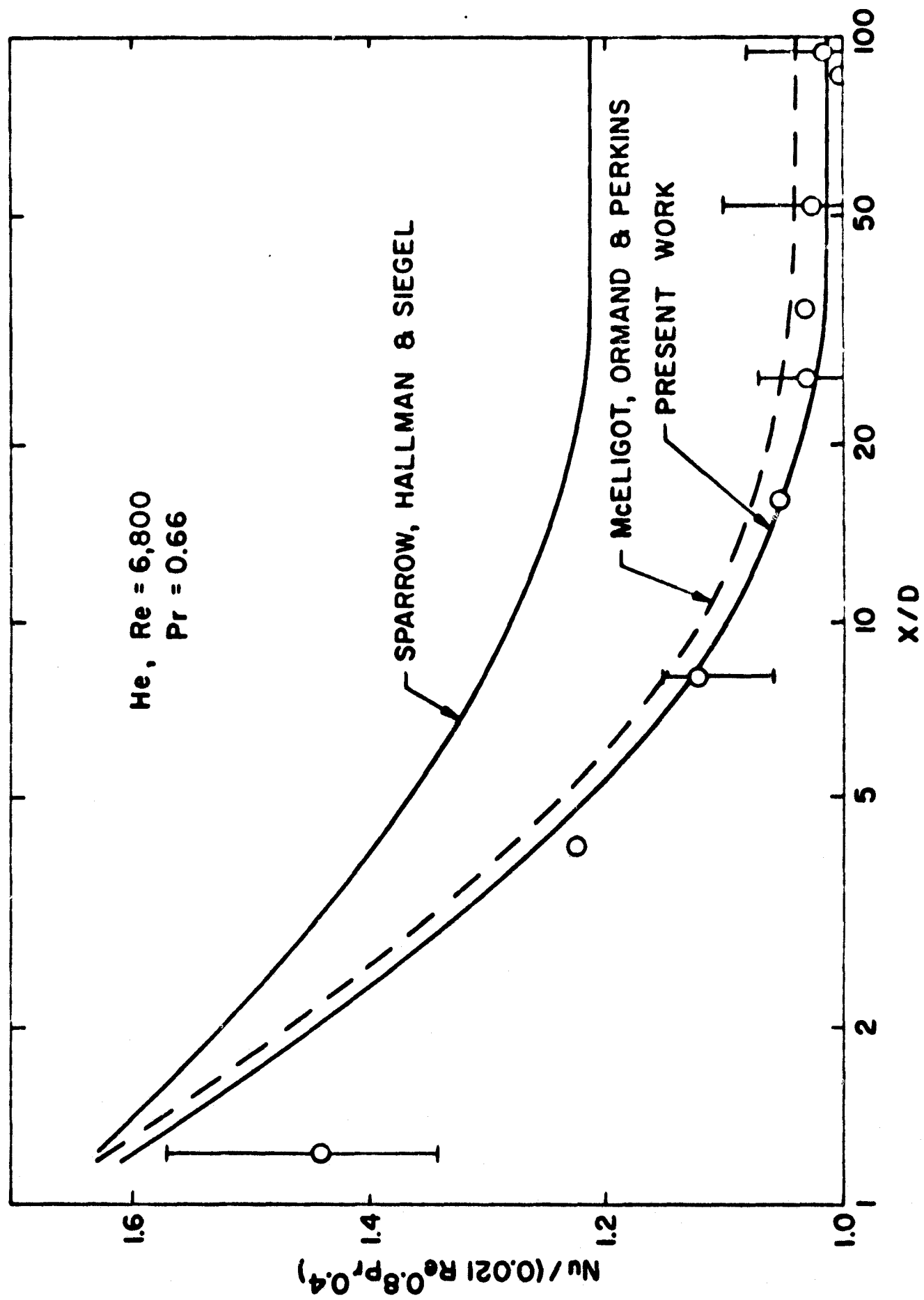
Figure 8. Thermal Entrance Solutions Compared with Experiment, $Re = 6800$

60
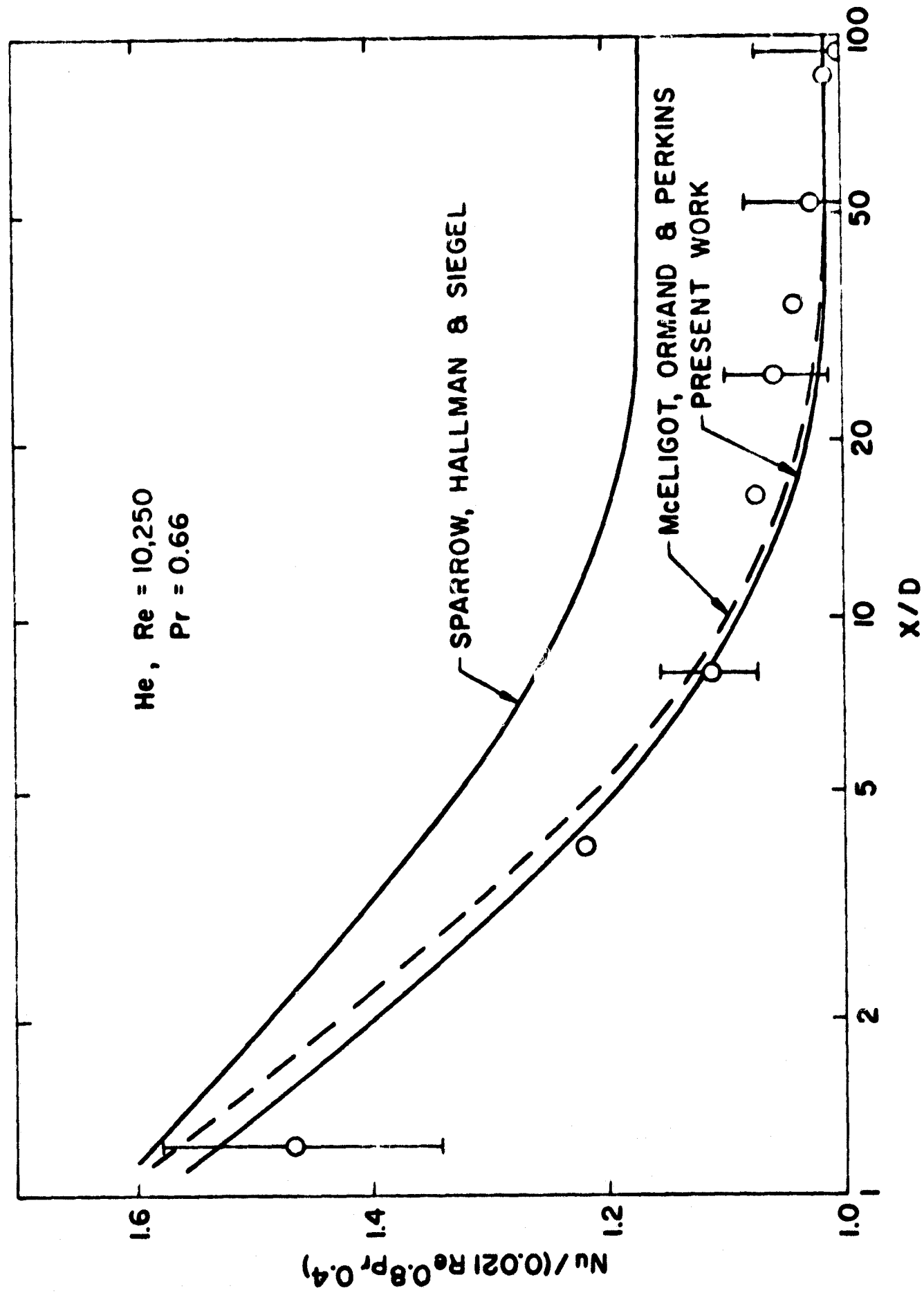
Figure 9. Thermal Entrance Solutions Compared with Experiment, Re = 10,250

$$\frac{Nu}{Nu_\infty} = \frac{(1 - e^{-mx^+})}{1 + \sum_k \frac{\lambda_k^2 A_k e^{-mx^+} - m A_k e^{-\lambda_k^2 x^+}}{\lambda_k^2 - m}}$$

This solution approaches the constant wall heat flux solution to within two per cent or less by $x/D = 4$ under the conditions of the present experiments.

The air data are observed to be consistently higher than the analysis, a trend which is consistent with the suspected low value of the measured flow rate mentioned earlier. Excluding these data and the values at $x/D = 1.21$, which are highly inaccurate due to axial conduction in the test section wall and to the small wall-to-bulk temperature differences which exist near the initiation of heating, the data are correlated to within five per cent by the present analysis. Including all data, correlation is obtained to within ten per cent.

From the present investigation, it cannot be definitely concluded whether a solution based on the present low Reynolds number velocity formulation, or on the McEligot, Ormand, and Perkins (9) formulation, is more accurate. Both correlate the data within the experimental uncertainty, and agree closely with each other, differing by a maximum of 6.7 per cent at a Reynolds number of 3000. Both satisfy continuity and converge to the Sparrow,

Hallman, and Siegel (35) solution at a Reynolds number of 50,000 as shown in Figure 10. A slightly better agreement is noted for the present solution (2 versus 4-3/4 per cent maximum difference). The present formulation is recommended over the McEligot, Ormand, and Perkins solution (9) since it predicts lower, and thus more conservative, Nusselt numbers at the low end of the Reynolds number range. In addition, the eddy diffusivity-velocity profile used is based on data covering the entire low Reynolds number range from 3000 to 15,000 and is theoretically more rigorous. The eddy diffusivity distribution satisfies the accepted requirements at the wall and centerline of the tube more completely than does the distribution of the earlier study.

Fully Developed Solution

The analytical prediction of Nusselt numbers for fully established conditions are compared with local data of the present work, and with the data presented by McEligot, Ormand, and Perkins (9), in Figure 11. Both of the low Reynolds number solutions correlate the data to within a few per cent and represent a substantial improvement over the analyses based on universal velocity type distributions. As mentioned earlier, the fully developed Nusselt numbers of the present analysis are approximated within 4 per cent by the Dittus-Boelter equation
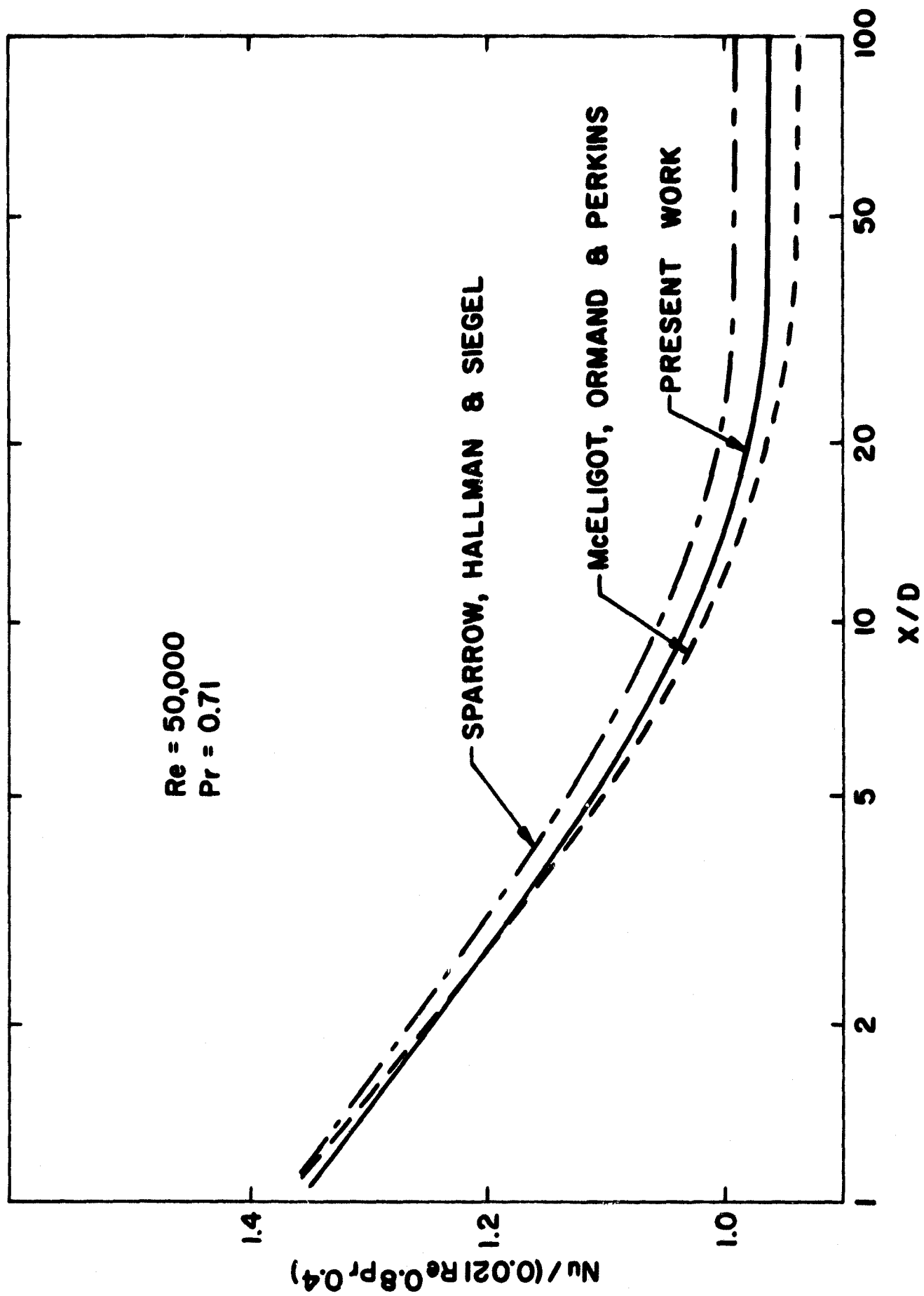
Figure 10. Thermal Entrance Solutions at Re = 50,000

64
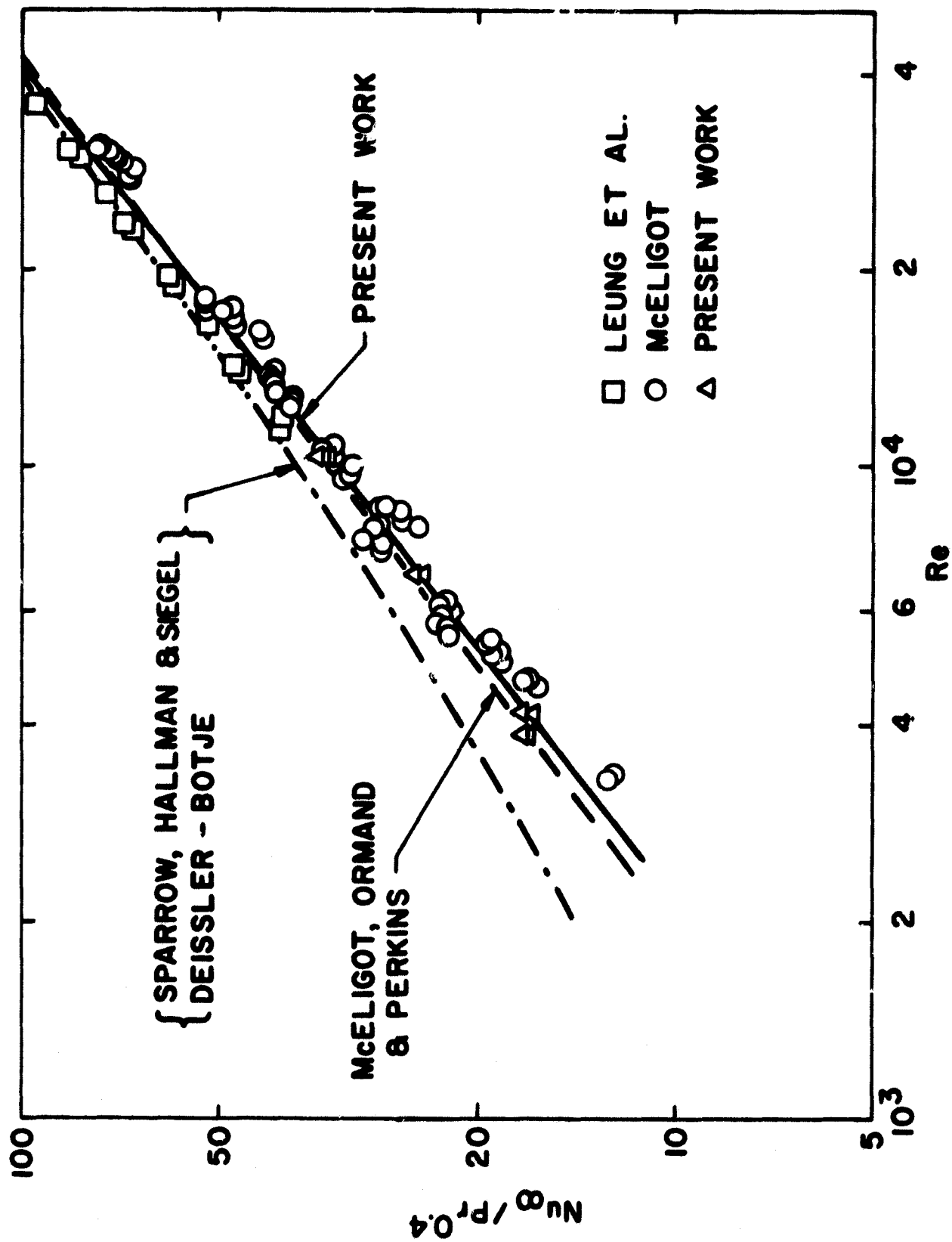
Figure 11. Heat Transfer in Fully Established Flow: Semi-Empirical Predictions Compared with Data

$$Nu_{\infty} = 0.021 \, Re^{0.8} \, Pr^{0.4} \qquad (8\text{-}1)$$

for the range of Reynolds numbers from 3000 to 50,000.

The present formulation predicts a slightly lower Nusselt number than the McEligot, Ormand, and Perkins (9) solution at the lower Reynolds numbers with the converse occurring above a Reynolds number of approximately 20,000.

CHAPTER IX

DISCUSSION OF HEAT TRANSFER STUDY

The success of the present entrance region solution for the low Reynolds number turbulent heat transfer yields additional support to the use of Reynolds analogy, $\epsilon_m = \epsilon_H$, in heat transfer analysis for gases. The data were correlated reasonably well by both of the low Reynolds number eddy diffusivity-velocity profiles considered, although they differed in several respects. The differences in the profiles indicate that a velocity profile is adequate for heat transfer predictions provided (a) it satisfies continuity, i.e., predicted friction factors agree with data, and (b) it agrees approximately with the observed deviation of the velocity data from the universal profile.

The eigenvalues of the present analysis provide the necessary building blocks for the prediction of heat transfer results for axially varying wall heat flux at low heating rates. For the treatment of the method of superposition presented by Kays (2) the nomenclature are related as $\gamma_m^2 = \lambda_n^2 \, RePr$ and $A_m = -2\gamma_m^2 \, A_n/Nu_\infty$, where λ_n^2, A_n, and Nu_∞ are the values predicted by the present solution. Care must be exercised if alternate references are used, since

the numerical values of the eigenvalues and the associated
constants will differ as the nondimensionalization differs.

The present analysis is not necessarily restricted
to Reynolds numbers below 50,000 since the semi-empirical
velocity formulation used is valid for all Reynolds numbers
for which the Blasius friction factor is acceptable.
Results were not presented beyond 50,000, since the
designer will probably wish to use the more familiar
Sparrow, Hallman, and Siegel (35) solution at the higher
Reynolds numbers. Below a Reynolds number of 50,000, the
present solution predicts slight increases in the entrance
length and strong increases in the normalized Nusselt
number in the entrance region with decreasing Reynolds
numbers. The latter effect is most prominent for distances
less than ten diameters. For a Reynolds number decrease
from 50,000 to 3000, increases of 3.5 per cent and 16 per
cent are observed in the normalized Nusselt number for
$x/D = 10$ and $x/D = 3$, respectively. In all cases, the
Nusselt number may be considered fully developed by
$x/D = 30$. As previously indicated, the above trends are
consistent with the data of Malina and Sparrow (42),
Hanratty and Johnk (11), and the present data. Above
Reynolds numbers of 50,000, a reversal in the trends of
the solution was observed. Very slight increases in both
the entrance length and the normalized Nusselt numbers
occurred with increasing Reynolds numbers. This reversal

agrees with the small increases shown by the solution of Sparrow, Hallman, and Siegel (35) for their published values of Reynolds numbers of 50,000, 100,000, and 500,000. The change in the direction of the trends at high Reynolds numbers may be due to the reduced thickness of the laminar sublayers, and/or numerical inaccuracies in the solution.

The reader's attention is also called to the requirement of fully turbulent flow, as defined by an intermittency factor equal to one. The velocity profile employed is valid only for this condition. It is incapable of describing intermittent laminar and turbulent flow, which exists for values of the intermittency factor less than one. Thus, these results should not be used for prediction during the axial transition from laminar to fully-turbulent flow.

For x/D values greater than four, the experimental Nusselt numbers were observed to decrease slightly as the wall-to-bulk temperature ratio increased from approximately 1 to 1.4. These data might be correlated by an equation of the form

$$ Nu = 0.021 \ Re^{0.8} \ Pr^{0.4} \ (\frac{T_w}{T_b})^a \qquad (9-1) $$

but experimental uncertainties prevent an accurate evaluation of the exponent, a, since the range of T_w/T_b is small.

The question--which of the two low Reynolds number, turbulent eddy diffusivity and velocity profile formulations considered best describes low Reynolds number turbulent flow--remains unresolved. The differences between the two profiles noted in Chapter IV, however, appear to have a minor effect on the prediction of the heat transfer parameters, so resolution is probably not necessary.

The use of the high Reynolds number expressions employed by Sparrow, Hallman, and Siegel (35) proved totally ineffective for thermal entrance region predictions in the low Reynolds number range. This is due to the use of a velocity formulation which neither satisfies continuity, nor describes the adiabatic profile accurately at low Reynolds numbers. For high Reynolds numbers, these requirements are fulfilled and the solution provides an accurate prediction of heat transfer characteristics for Reynolds numbers over 50,000. The agreement at high Reynolds numbers further confirms that adequate heat transfer predictions are possible only if both of these requirements are met for the velocity profile.

CHAPTER X

CONCLUSIONS

The lack of accurate predictions of thermal entry heat transfer characteristics for low Reynolds number, constant property, turbulent flow has been eliminated. Design equations have been developed from this study to provide the engineer with a convenient method of analysis. The following conclusions can be drawn:

1. A universal velocity profile does not provide an adequate prediction of the friction factor for low Reynolds number flow. It satisfies continuity only for Reynolds numbers in excess of approximately 30,000.

2. To be valid, a velocity formulation must predict both friction factor and velocity magnitudes consistent with the experimental data. The present modified form of Reichardt's eddy diffusivity yields a velocity profile which meets these requirements in both the low and high Reynolds number ranges. It is valid for all Reynolds numbers for which the Blasius friction factor is reasonable.

3. A universal velocity profile is inadequate for use in the prediction of heat transfer characteristics of low Reynolds number turbulent flow.

4. The use of the present low Reynolds number formulation leads to an accurate prediction of the Nusselt number for the thermal entrance and downstream, fully developed regions. For a constant wall heat flux, the results are described by the eigenvalue table and are correlated by the expressions presented in Chapter VI.

5. The eigenvalue results (or the correlations for the eigenvalues and associated constants) provide the necessary information needed for the solution of the variable wall heat flux problem.

6. It is not necessary to modify Reynolds analogy, $\epsilon_H = \epsilon_m$, to obtain good heat transfer predictions for the conditions in this study.

APPENDIX A

DETAILS OF EXPERIMENTAL VELOCITY STUDY

Introduction

This appendix presents details of the adiabatic velocity measurements taken at Texas Technological College, Lubbock, Texas, the data reduction procedure, and specifics of the uncertainty analysis. The uncertainty analysis includes consideration of the effect of neglecting probe corrections in relation to the uncertainty in the velocity and transverse position. The estimates are based on the expressions suggested by Daily and Hardison (27) in their impact probe literature survey. A brief discussion of these corrections is also included.

Experimental Equipment

Details of the experimental facility are presented in reference (25). The major characteristics, plus modifications performed for the present study, are documented in the main body of this work. The experimental facility is shown schematically in Figure A-1. The probe installation, including the probe housing and wall static tap, is shown in Figure A-2. The radiation shield and insulation described in reference 25 were not in place when the present measurements were taken.
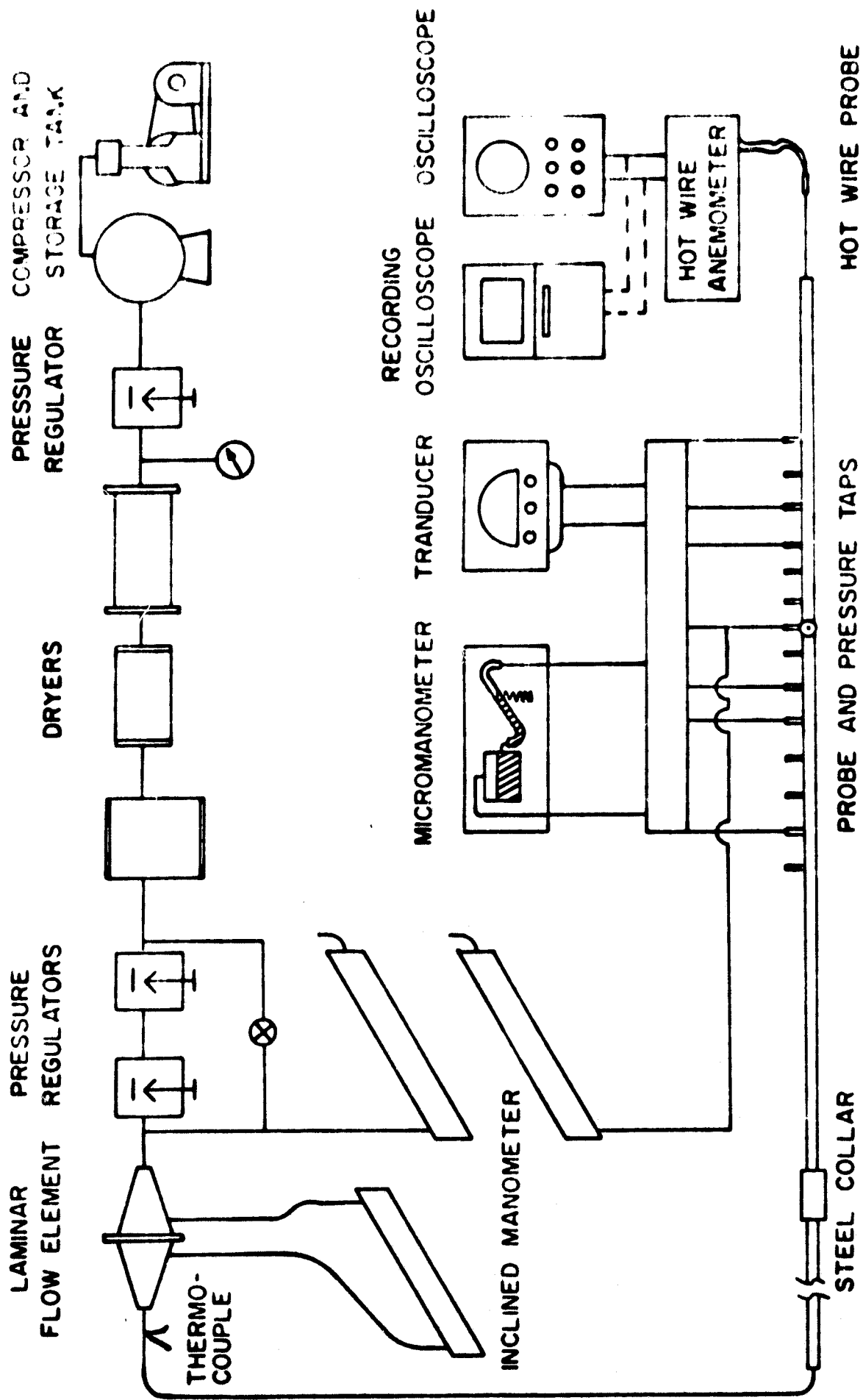
Figure A-1. Adiabatic Velocity Profile Apparatus

STATIC HOLE

INCONEL RING

STATIC PRESSURE TAP

INCONEL PIPE

SPINDLE

TEMPERATURE PROBE HOUSING

VELOCITY PROBE

VELOCITY PROBE HOUSING
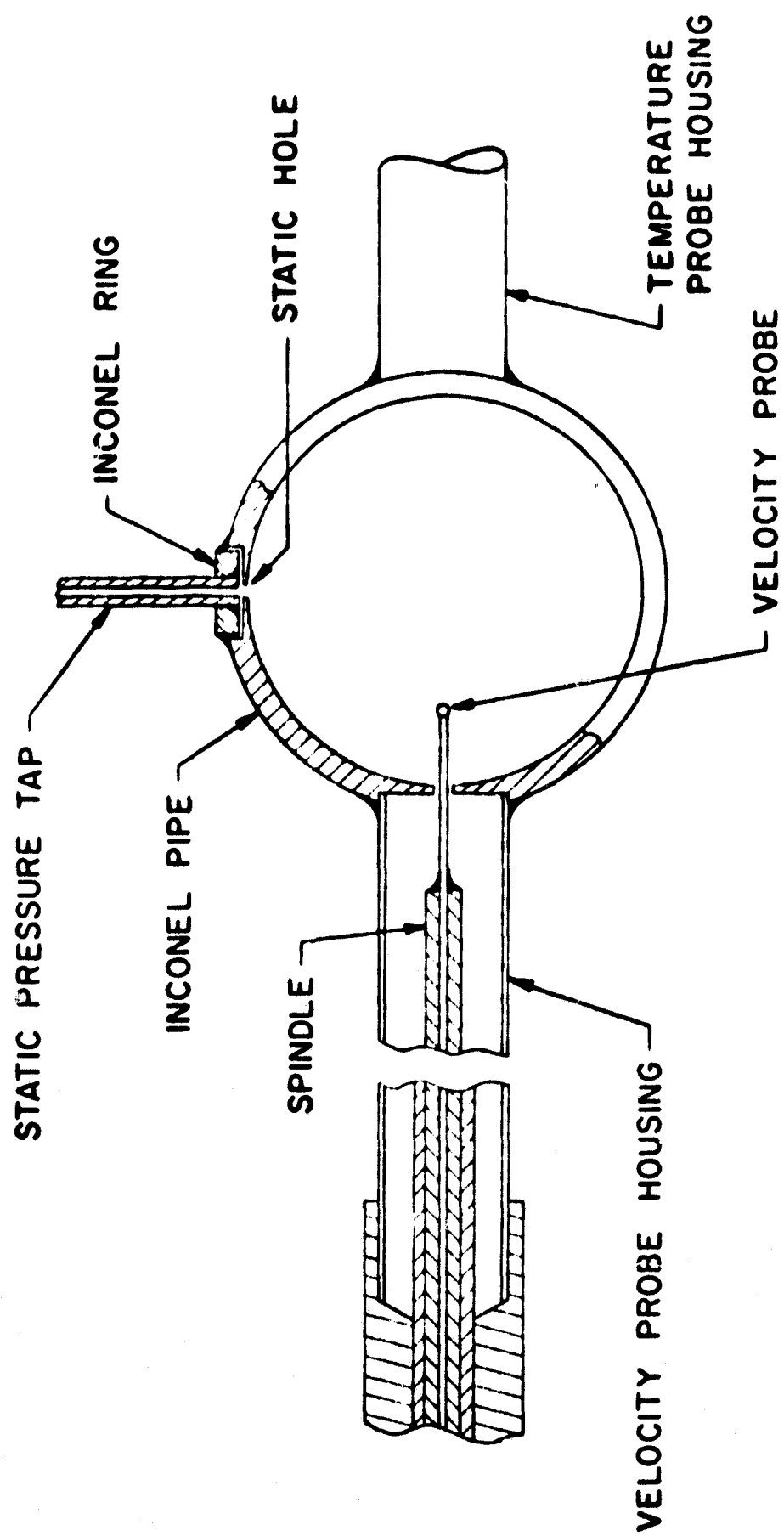
Figure A-2. Probe Installation

The manifold used in the pressure measurements was constructed from 1/4 inch diameter Polypenco tubing and 1/8 inch Swagelok tees. Six 1/8 inch Whitey and four 1/8 inch Robbins valves with Swagelok connections were used. The six Whitey valves were connected to the tube wall static pressure taps. The remaining twenty-one wall taps were sealed by plugging the open end of the Swagelok connectors on the 1/8 inch wall pressure tap extensions. One-eighth inch diameter copper tubing, sealed at one end, was used for this purpose. The impact probe and its wall static tap were connected to the manifold through two Robbins valves. Approximately six to eight feet sections of 1/8 inch Polypenco tubing were used for these connections. The high pressure and low pressure sides of the manifold were connected through two Robbins valves to a Flow Corporation Model MM3 Micromanometer with 1/4 inch Tygon tubing. They were also connected directly with 1/8 inch Polypenco tubing to a Decker Model 306-2 differential pressure transducer and indicator. This arrangement allowed the pressure drop between any of three pairs of wall static taps, or the impact probe and its wall static tap, to be read by opening the appropriate valves on the Micromanometer and/or pressure transducer. The Micromanometer has an accuracy of ± 0.0002 inches of butyl alcohol with a resolution of ± 0.0001 inch. The manifold was mounted on a 1/4 inch sheet of plywood reinforced with

slotted angle iron. It was clamped to a large sturdy table located next to the test section. The Micromanometer and transducer were also located on the table.

A Flow Corporation Model HWB3 Constant Current Hot Wire Anemometer was used to obtain qualitative fluctuating velocity component measurements. The output was observed on a Hewlett Packard 130-C oscilloscope, and a Sandborn 4500 Series high speed recording oscilloscope was used to record u' traces. Due to an impedance matching problem between the high impedance hot wire equipment and the moderate impedance Sandborn, the Sandborn would not record the u' output directly from the hot wire. Impedance matching was obtained by inserting a 20 microfarad capacitor in the positive leg of the hot wire output. Several resistances ranging from 100kΩ to 1.5mΩ were also tried, but traces could not be recorded until the 20 microfarad capacitor was inserted in the system. The traces recorded in this manner were found to be superimposed on a sine wave of small amplitude and large period. Consequently, the traces obtained are only useful as an indication of the oscilloscope output.

The Flow Corporation hot wire probe, used to measure the u' fluctuations, was held with its axis coincident with the test sections by two circular oak spacers attached to the shaft of the hot wire probe. The spacers were 1.6 inch diameter wheels with three spokes and a 1/2 inch thick rim.

The spacers contained ample flow passages to prevent flow
blockage. Access to the test section was gained through
the exit of the 1.61 ID tube. The probe was positioned at
the two stations at which u' measurements were taken by
means of a 1/4 inch dowel attached to the Amphenol connector
at the end of the probe. Scribed reference lines on the
dowel and tube were used to reproduce the same relative
alignment of the hot wire at the two stations. This
apparatus was not present in the tube when velocity
traverse data were taken.

Air was supplied by a compressor, capable of
pumping 40 cubic feet per minute, with the primary pressure
varying from 85 to 125 psig. Flow control was maintained
by a high capacity regulator and two Minneapolis Honeywell
pressure regulators. The last regulator, a model 356529,
was capable of maintaining control with 0.01 psig sensi-
tivity and 0.013 psi drift in fifteen hours for pressures
in the range of 0 to 25 psig. For low flow rates, all
regulators were used in series. Capacity limitations
prevented the use of the Honeywell regulators for Reynolds
numbers of 7000 and above, in which case they were by-
passed.

Bulk flow rates were measured with a Model 50 MC
2-2P Meriam Laminar Flow Element. The reading was obtained
directly in scfm on an inclined Meriam Manometer supplied
with the unit. It was then corrected for pressure and

temperature effects. The combination has a stated accuracy of 1/2 of one per cent of reading over the entire 0.2 to 20 scfm range. The temperature immediately downstream of the laminar flow element was measured with a Chromel-Alumel thermocouple. Pressure level was measured with either an 8 inch inclined or 60 inch vertical water manometer.

A filtering system consisting of a Cuno cartridge filter, a silica gel dryer, and a Poro-Stone air filter was an integral part of the existing facility. To check the moisture content of the air, dew point measurements were obtained with an Electro Dryer dew point apparatus attached to the last pressure tap on the test section. The instrument yields a dew point temperature accurate to within ± 3 degrees centigrade.

The wall static pressure taps consisted of 1/16 inch diameter holes in the tube, and 1/8 inch Inconel tube extensions 11-1/2 inches in length. The taps were constructed by machining two concentric holes in the tube wall; a 1/2 inch milled hole approximately 3/4 of the way through the tube, and a 1/16 inch hole drilled through the remainder of the wall. The burrs were cut from the inside of the test section and the pipe was honed. Circular slugs, 1/8 inch in thickness, to which the 1/8 inch Inconel extensions had been welded, were fitted into the 1/2 inch holes and welded to the test section.

Impact Probe Calibration

The impact probe was calibrated in an undisturbed laminar flow stream to determine the viscous effects discussed in the literature survey of Daily and Hardison (27). The probe error was determined by comparison of centerline measurements with the centerline velocity calculated from the measured bulk flow rate. The calibration, supplied by Texas Technological College, is presented in Figure A-3. A maximum overprediction of 0.02 per cent of the velocity is observed for local probe Reynolds numbers greater than 20.

Experimental Procedure

Preliminary Check of Equipment and System

Before data were collected, the experimental apparatus was leak checked and preliminary pressure drop measurements were obtained to check the instrumentation. The test section exit was sealed and the system leak checked under 50 psig pressure with "Snoop" leak detecting fluid. During this phase, all valves on the manifold were open, except those to the micromanometer, and the leads to the Decker transducer were disconnected and plugged. After a few initial leaks were discovered and sealed with U. S. Royal industrial adhesive (epoxy), no further leaks were found by this method. However, the existence of minute leaks, estimated to be of the order of the accuracy of the micromanometer, was indicated by the initial pressure drop
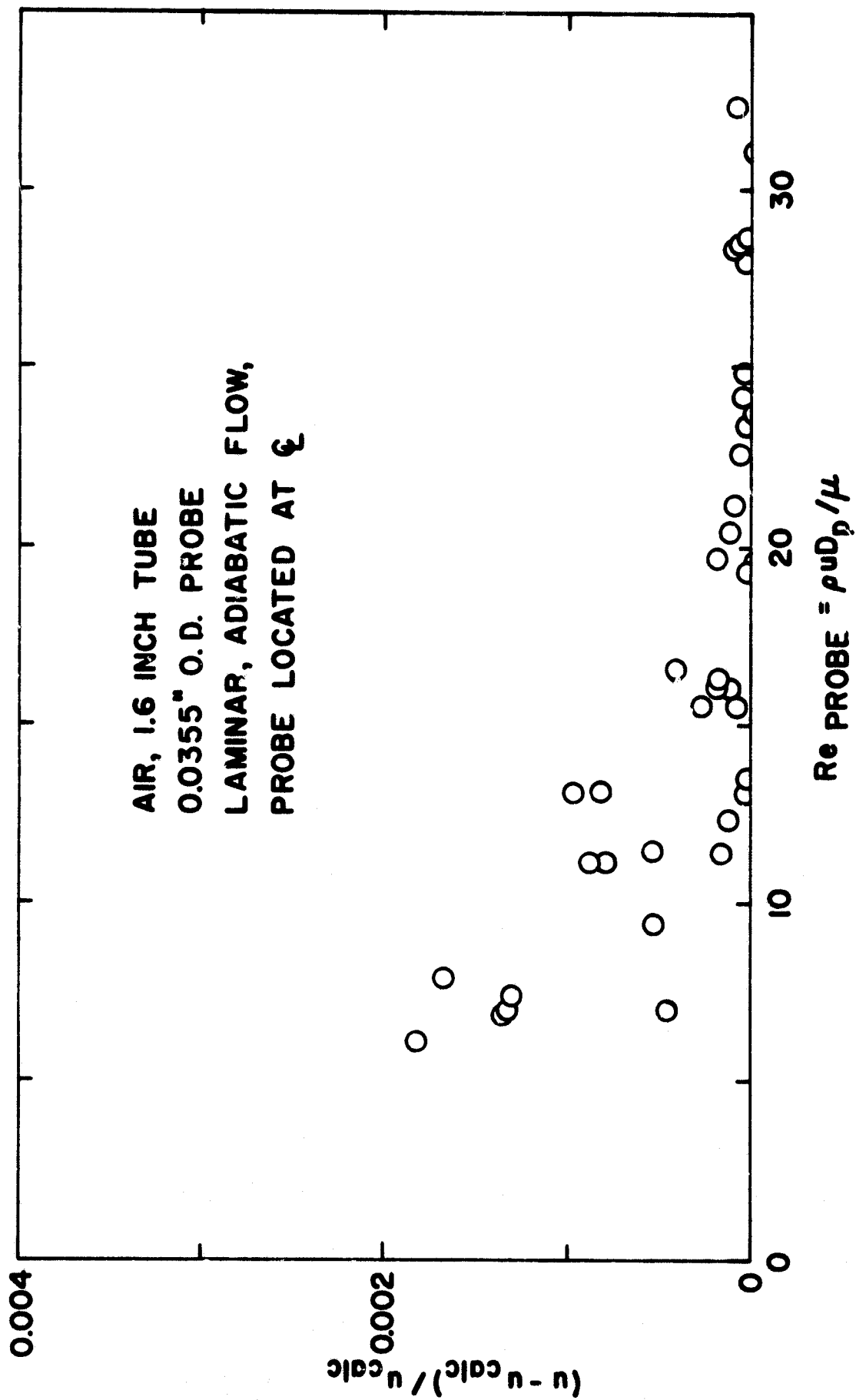
Figure A-3. Probe Calibration

readings taken with flow. The readings obtained were highly erratic on the micromanometer. In such cases, the micromanometer would continuously drift in a given direction. Tightening existing fittings and additional leak checking under pressure proved futile. Discussion with Dr. M. Davenport and Mr. L. Chance of Texas Technological College revealed, that while not mentioned in reference (50), H. Ferrell encountered the same problem. The problem was solved by coating all fittings and unions with paraffin. A systematic application of this technique to the present system eliminated the remaining leaks.

Agreement between the Decker Pressure Transducer and the micromanometer could not be obtained, for identical pressure drop measurements, in the subsequent instrument check out. The transducer proved to be erratic over short, unpredictable intervals, yielding both positive and negative voltage readings. Instead of the stated fifteen minute warm up period, four to five hours sometimes elapsed before the zero balance could be obtained. In some cases, long periods of stability existed during which the output remained steady but differed from the micromanometer. These periods were terminated by instability of the instrument output and an inability to set the zero balance.

An attempt to repair the transducer, following the instructions supplied with the instrument, proved futile. It was observed that, during the null balancing of the

micromanometer, changes in the fluid level of the instrument induced oscillations between the micromanometer and the pressure transducer. It was also observed that the opening and closing of valves on the manifold caused oscillations of the same nature. The transducer output was more sensitive to these oscillations than the micromanometer.

Based on the results of the preliminary adiabatic friction factor measurements, only the micromanometer was used to collect the pressure drop data for this investigation. A separate set of data was also collected with the Decker transducer during one of its periods of relative stability. These data were not used in this work due to the following reasons: (1) disagreement with micromanometer results; (2) an inability to obtain a consistent calibration of the transducer following the procedure originally used by Texas Technological College; and (3) the observed periods of instability discussed above. The data were recorded in data log book number 3, on file with the Energy, Mass and Momentum Transfer Laboratory of the Department of Aerospace and Mechanical Engineering, University of Arizona.

Fluctuating Axial Centerline Velocity Component, u'

The qualitative turbulence measurements consisted of visual observations and chart recordings of the

centerline fluctuating axial velocity component, u', and the measurement of flow rates. All hot wire settings, the zero velocity current, peak-to-peak values of the calibration square wave and chart speeds were also recorded but were not used in the data reduction. Data were collected at two different axial positions for Reynolds numbers of 2000, 2300, 2500, 2700, and 3000. These data were used to establish the limiting Reynolds number for which the flow at the probe was considered fully turbulent. Visual observation of the hot wire output is sufficient to indicate the Reynolds number at which the intermittency factor (17) has a value of one. Moreover, as mentioned previously, superposition of the u' traces on a sine wave of small amplitude and large period preclude quantitative evaluation based on the chart recordings.

The hot wire data were obtained as follows. The hot wire probe and extension arm described in the equipment section were inserted into the test section exit and located at the probe station. The hot wire calibration square wave was then reproduced on the oscilloscope and Sandborn recorder to assure that representation of the hot wire output was being obtained. Following this preliminary step, a desired flow rate was set and the gas temperature and pressure recorded, as described in the next section. The hot wire output was then observed for several minutes on the oscilloscope and the observed flow patterns and

axial positions were indicated in the data book. The hot wire output was then fed into the Sandborn Recorder and a trace of the output obtained on light sensitive recording paper. Without changing the flow settings, the probe was then moved to the second axial position and the observation and recording process repeated. Next, a new flow setting was established and the entire procedure repeated for the two axial positions.

At the completion of the test, the flow was turned off by closing the high capacity flow regulator. The hot wire calibration square wave was then reproduced again on the oscilloscope and Sandborn recorder to assure that the output of the hot wire equipment was still being obtained.

Adiabatic Flow Runs

The adiabatic flow runs consisted of measurements of wall friction factors for three different pressure tap pairs, impact (velocity) probe traverse data, and flow rates. Data were collected at bulk Reynolds numbers of 3020, 4080, 5010, 7030, 10,100, and 15,000. All runs were performed during the evening hours from 7 p.m. to 3 a.m. This procedure was necessitated by the extreme sensitivity of the micromanometer, which was affected by the rapid changes in atmosphere conditions that occurred during the day, as well as by air currents induced by the evaporative cooling system.

The procedure employed for a given flow run was as
follows. Approximately two hours before testing began, the
evaporative cooling system was shut off. At the end of the
two hour period, the air compressor was turned on with all
three of the flow (pressure) regulators, and the main flow
valve closed. When the pressure tanks were filled with
compressed air at 125 psig, the regulators were adjusted to
give the approximate desired flow rate. The barometric
pressure was measured. Based on temperature and pressure
measurements of the flowing gas, the laminar flow element
output necessary to produce the desired Reynolds number
was computed. This output was then set on the laminar flow
element by fine adjustment of the regulators. For low flow
rates (Reynolds numbers below 7000) all three regulators
were used in series. For high flow rates, the two low
capacity regulators were bypassed.

The time was then recorded and the dew point
temperature of the air determined. The level of the
micromanometer was checked with the integral circular
spirit level and adjusted if necessary. The micro-
manometer zero ($\Delta P = 0$) was then determined. Adiabatic
wall friction data were then collected for the three
different wall pressure tap pairs. These data consisted
of the pressure drops obtained by null balance of the
micromanometer, in inches of butyl alcohol, and the alcohol
temperature. For the first and third pressure tap pairs

the laminar flow element output in scfm, the gas temperature and pressure, and the barometric pressure and temperature were also recorded.

The velocity traverse was then initiated. Following a check of the micromanometer zero, the difference between the probe impact pressure and wall static pressure, in inches of butyl alcohol, and the temperature of the alcohol were recorded for a given micrometer reading of the traversing mechanism. A traverse, consisting of 17 to 20 positions, was performed with the probe moving from the wall towards the centerline. Small, radial changes were employed near the wall, increasing in size from approximately 0.01 inches to 0.075 inches in the vicinity of the centerline. Starting with the first probe setting, the laminar flow element output in scfm, gas temperature and pressure, and the barometric pressure and temperature were recorded for approximately every second or fifth probe setting. Due to the high sensitivity of the micromanometer and its null technique of measurement, the flow runs were quite lengthy, averaging from 2-1/2 to 3-1/2 hours per run.

At the conclusion of a traverse, the micromanometer zero was rechecked and the time recorded. If time permitted, a new flow setting was set and the process repeated. Otherwise, the system was shut down. The shut down sequence consisted of placing the micromanometer and laminar flow element off line and opening their bypass

valves. The main flow valve and the regulators in use were then closed, the compressor turned off, and the evaporative cooling system turned back on.

Data Reduction

Fluctuating Axial Centerline Velocity Component, u'

For the hot wire anemometer measurements of the fluctuating axial centerline velocity component, data reduction was not attempted. The traces were examined visually on the oscilloscope to yield a qualitative measurement of the Reynolds number above which fully turbulent flow existed at the measurement station. Representative traces at the probe location, recorded by the Sandborn recorder, are presented in Figure A-4. The decay of the laminar segment observed on the middle trace is probably due to the electronic circuitry. On the Hewlett Packard Oscilloscope, laminar flow appeared as a straight, uniform, smooth line.

Adiabatic Flow Runs

Values for the viscosity, μ, and the compressibility factor, Z, used in the velocity and friction data reduction were taken from Hilsenrath et al. (51). Two way interpolation on pressure and temperature was employed in all cases. Measurement of extremely low dew point
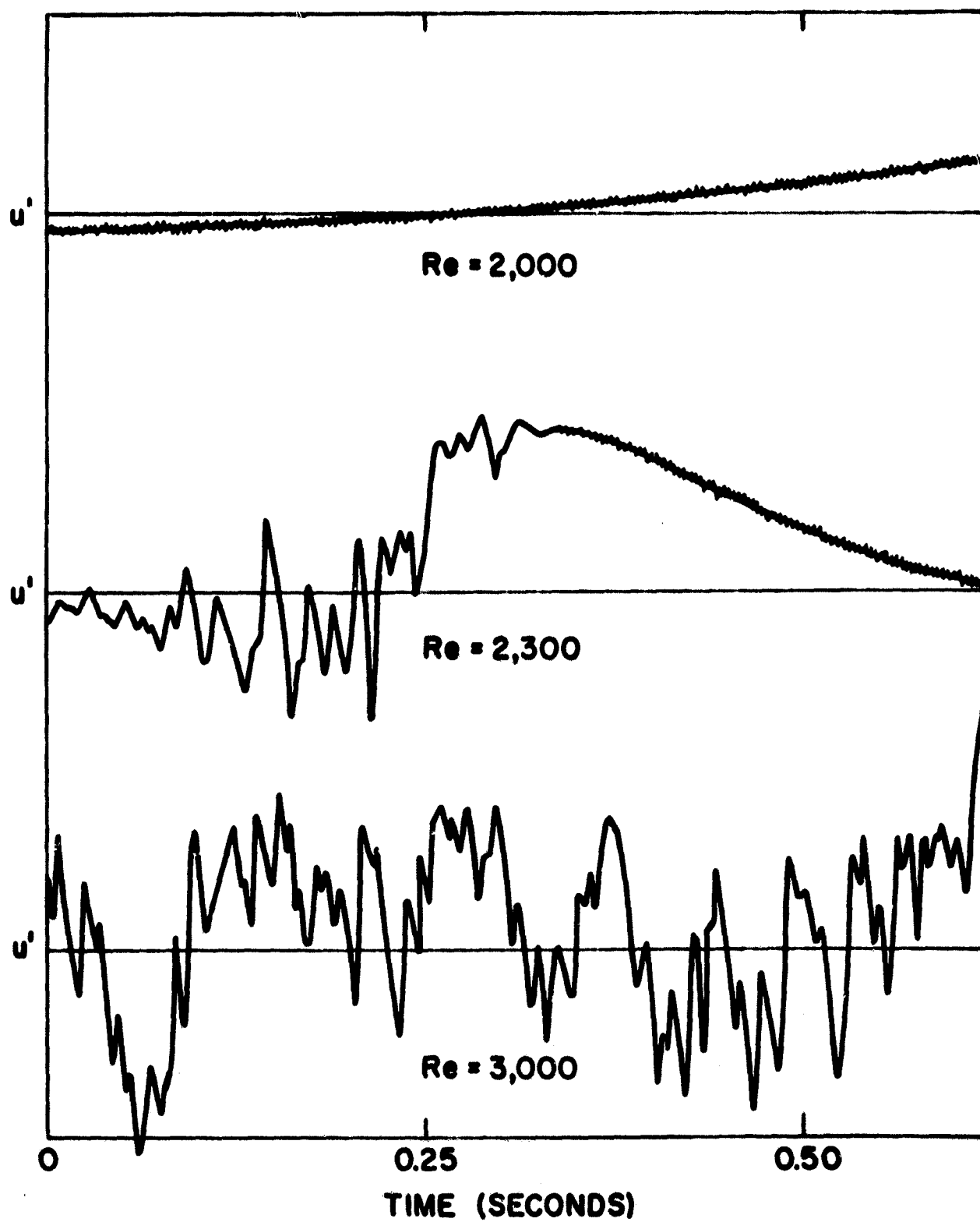
Figure A-4. Representative u' Traces

temperatures, in the vicinity of -48 degrees Fahrenheit for
all tests, justified the use of dry air properties.

The mass flow rate was calculated from the scfm
output of the Meriam Laminar Flow Element, with corrections
for temperature and pressure effects. The density was
calculated from the equation of state, including the
compressibility factor. For the Reynolds number, the
viscosity was evaluated at the gas temperature and pressure.
The wall shear stress was obtained by a force balance
between any two pressure taps with the pressure drop
measured by the micromanometer. The friction factor was
evaluated from the Fanning friction factor expression.

The velocity was calculated from the expression

$$u(y) = \sqrt{\frac{2g_c \Delta P}{\rho}} \qquad (A-1)$$

The pressure drop between the impact probe and its wall
static tap, ΔP, was obtained from micromanometer readings
in inches of butyl alcohol. The alcohol density was
evaluated as a function of temperature from the information
supplied with the micromanometer. An estimation of the
effect of neglecting the contribution of the fluctuating
velocity components in the above equation is included in
the uncertainty analysis, presented in the next section.
The nondimensional velocity, u^+, and distance, y^+, are

$$u^+ = \frac{u(y)}{\sqrt{\tau_w g_c / \rho}}, \quad y^+ = \frac{y\sqrt{\tau_w g_c / \rho}}{\nu} \qquad (A-2)$$

In forming these two groups, the properties were evaluated at the measured gas temperature and pressure. The experimental values of wall shear stress were used.

The local probe Reynolds number was calculated for each probe position from the expression

$$Re_p = \frac{u(r) D_p}{\nu} \qquad (A-3)$$

Corrections from the probe calibration presented in Figure A-2 were unnecessary since the probe Reynolds number always exceeded twenty.

The bulk velocity was determined in two different ways: directly from measurements of the bulk flow rate, and from a graphical integration of the velocity profile, $u(y)$. A comparison of the two values is presented in Appendix C.

Uncertainty Analysis

Important considerations of the uncertainty analysis, which is an estimate of the cumulative effect of individual errors, are presented below. The method employed was that presented by Kline and McClintock (30). The uncertainties in the directly measured quantities are presented in Table A-1. These values were based on consideration of the manufacturer's specifications (where available), the estimated reading error, and experience.

Table A-1.   Velocity Study: Uncertainty Intervals of
            Measured Quantities

Item	Uncertainty
Laminar Flow Element (Flow Rate)	$\pm 1/2\%$ of reading
Micromanometer (Pressure Drop)	± 0.00002 psi
Gas Pressure (above barometric)	± 0.005 in H_2O
Barometric Pressure	± 0.0204 psi
Probe Location (Micrometer)	± 0.0005 inch
Temperature	$\pm 3°F$
Tube Diameter	± 0.001 inch
Distance Between Pressure Taps	± 0.006 inch
Viscosity	± 0.01 lbm/ft sec

The uncertainties in the deduced results are presented with the tabulated results in Appendix B.

Probe "Error" Uncertainties

An estimate of the magnitude of the error caused by neglecting probe corrections was made. As discussed in Daily and Hardison (27), the effect of turbulence on impact probe readings, referred to a datum pressure measured at the wall, is expressed by the relation

$$g_c(P - P_w) = \frac{\overline{\rho_1^2}}{2} + \frac{\overline{\rho_{u'}^2}}{2} + \rho \overline{v'^2} + \rho \int_{r_w}^{r} \frac{\overline{w'^2} - \overline{v'^2}}{r} \, dr \qquad (A-4)$$

The velocity is seen to be

$$u = \sqrt{\frac{2g_c(P - P_w)}{\rho} + C} \qquad (A-5)$$

where

$$C = -\overline{u'^2} - 2\overline{v'^2} - 2 \int_{r_w}^{r} \frac{\overline{w'^2} - \overline{v'^2}}{r} \, dr \qquad (A-6)$$

A common procedure, employed by Laufer (52) and others who have made probe corrections, has been to neglect the turbulence effect on the wall static probe (the last two terms) in using the above correction. Complete neglect of correction C is equivalent to introducing a maximum error, W_c, in u

$$W_c = \sqrt{\frac{2g_c \Delta P}{\rho} + C} - \sqrt{\frac{2g_c \Delta P}{\rho}} \tag{A-7}$$

or, conversely, a maximum percentage error in u of

$$\frac{W_c}{u} = \sqrt{1 + \frac{C}{\frac{2g_c \Delta P}{\rho}}} - 1 \tag{A-8}$$

This error is now treated as an effective uncertainty in the velocity. The total uncertainty in the velocity becomes

$$\frac{W_u}{u} = \left[\left(\frac{1}{2} \frac{W_{\Delta P}}{\Delta P}\right)^2 + \left(\frac{1}{2} \frac{W_P}{P}\right)^2 + \left(\frac{1}{2} \frac{W_T}{T}\right)^2 + \left(\frac{W_c}{u}\right)^2 \right]^{1/2} \tag{A-9}$$

To estimate the importance of $\frac{W_c}{u}$, a logarithmic extrapolation of C was performed. Sandborn's (26) normalized turbulence measurements, obtained at Reynolds numbers of 25,000 and 50,000, were used in this evaluation of the correction term. In Table A-2 values of $\frac{W_c}{u}$ are compared with the sum of the other three uncertainty terms for a Reynolds number of 4080. The other terms dominate. Subsequently, this term was neglected in estimating the uncertainty of the velocity.

Effective Center Displacement Effect

Insertion of a finite probe into a shear flow, or flow near a boundary, causes an "effective center displacement" of the probe. In effect, the probe may be considered to measure the stagnation pressure of a

Table A-2.   Importance of Turbulence Velocity Correction

y/r_w	y^+	Re = 4080 Term $(\frac{W_c}{u})^2$	All other terms, equation A-9
0.0472	.744	1.42	11.91
0.1093	15.61	0.307	6.64
0.2335	33.36	0.0984	3.61

streamline which is shifted from its upstream course due to the presence of the probe. Normally the displacement of the streamline has been considered as away from the wall. Thus, the velocity measured by the probe is closer to the wall than the location of the probe centerline. However, streamline displacements toward the wall have been reported (27). No comprehensive data are available upon which to base a correction (27). To estimate the possible error caused by this effect, Fage (29) analytically extended experimental results obtained by Young and Maas (see 27). In the present work the effective center displacement, Δ, given by Fage's expressions,

$$\Delta = 90(0.131 + 0.08 \cdot d_i/d_o)y(\frac{d_o}{r_w})^2 \qquad 0 \leq y/r_w \leq 0.15$$

and
$$(A-10)$$

$$\Delta = 16(0.131 + 0.082 \, d_i/d_o)(r_w - y)(\frac{d_o}{r_w})^2 \qquad 0.15 \leq y/r_w \leq 1$$

was considered as one of the errors in the probe position. Thus, the total uncertainty in the position of the velocity was evaluated from

$$\frac{W_y}{y} = \sqrt{(\frac{W_{ym}}{y})^2 + (\frac{\Delta}{y})^2}$$

where W_{ym} is the uncertainty interval of the probe micrometer positioning mechanism.

Effect of Slot in Tube Wall

In the vicinity of the wall a large discrepancy is observed between the velocity data and accepted viscous profiles. The uncertainty analysis is completely unable to account for this divergence, which is believed to be caused by the small rectangular slot milled in the tube wall to accommodate the probe traversing mechanism. The width of the slot is approximately 1 per cent of the tube circumference. It could cause changes in the turbulence level and/or an effect comparable to the effective center displacement.

Haugen and Dhanak (31) have presented experimental velocity profiles for boundary layer flow over rectangular slots, at estimated boundary layer Reynolds numbers of 12,900, 38,600, and 64,000. An attempt was made to predict the y^+ values at which disagreement between these profiles (presented in graphical form) and Spalding's law of the wall profile (53) would first occur. Agreement was found for the smallest distance from the wall which could be accurately plotted on the graphs. Unfortunately, the distance represented a sizeable y^+ value (approximately 60), and a comparison near the wall was not possible. Consequently, the results only indicate a point at which the effect of the slot is known to be negligible. The ratio of this distance over the boundary layer thickness was plotted against the boundary layer Reynolds number, for

each of the three values above, on logarithmic coordinates.
Extrapolation to the Reynolds numbers of the present study
yielded a value of y^+ of approximately forty for all of the
tests.

From a qualitative examination of the present data,
it appears the slot effect is no longer felt beyond y/r_w
ranging from approximately 0.09 to 0.05 (y^+ = 9.7 to 21.8),
corresponding to the lowest and highest flow rates of the
present study. This range of y/r_w represents the locations
at which agreement between the velocity data and accepted
viscous profiles (where appropriate) and/or strong changes
in slope, du^+/dy^+, are first observed. As indicated
previously, the effect can be conservatively considered
negligible by y^+ = 40.

Errors Due to Selection of Wall Shear Stress

The values calculated for y^+ and u^+ are directly
dependent on the expression or method utilized to evaluate
the wall shear stress since it appears in the shear velocity

$$u^* = \sqrt{\frac{g_c \mathcal{T}_w}{\rho}} \qquad (A-12)$$

used in their definitions. Two approaches have been taken
to this problem: (a) use of an analytical expression for
the friction factor, or (b) evaluation of $\mathcal{T}_w$ from experi-
mental data taken during the velocity investigation.
Senecal (4) employed a friction factor evaluated from

Blasius' expression. The second alternative was used in the present study, but, when reduced by both methods, the resulting values of u* show a difference of only 0.5 per cent. At low Reynolds numbers this difference may exist in comparisons between the present formulation and the McEligot, Ormand and Perkins profile (9), which was based on Senecal's data.

APPENDIX B

EXPERIMENTAL EDDY DIFFUSIVITY VALUES

Values of the eddy diffusivity determined from the present velocity profile data (via equation B-1 below) are presented in Figure B-1. These profiles were employed as an aid in the selection of the values of y_1^+ and $\mathcal{K}$ which appear in equation 3-5. The method of formulation and subsequent use of these values are discussed in the section, Semi-empirical Profile.

Eddy diffusivity distributions predicted from the combined form of Reichardt's wall and center laws (24), with his original values for y_1^+ and $\mathcal{K}$, are presented for Reynolds numbers of 3020 and 15,000 in the figure.

It is observed that the experimental values tend to fall towards negative values for values of y/r_w in excess of 0.6. This drop is a direct consequence of the inability to obtain accurate experimental results for the eddy diffusivity from the defining equation

$$\frac{\epsilon_m}{\mathcal{U}} = \frac{(1 - y^+/y_{\mathfrak{q}}^+)}{\dfrac{du^+}{dy^+}} - 1 \qquad (B-1)$$

which was used to obtain $\dfrac{\epsilon_m}{\mathcal{U}}$ from the velocity data. Analytically, this expression tends to an indeterminate
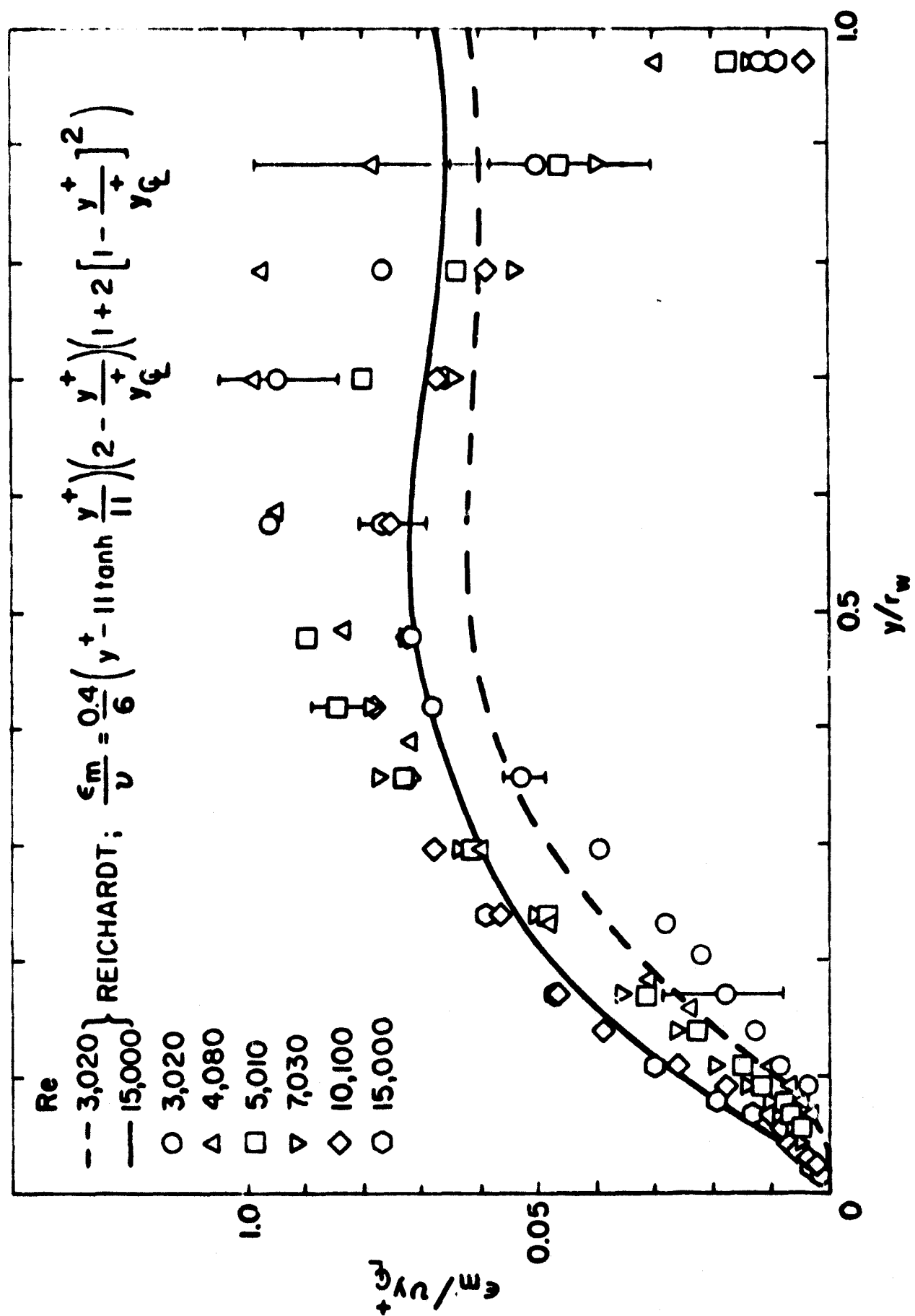
Figure B-1. Experimental Eddy Diffusivity Results

form as the centerline is approached. However, in data reduction the percentage uncertainty in du^+/dy^+ becomes large despite precise velocity determination a zero value of the slope is seldom obtained. Accurate experimental values of the eddy diffusivity in the vicinity of the centerline have been determined from hot wire turbulence measurements by several investigators (32). These yield a finite value of $\dfrac{\epsilon_m}{\upsilon y_{\mathcal{C}}^+}$ at the centerline of approximately 0.07 rather than the steep drop observed in Figure B-1.

The values shown for $\dfrac{y}{r_w}$ less than 0.1 are probably of little use due to the errors in the velocity near the wall, as discussed earlier. Conservatively, the most valid data thus fall in the region $0.2 \gtrsim \dfrac{y}{r_w} \gtrsim 0.7$.

APPENDIX C

ADIABATIC BULK VELOCITY COMPARISON

As an overall check on the experimental velocity profiles, the bulk velocity was determined by graphical integration of the velocity data. The integral appearing in the definition of the bulk velocity was determined by plotting the profile and evaluating the area with a planimeter. In Table C-1 the results are compared with values of bulk velocity determined from the measured mass flow rate. The approximate "percentage over estimation" of the bulk velocity, obtained in the integration, due to the effective center displacement effect is also included. This estimation was obtained using Fage's expression (29),

$$\frac{V_{b_{correct}} - V_b}{V_b} = 190 \frac{g_c \mathcal{T}_w}{\rho V_b^2} + 190 \left(\frac{d_o}{r_w}\right)^2 + 120 \frac{d_i d_o}{r_w^2} \qquad (C-1)$$

However, Fage's formulation was not based on comprehensive data (27) and must be considered only as an indication of the error in bulk velocity obtained by integration. More-over, since both positive and negative effective center displacements have been reported, this approximation probably should be considered as representing a possible

103

Table C-1. Comparison of Bulk Velocity Calculations

Re	V_{bi} integration ft/sec	V_{bm} measured ft/sec	% difference $\dfrac{V_{bi} - V_{bm}}{V_{bi}}$	% "overestimation" in V_b integration (Fage)
3,020	4.53	4.37	+3.53	±1.41
4,080	5.85	5.83	+0.342	±1.34
5,010	6.97	7.03	-0.86	±1.305
7,030	9.55	9.65	-1.04	±1.24
10,100	13.99	14.19	-1.43	±1.16
15,000	19.99	20.41	-2.10	±1.08

bound on the error in the bulk velocity without regard to direction.

APPENDIX D

TABULATED VELOCITY DATA AND UNCERTAINTIES

Adiabatic Velocity Data: Air

Run 1 Re = 4077

$$f = 0.00982, \ 0.00929, \ 0.01052$$

x/D range 234-251, 247-264, 259-275

$$T_{av} = 88°F, \ P_{av} = 27.015 \text{ in Hg. abs.}$$

y inches	u ft/sec	y^+	u^+	$(\delta y^+)/y^+$ % uncertainty	$(\delta u^+)/u^+$ % uncertainty
0.004	2.026	0.710	4.957	13.0	34.6
0.012	2.219	2.130	5.430	5.5	28.9
0.028	2.718	4.969	6.651	4.1	19.3
0.038	3.450	6.744	8.442	3.9	12.2
0.044	3.624	7.809	8.868	3.8	11.1
0.053	3.680	9.406	9.005	3.8	10.7
0.063	3.949	11.181	9.663	3.7	9.4
0.073	4.201	12.956	10.279	3.7	8.4
0.088	4.620	15.618	11.304	3.7	7.1
0.129	5.695	22.894	13.933	3.6	5.0
0.148	5.907	26.266	14.453	3.3	4.7
0.188	6.277	33.365	15.359	3.0	4.3
0.238	6.502	42.239	15.909	2.9	4.1
0.313	6.841	55.550	16.737	2.7	3.9
0.391	7.048	69.393	17.244	2.7	3.7
0.471	7.361	83.591	18.010	2.7	3.6
0.563	7.581	99.918	18.548	2.6	3.5
0.638	7.635	113.229	18.680	2.6	3.4
0.713	7.662	126.539	18.746	2.6	3.4
0.788	7.688	139.850	18.811	2.6	3.4

Adiabatic Velocity Data: Air

Run 2   Re = 3017

f = 0.01216, 0.01056, 0.01031

x/D range = 234-251, 247-264, 259-275

T_{av} = 91.4°F, P_{av} = 26.970 in Hg. abs.

y inches	u ft/sec	y^+	u^+	$(\delta y^+)/y^+$ % uncertainty	$(\delta u^+)/u^+$ % uncertainty
0.013	2.131	1.770	6.712	6.2	31.7
0.028	2.649	3.813	8.344	5.2	20.7
0.038	2.726	5.175	8.586	5.1	19.6
0.044	2.801	5.992	8.821	5.0	18.7
0.053	2.944	7.217	9.274	5.0	17.0
0.063	3.014	8.579	9.492	4.9	16.2
0.073	3.276	9.941	10.319	4.9	13.9
0.088	3.577	11.984	11.268	4.9	11.9
0.113	3.908	15.388	12.310	4.9	10.2
0.138	4.310	18.793	13.576	4.7	8.7
0.163	4.678	22.197	14.733	4.5	7.7
0.188	4.851	25.602	15.279	4.4	7.3
0.238	5.140	32.410	16.190	4.3	6.7
0.288	5.376	39.219	16.932	4.2	6.4
0.338	5.638	46.028	17.758	4.2	6.0
0.388	5.711	52.837	17.988	4.2	5.9
0.463	5.854	63.051	18.437	4.2	5.8
0.563	5.924	76.668	18.658	4.2	5.7
0.638	6.028	86.882	18.985	4.2	5.6
0.713	6.130	97.095	19.305	4.2	5.5
0.788	6.163	107.309	19.411	4.2	5.5

Adiabatic Velocity Data: Air

Run 3   Re = 10070

f = 0.00780, 0.00783, 0.00774

x/D range = 234-251, 247-264, 259-275

T_{av} = 87.7°F, P_{av} = 27.400 in Hg. abs.

y inches	u ft/sec	y^+	u^+	$(\delta y^+)/y^+$ % uncertainty	$(\delta u^+)/u^+$ % uncertainty
0.013	1.680	5.087	1.893	4.8	49.5
0.020	5.538	7.827	6.238	3.8	4.6
0.028	6.812	10.957	7.673	3.3	3.1
0.033	8.085	12.914	9.107	3.2	2.2
0.038	8.307	14.871	9.356	3.1	2.1
0.044	9.655	17.219	10.875	3.0	1.6
0.053	10.144	20.741	11.426	3.0	1.5
0.063	10.892	24.654	12.268	2.9	1.3
0.073	12.002	28.567	13.519	2.9	1.1
0.088	12.399	34.437	13.966	2.9	1.0
0.113	12.972	44.221	14.611	2.8	1.0
0.138	13.565	54.004	15.279	2.5	0.9
0.188	14.261	73.571	16.063	1.9	0.9
0.238	14.679	93.138	16.534	1.6	0.8
0.288	15.232	112.704	17.157	1.4	0.8
0.388	16.307	151.838	18.368	1.3	0.7
0.463	16.722	181.188	18.836	1.2	0.7
0.563	17.292	220.321	19.477	1.2	0.7
0.638	17.821	249.671	20.073	1.2	0.7
0.713	17.933	279.021	20.200	1.2	0.7
0.788	17.990	308.371	20.263	1.2	0.7

Adiabatic Velocity Data: Air

Run 4   Re = 5010

f = 0.00927, 0.00964, erratic

x/D range = 234-251, 247-264, 259-275

T_{av} = 81.63°F, P_{av} = 26.979 in Hg. abs.

y inches	u ft/sec	y^+	u^+	$(\delta y^+)/y^+$ % uncertainty	$(\delta u^+)/u^+$ % uncertainty
0.013	1.105	2.754	2.310	5.0	114.9
0.038	2.707	8.051	5.658	3.5	19.2
0.044	3.552	9.322	7.425	3.5	11.3
0.053	3.933	11.229	8.221	3.4	9.2
0.063	4.420	13.348	9.239	3.4	7.4
0.073	5.525	15.467	11.549	3.3	4.9
0.088	5.882	18.645	12.295	3.3	4.4
0.113	6.444	23.942	13.468	3.3	3.8
0.138	6.931	29.239	14.486	3.0	3.4
0.188	7.386	39.832	15.437	2.5	3.1
0.238	7.709	50.426	16.113	2.3	2.9
0.288	7.943	61.020	16.603	2.2	2.8
0.388	8.319	82.207	17.387	2.1	2.7
0.463	8.560	98.098	17.891	2.1	2.6
0.563	8.841	119.286	18.478	2.0	2.5
0.638	8.955	135.176	18.717	2.0	2.5
0.713	9.091	151.067	19.000	2.0	2.4
0.788	9.135	166.957	19.094	2.0	2.4

Adiabatic Velocity Data: Air

Run 5   Re = 7025

f = 0.00849, 0.00855, 0.00845

x/D range = 234-251, 247-264, 259-275

T_{av} = 79.75 , P_{av} = 27.107 in Hg. abs.

y inches	u ft/sec	y^+	u^+	$(\delta y^+)/y^+$ % uncertainty	$(\delta u^+)/u^+$ % uncertainty
0.013	1.270	3.708	1.994	4.8	86.2
0.038	4.538	10.840	7.119	3.2	6.8
0.044	5.927	12.551	9.298	3.1	4.1
0.053	6.226	15.119	9.767	3.1	3.7
0.063	6.989	17.971	10.966	3.0	3.0
0.073	7.860	20.824	12.331	3.0	2.5
0.88	8.236	25.103	12.921	3.0	2.3
0.113	8.896	32.234	13.956	2.9	2.0
0.138	9.339	39.366	14.651	2.6	1.9
0.188	9.986	53.629	15.667	2.1	1.7
0.238	10.285	67.892	16.136	1.8	1.6
0.288	10.840	82.155	17.006	1.7	1.5
0.388	11.242	110.681	17.637	1.5	1.5
0.463	11.613	132.075	18.219	1.5	1.4
0.563	12.106	160.601	18.993	1.4	1.4
0.638	12.239	181.996	19.201	1.4	1.4
0.713	12.419	203.390	19.484	1.4	1.3
0.788	12.565	224.784	19.712	1.4	1.3

Adiabatic Velocity Data: Air

Run 6   Re = 15031

f = 0.00706, 0.00704, erratic

x/D range = 234-251, 247-264, 259-275

T_{av} = 78.50°F, P_{av} = 27.574 in Hg. abs.

y inches	u ft/sec	y^+	u^+	$(\delta y^+)/y^+$ % uncertainty	$(\delta u^+)/u^+$ % uncertainty
0.013	4.361	7.210	3.595	4.7	7.2
0.018	6.480	9.983	5.342	3.9	3.3
0.023	8.902	12.756	7.338	3.5	1.7
0.028	10.645	15.529	8.775	3.3	1.2
0.033	11.876	18.302	9.790	3.2	1.0
0.038	13.143	21.075	10.834	3.1	0.8
0.044	14.962	24.403	12.334	3.0	0.7
0.053	15.483	29.394	12.763	2.9	0.6
0.063	16.317	34.940	13.451	2.9	0.6
0.088	17.948	48.805	14.795	2.8	0.5
0.138	19.237	76.535	15.858	2.5	0.5
0.188	20.309	104.266	16.741	1.9	0.4
0.238	21.131	131.996	17.419	1.5	0.4
0.388	23.102	215.187	19.044	1.2	0.4
0.463	23.795	256.782	19.615	1.1	0.4
0.563	24.878	312.243	20.507	1.1	0.4
0.638	25.241	353.838	20.807	1.1	0.4
0.788	25.770	437.029	21.242	1.1	0.4

APPENDIX E

DETAILS OF EXPERIMENTAL HEAT TRANSFER MEASUREMENTS

Experimental Apparatus

The experimental gas loop is shown schematically in Figure E-1. The gas supply consisted of four large commercial compressed gas cylinders. The test gas was reduced to operating pressures by the two pressure regulators and flowed through the primary and secondary flow meters to the inlet mixer where its bulk temperature was measured. It then passed through the vertical, resistively heated, circular test section and entered a shell and tube heat exchanger where the hot gas was cooled. It was exhausted through the downstream control valves to the atmosphere. Measurements of the test section pressure, overall pressure drop, wall temperature profile, and approximate exit bulk temperature were obtained. The test section was enclosed in a vacuum chamber to reduce the heat loss and allow localized heat loss calibration. The vacuum reduced the time necessary to reach equilibrium with heating.
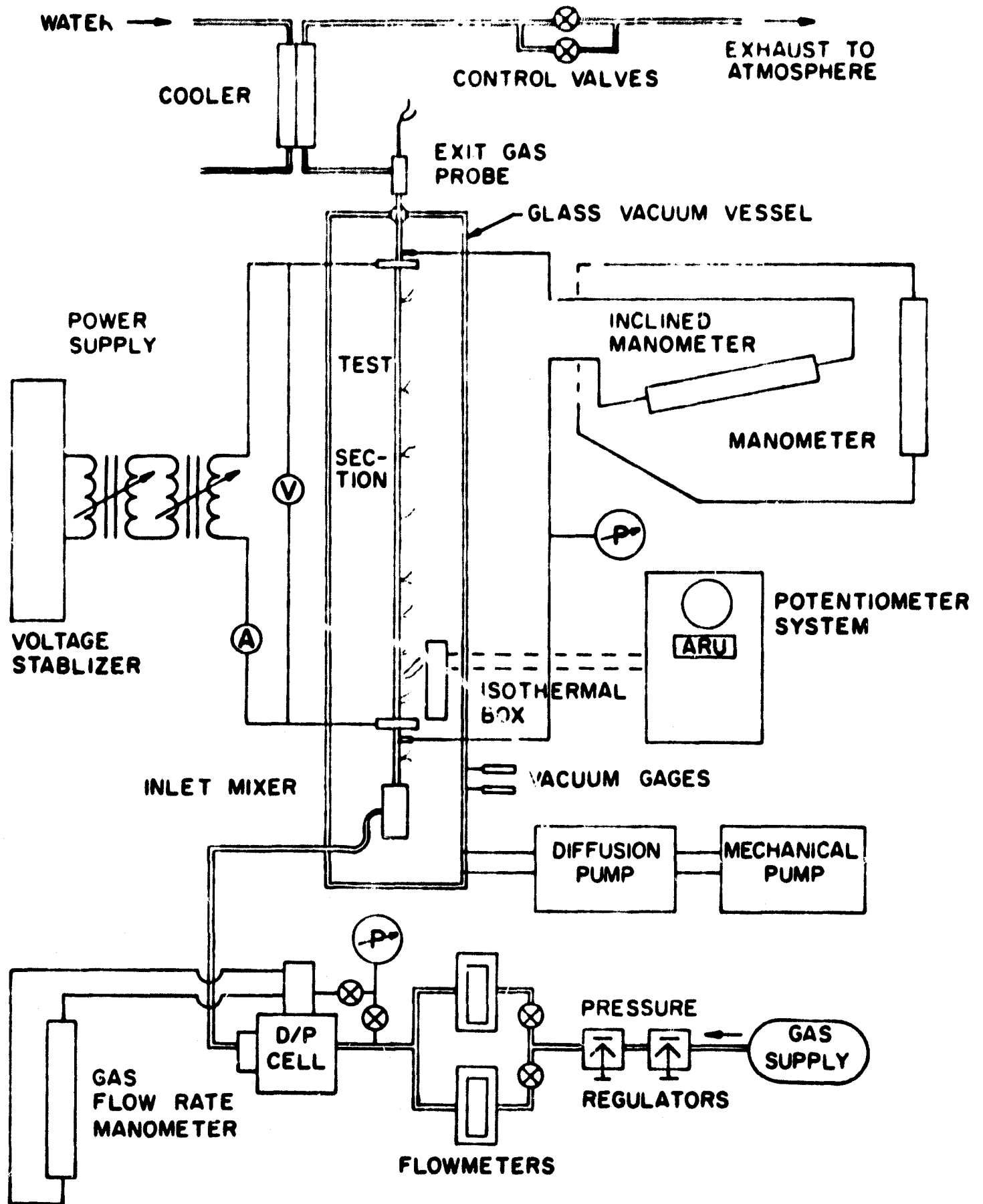
Figure E-1. Heat Transfer Apparatus

Test Section and Vacuum Chamber

General Details

The test section was fabricated from a 0.250 OD
Inconel tube with a 0.010 inch wall. The exit end was
brazed to a 3/8 inch thick wall stainless steel tube
approximately 10 inches in length. The entire section was
hung from a vertical stainless steel flange, by means of a
Conax fitting, inside a 6 foot long, 6 inch diameter glass
vacuum chamber. The glass cylinder was located on top of a
large glass cross of equal diameter, the three free arms of
which were sealed by stainless steel flanges. A flexible
5/8 inch OD high pressure hose was used to connect the
test section inlet to a fitting, welded to one of the
flanges. The flexible hose allowed the test section to
expand under its own weight when heated. Vertical align-
ment of the test section was ensured by Teflon and
plexiglass guides in unheated regions.

Particulars of the test section are presented in
Table E-1. Thermocouples of 36 gage (0.005 inch) Chromel-
Alumel wire were spot welded to the test section using a
Weldmatic Model 1015-C Capacitor-Discharge spot welder.
Twenty gage (0.0321 inch) thermocouple wire was used
between the fine wires and the two isothermal junction
boxes, where a conversion to copper wire was made. The
isothermal box for thermocouples 1 through 13 and the inlet

Table E-1.   Test Section Information*

Material	Inconel 600
Inside diameter	0.2302
Outside diameter	0.2502
Hydrodynamic entrance length	23.0
Heated length	25.0068
Pressure tap holes	0.040

Item No. Location		Item No. Location	

Location of pressure taps

1	-1.6862	2	27.2068

Wall Thermocouple locations

1	-3.3051	9	5.9620
2	-2.1798	10	7.9610
3	-0.5962	11	11.9612
4	0.0 (L. E.)	12	19.9498
5	0.2781	13	22.0068
6	0.9387	14	25.0068 (U. E.)
7	1.8718	15	25.5010
8	3.6996	16	26.6905

(L. E. = Lower Electrode, U. E. = Upper Electrode)

Glass thermocouple locations with reference to lower electrode

1	30.2568	4	1.2568
2	22.0068	5	-9.7432
3	12.2568		

*All dimensions in inches.

bulk temperature was located inside the vacuum chamber.
Its isothermal reference temperature was given by a
precision mercury-in-glass thermometer. For all other
thermocouples, the reference junction was an ice bath.

Test Section Diameter

The transverse dimensions of the test section were
measured by several different means, using tubing obtained
from the same mill run. Results are presented in Table E-2.
Values chosen for the ID and OD were 0.2302 and 0.2502
inches.

Instrumentation and Equipment

The supply gas pressure was reduced to the desired
operating pressures by means of a two stage Victor regulator,
Model VTS 431-250, and a Wilkerson Model 2001-4 pressure
regulator, connected in series. The flow rate was measured
by a Brooks Model 1112 A Variable area flowmeter (helium),
or a Brooks Model 150 Sho-Rate flowmeter (air), with stated
accuracy of ±1 per cent of full scale reading. A Foxboro
Model 13-A differential pressure transmitter, with integral
orfices, served as a secondary check.

The thermocouple signals were fed to a Honeywell
Electronik 18 self balancing indicating potentiometer
through an adjustable range unit. The Electronik 18,
calibrated by Honeywell, has an accuracy of ±0.25 per cent
of span (5mv) and the range unit has an accuracy of ±0.1

Table E-2. Measurements of Tube Dimensions

Test	Instruments	ID inches	WALL inches	OD inches
1	Starret micrometer & small hole gage (Average--5 readings)	0.2302	--	0.25007
2	Millers Falls micrometer & small hole gage	0.230	--	0.250
3	Craftsman #40161-DJ helio vernier calipers	0.228	0.011	0.250
4	Pratt and Whitney electrolimit gage	--	--	0.252(max) 0.2507(min)
5	Unitron Model MEC inverted stage metallurgical microscope	0.23043	0.010250	0.24888

Tests 2, 3, and 4 used the same sample.

per cent of scale suppression. The accuracy of this
combination is greater than the accuracy of the thermo-
couples used. Premium grade Chromel-Alumel thermocouple
wire, accurate to $\pm 2°F$ below 530°F and ± 0.375 per cent of
reading above 530°F, was used throughout the system. The
test section thermocouples were spot welded to the outside
of the test section; those located on the heated length
were calibrated in place for thermocouple conduction error
as described in the section--Experimental Procedure. The
entering gas bulk temperature was measured in an inlet gas
mixer. A mercury-in-glass NBS Certified Bomb Calorimeter
thermometer, with a least scale division of 0.05°F, was
used to measure the temperature of the isothermal junction
box located inside the vacuum chamber.

The pressure drop was measured either on a Meriam
Model 34FB2 Micromanometer, on a 10 inch inclined manometer,
or on a 60 inch water manometer. These instruments were
accurate to about 0.001, 0.01, and 0.05 inches, respec-
tively. For the heating runs, which were at "high"
pressures, the micromanometer was not employed and the test
section and flow meter pressure levels were measured on a
150 psi Heise gage, accurate to 0.15 psi. For some
preliminary adiabatic runs either a water manometer or a
mercury manometer was used to measure the pressure levels.
A Welch Model 1215 mercurial barometer was used to measure

the atmospheric pressure, which was corrected for temperature and local gravity effects.

The test section voltage drop was measured with a Weston Model 341 Voltmeter, accurate to 0.25 per cent of full scale. (For the air data a Fluke Model 883A AC/DC Null Voltmeter, with uncertainty of $\pm$0.1 per cent of reading, was used.) The voltage measurements provided a check of the overall test section resistance and the local energy generation. The current was measured with a Weston Model 370 Ammeter and Weston Model 327-Type 2 Current Transformer. The ammeter and current transformer have a combined uncertainty of about 0.25 per cent of full scale. These voltmeters and the ammeter were used in the calibration for the test section resistance. The calibration is discussed in Chapter VII.

Power for the electrical heating was provided by a surplus 3KVA GE Model 61C-75 transformer. The 110 V, 60 cycle AC input of the transformer was stabilized to within $\pm$0.01 per cent by a Sorenson Model 250-1 voltage regulator. The input current was controlled by an Ohmite Model VT 20 NB Variable Transformer. Above approximately 80 amperes a Lincoln Model TM-500 AC/DC welder was used in place of the above power supply package.

The vacuum pumps, which maintained the system below 1.5×10^{-5} torr, consisted of a 2 inch Consolidated Vacuum Corporation Model PMC-115 diffusion pump and a Welch

Duo-Seal Model 1402B mechanical pump. Vacuum pressures
were measured with either a Pirani gage tube and a
Consolidated Vacuum Corporation Type GP-140 indicator, or a
General Vacuum Industries Model 700 cold cathode vacuum
gage.

Experimental Procedure

Preliminary Tests and Calibrations

Before collection of the heat transfer data was
undertaken, preliminary tests and calibrations, designed to
increase the accuracy of the data and to assure correct
operation of the equipment, were performed. These tests
are described below.

Leak checks. Leaks in the flow system were detected
by pressurizing the system to 100 psig with helium and
coating all fittings with a soap solution. The system was
considered leak tight when no observable change in the
Heise pressure gages could be detected over a span of
several hours. Leaks in the manometers were detected by
isolating 100 psig on each leg of the manometer and
observing if any change in the fluid column occurred with
time. The micromanometer was checked at approximately
15 psig due to pressure limitations of the instrument.
This process was repeated several times during the course
of the investigation to insure system integrity. Pressure
level manometers were only checked once (at the beginning

of the testing) since the atmospheric side had to be connected into the flow system in order to provide a means of subjecting both sides of the fluid column to an equal pressure.

A continuous check of the vacuum system pressure was provided by the vacuum gages present in the system.

Differential pressure cell calibration. The Foxboro integral orifice, differential pressure cell was used as a secondary check of the primary flow measurement instruments. The 0.034 and 0.0595 inch Foxboro orifices were calibrated by measuring the discharge of nitrogen from a cylinder of known volume. The procedure employed was essentially the same as that used by Magee (54) except the cylinder, fabricated from a standard compressed gas bottle, was not immersed in an isothermal bath. A long pressure tap and a Chromel-Alumel thermocouple were placed inside the cylinder through a cylindrical steel plug located at the top of the bottle. The time history of conditions in the cylinder, of conditions at the outlet of the orifice, and of the D.P. cell output during the blow-down allowed the orifice constant to be determined by numerical integration. An empirical expression for the net orifice expansion factor, obtained from the ASME study of fluid meters (55), was included in the data reduction. The results differed from the factory supplied calibration curves by a maximum of 4 per cent, for the smaller orifice.

The orifice constant for the 0.0995 orifice, used in the two highest Reynolds number runs, was determined from the factory calibration; limited capacity of the cylinder prohibited blow down runs of any reasonable time duration for this orifice.

Thermocouple conduction error. A thermocouple attached to a heated surface changes the heat loss at the point of attachment, due to conduction along the wires. Local surface temperature is thus reduced. To provide a correction for this effect, the thermocouples were calibrated in place for a number of different power levels without fluid flow with a procedure comparable to the preliminary study of Hess (48). A ceramic thermocouple probe was inserted through the exit of the test section. The conduction error was estimated by obtaining the inside tube wall temperature at several locations, far enough removed from the wall thermocouple to be uneffected by the thermocouple attachment. The wall temperature that would have existed at the wall thermocouple location if it were not present was predicted from a curve fit[1] of the probe temperatures. Correction of this value for the temperature drop through the wall yielded an estimated "undisturbed," outside wall temperature which was then compared with the value measured by the thermocouple welded there. The

_____

1. Procedure FIT, reference 49.

ceramic probe was located by means of an external scale and reference positions marked on the probe. The zero reference was obtained by null balance of a DC voltage signal between the probe tip and a wall thermocouple located in the unheated region above the upper electrode. An estimate of the thermal expansion of the tube was included in the calculation of position. The maximum error in the location due to the difference in the thermal expansion of the two different materials was estimated to be less than 0.048 inches at 800°F. The correction obtained was expressed as a linear function of the wall temperature.

Heat loss calibration. Data for the heat loss calibration were collected simultaneously with the thermocouple conduction calibration data. In addition to the probe and test section wall temperatures, the current, voltage, vacuum pressure, and the temperature distribution along the glass vacuum vessel were recorded with each probe reading.

The procedure for evaluating the heat loss was developed and was programmed by A. F. Deardorff. Local radiation heat loss was determined by subtracting the local energy loss due to axial conduction from the average resistive heating. The points were referenced to 1/4 inch intervals on the unexpanded tube and were corrected for expansion when heated. Small cylindrical, isothermal elements were considered to be located at these points.

Each element was assumed to be surrounded by a 6 inch
diameter cylinder centered on the point and divided into
seven equal isothermal elements. A radiation network
describing diffuse energy radiation from each inner element
i was constructed and solved by electrical analogy (56).
The element i was considered as a small gray body in a
large enclosure. The resulting expression for the radiated
heat flux,

$$q''_{r,i} = e_i(T_{iw})(T^4_{iw} - \sum_{n=1}^{8} F_{in}T^4_n) \tag{E-1}$$

was then used to evaluate the emissivity. For several
different power settings, the emissivity data at each
location, i, were correlated with a straight line least
squares fit.

Geometric view factors, F_{in}, from the inner element
to the seven outer isothermal glass elements, were
evaluated from the defining expression for view factors
(56). A numerical solution generated and programmed by
Mills (57), for evaluation of view factors in a non-
isothermal annulus, was used to obtain these values. The
angles in the definition for the view factor were evaluated
using vector algebra. The view factors for the two end
disks, at assumed constant temperatures of 530°R, were
evaluated using flux algebra,

$$F_{i8} = 1 - \sum_{n=1}^{7} F_{in} \qquad (E.2)$$

An average temperature for each 5 inch isothermal glass element, T_n, was evaluated from an interpolation of the measured glass temperature profile. The temperature at the point i on the test section was evaluated using the corrected temperatures and Procedure FIT (49).

Adiabatic friction factor checks. Over fifty adiabatic friction factor runs were made, using air and helium, prior to the collection of the heat transfer data. The pressure taps were located 28.893 inches apart and the flow covered the bulk Reynolds number range from 750 to 38,000. Comparison of the laminar results with the laminar prediction and the turbulent results with the prediction of Drew, Koo and McAdams (1) provided a check of the system integrity and correct operation of the flow and pressure drop measurement equipment. Results of some of the later turbulent runs have been included in Figure 1.

Heat Transfer Runs

The heat transfer runs consisted of measurements of the test section current, voltage, overall pressure drop, pressure at the first pressure tap, wall temperatures, the mass flow rate, inlet and outlet bulk temperatures, the vacuum system pressure, and the temperature distribution of the vacuum chamber wall. The mass flow rate

measurements consisted of the primary and secondary flow meter readings and the gas temperature and pressure downstream from the meters.

The successive procedure follows. Zeroes of all manometers and Heise gages were set under atmospheric conditions. The system was then pressurized to approximately 100 psia. The fluid levels in the pressure drop manometers were alternately raised and lowered, by opening and closing bypass valves and vents, until the zero was consistently reproduced. This step was necessary to assure that only test gas was present in all of the manometer lines and in both legs of the manometers. The bypass valves were then closed and the system leak checked for a period of one hour.

The Foxboro Differential Pressure Cell zero was then set, and the ice reference and zeroes of the manometers and meters checked. Correct operation of the Electronic-18 over the expected temperature range was checked by means of a calibration feature of the ARU unit.

The desired inlet flow rate was then set and an adiabatic friction factor run made to determine the validity of the pressure drop and flow measurements for the heating runs at these settings. The test section power leads were then connected to the power supply and the current adjusted to give desired wall temperatures. Care was taken to assure that the current for the setting was

near full scale on the ammeter. When steady state was
obtained, as indicated by no further changes in the
readings of the last three or four thermocouples located
on the heated portion of the test section, the data
described earlier were recorded in the data book. The
meters used and the current transformer setting were also
recorded. Overall test section resistance was computed
from the voltage and current measurements, and a field plot
of wall temperature prepared. After checking any readings
that appeared out of line, a new power setting was set, if
adequate supply gas remained, and the process was repeated.
At the completion of the heating runs, the power supply was
disconnected and an adiabatic friction factor run taken
when steady state was reached.

Data Reduction

Except for changes in the calculation of the local
energy generation, heat loss, gas stagnation enthalpy, and
the mass flow rate, as necessitated by changes in the
experimental loop, the data reduction formulae developed by
McEligot (49) were employed throughout the heat transfer
study.

Gas Bulk Stagnation Enthalpy

The bulk stagnation enthalpy at a thermocouple, n,
was obtained by an energy balance on a control volume
comprised of the tube and fluid, as shown in Figure E-2.
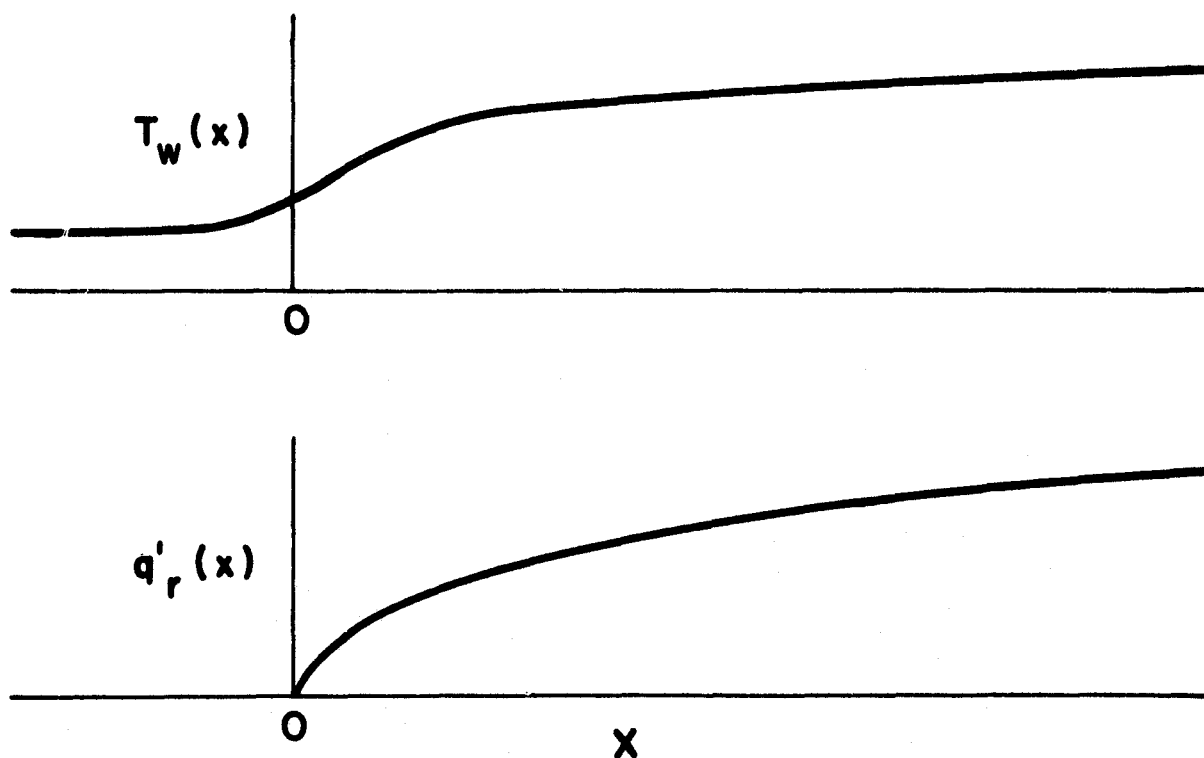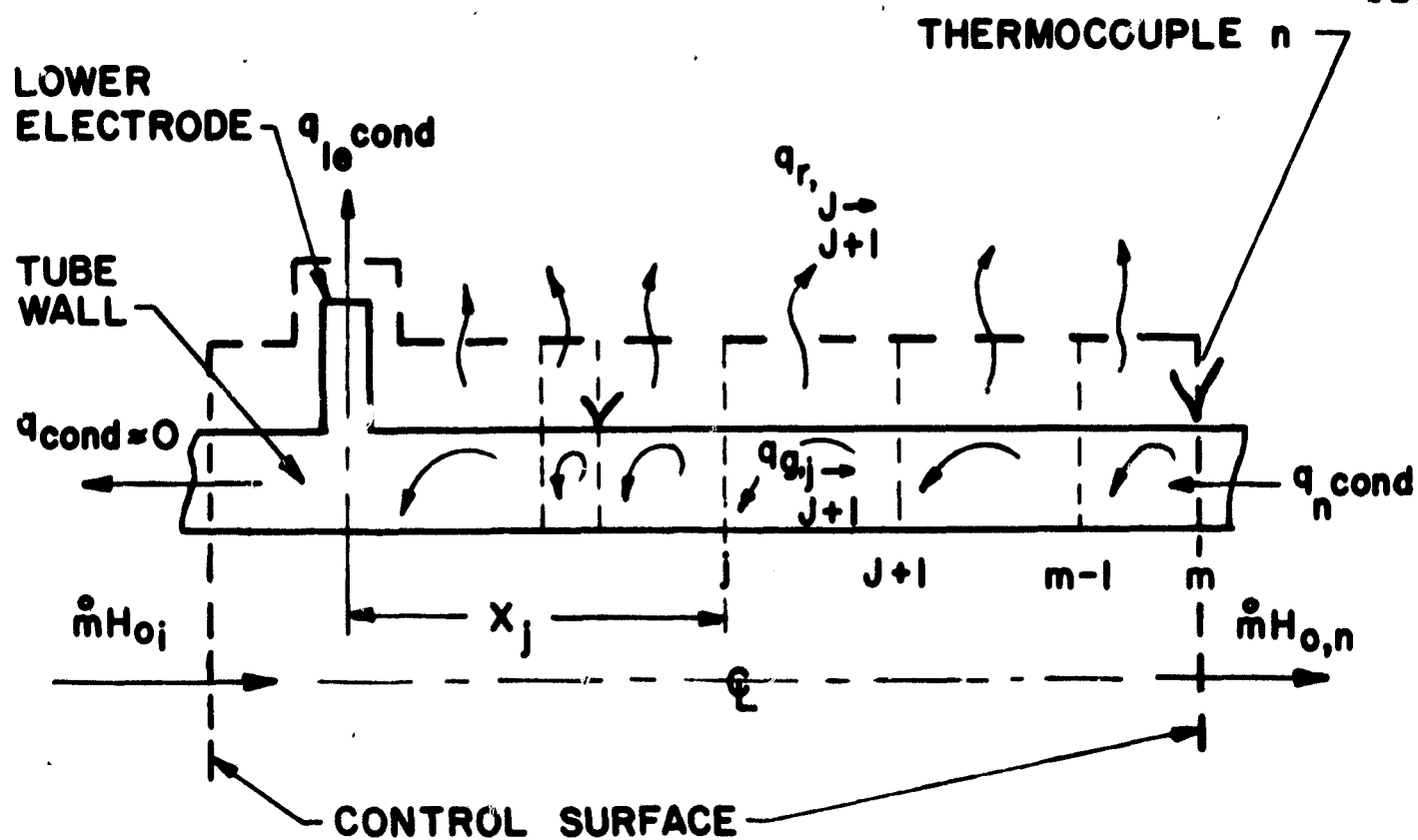
Figure E-2.   Control Volume for Calculation of Bulk
               Stagnation Enthalpy and Typical Axial
               Profiles

Trapezoidal integration was used to find the net difference between the energy generation and the radiation heat loss, in the energy balance,

$$H_{o,n} = H_{o,i} + \frac{1}{\dot{m}} \left\{ -q_{le} + q_{cond,n} + \sum_{j=1}^{m-1} \left[(q'_g - q'_r)_{j+1} + (q'_g - q'_r)_j \right] \left[\frac{x_{j+1} - x_j}{2} \right] \right\}$$

(E-3)

where $q'_{g,j}$ and $q'_{r,j}$ represent the energy generation per foot and the radiation loss per foot at the location j. The assumption was made that the small amount of energy conducted down the tube below the lower electrode all entered the gas. Calculations, based on temperature measurements at the electrode and on the wall below the electrode, showed that this assumption introduces a maximum error of less than 0.1 per cent in the bulk temperature at the lower electrode, for the air run at a Reynolds number of 3860.

Conduction Heat Loss

The heat loss at the lower electrode, q_{le}, was estimated by considering the electrode as a thin circular radiating fin. The resulting expression (48)

$$q_{le} = \sqrt{\frac{4}{5} r_{le}^3 \pi^2 \sigma k_{le} e_{le}} \; (T_{le}^5 - 5T_{le}T_\infty^4 + 4T_\infty^5)^{1/2}$$

(E-4)

was found to be closely approximated (for the present stainless steel electrode) by

$$q_{le} = 0.0224(T_{le} - T_\infty) \qquad 90 \leq T_{le} \leq 400°F \qquad (E-5)$$

The latter expression was employed for the calculation of q_{le} in the energy balance. A 100 per cent error in this approximation would cause a maximum error of less than 2 per cent in the bulk temperature at the lower electrode. This error would occur for the air data at a Reynolds number of 3860.

The conduction heat loss was evaluated from the expression

$$q_{cond_n} = -k(T_n)A\perp \frac{dT_n}{dx} \qquad (E-6)$$

Procedure FIT (49) was used to determine $\frac{dT_n}{dx}$.

Local Energy Generation

The local energy generation was calculated both at 1/4 inch intervals and at the thermocouple locations from the expression

$$q'_{g,j} = I^2 R'(T_j) \qquad (E-7)$$

The positions were corrected for tube expansion. Procedure FIT (49) was used to obtain the temperature at the 1/4 inch intervals from the corrected thermocouple temperatures.

The local test section resistance was evaluated as a
function of temperature from the experimental expression

$$R'(T_j) = \frac{0.12452 + 1.058 \times 10^{-5} (T_j - 80°F)}{L_{exp}} \Omega/FT \quad (E-8)$$

The calibration for the variation of the resistance with
temperature is described in Chapter VII. The major portion
of the calibration, including a measurement of the axial
variation of resistance for the test section, was performed
by R. W. Shumway (58). The straight line correlation used
for the resistance in this study is slightly lower, and
approximately parallels the result obtained by Shumway (58).
The new correlation was based on consideration of more
recent data and the observed decrease of resistance with
time, as indicated in Chapter VII.

Radiation Heat Loss

For the radiation calculations the test section and
the vacuum chamber were considered to be a non isothermal
annulus. The radiation heat loss at points located at 1/4
inch intervals on the unexpanded tube, corrected for
expansion when heated, was calculated from

$$q'_{r,j} = e_j(T_j) \, \sigma \, (T_j^4 - \sum_{n=1}^{8} F_{j,n} T_n^4) \quad (E-9)$$

where $e_j(T_j)$ was evaluated from an expression of the form

$$e_j(T_j) = a_j T_j + b_j \qquad (E\text{-}10)$$

The a_j and b_j coefficients were obtained from the heat loss calibration. The calculation procedure is the same as that presented in the section--Heat Loss Calibration--with the exception that $e_j(T_j)$ is now the known quantity, and $q'_{r,j}$ is the unknown.

The radiation heat loss at a given thermocouple was evaluated from a straight line interpolation of the values of $q'_{r,j}/T_j^4$ on either side of the thermocouple.

Mass Flow Rate

The mass flow rate was calculated from

$$\overset{\circ}{m} = scfm_c \, \rho_{std} \sqrt{\frac{\rho}{\rho_c}} \qquad (E\text{-}11)$$

ρ_{std} = air density at 68°F, 14.7 psia (Brooks "standard conditions"),

ρ_c = fluid density at calibration conditions,

ρ = actual operating density at the flowmeter,

$scfm_c$ = reading from calibration charts.

Local Heat Flux

The heat flux at each thermocouple was calculated from the expression

$$q''_{w,n} = \frac{q'_{g,n} - q'_{r,n}}{\pi D_{exp}} - k(T_n) A_\perp \, \frac{d^2 T_n}{dx^2} \qquad (E\text{-}12)$$

where D_{exp} is the expanded diameter of the test section. Procedure FIT (49) was used to evaluate d^2T_n/dx^2.

Constant Property Extrapolation

The constant property extrapolation is explained in sufficient detail in Chapter VII and will not be repeated here. The procedure is illustrated in Figure 5, which presents the extrapolation for the indicated thermocouples for the series of six heating runs taken at an inlet Reynolds number of 6800. Uncertainty intervals, discussed in the following section, are also included.

Uncertainty Analysis

An uncertainty analysis was performed by the method of Kline and McClintock (30) to estimate the uncertainty in the experimental data. The uncertainties in the directly measured quantities are presented in Table E-3. These values are based on experience and manufacturers' specifications, where available.

The uncertainties of the extrapolated constant property Nusselt Numbers presented in Figures 6, 7, 8, and 9 were obtained by plotting the uncertainty intervals of the data for the different heating runs on the logarithmic plots used for the extrapolation. From these values a straight line uncertainty band was estimated. The values of the band at a wall to bulk ratio of one were used for the uncertainty in the constant property Nusselt Number.

Table E-3. Heat Transfer Study: Uncertainty Intervals of Measured Quantities

Item	Uncertainty
Current	$\pm$0.25% full scale
Voltage:	
Fluke	$\pm$0.1% of reading
Weston	$\pm$0.25% full scale
Brooks Variable Area Flowmeter	
Model 1112A	$\pm$0.0221 scfm$_c$ (1% full scale)
Model 150	$\pm$0.00414 scfm$_c$
Foxboro D. P. Cell	
0.034 orifice	$\pm$0.54% of flow rate
0.0595	$\pm$2.5% of flow rate
0.0995	$\pm$5.0% full scale
Wall Temperature	$\pm$2°F, 3/8% of reading above 535°F
Inlet Bulk Temperature	
Thermocouple location	$\pm$0.005 inches
Pressure tap location	
Resistance	$\pm$0.002 Ω
Diameter	$\pm$0.0009 inches
Pressure (Heise)	$\pm$0.15 psi
Pressure Drop	
10" Inclined Manometer	$\pm$0.01 in H_2O
60" Vertical Manometer	$\pm$0.5 in H_2O

Representative uncertainty values for two of the heating runs at a Reynolds number of 6800 are presented in Table E-4. Values are also presented in Figure 5, which illustrate the constant property extrapolation.

Table E-4. Representative Uncertainty Values for Nusselt
Number Data With Heating

Run $(T_w/T_b)_{max}$ x/D	Re = 6800, Helium 53 1.090 Percentage	55 1.379 Uncertainty
1.21	8.5	3.0
8.14	6.4	2.5
25.92	6.2	2.8
52.01	5.6	3.7
95.68	7.6	6.1

APPENDIX F

DERIVATION OF HEAT TRANSFER ANALYSIS

The following derivation closely follows the method presented by Sparrow, Hallman and Siegel (35) and summarized by Kays (2). The major differences have been discussed in Chapter VI.

The energy equation for turbulent flow in a tube is derived for the conditions:

1. Constant fluid properties,

2. Fully developed velocity profiles,

3. Negligible viscous dissipation and axial conduction,

4. Steady, incompressible flow,

5. No internal energy generation.

The energy equation reduces to

$$\frac{1}{y_c^+(1-\overline{y})} \frac{\partial}{\partial \overline{y}} \left(1 - \overline{y}\right)\beta(\overline{y}) \frac{\partial \theta}{\partial \overline{y}} = u^+(\overline{y}) \frac{\partial \theta}{\partial x^+} \qquad (F-1)$$

where

$$\beta(\overline{y}) \triangleq \frac{\epsilon_H}{\nu}(\overline{y}) + \frac{1}{Pr} \text{ and } \theta(x^+,\overline{y}) = \frac{T - T_i}{q_w'' r_w / k} \qquad (F-2)$$

For a constant wall heat flux and an initial uniform fluid temperature, T_i, the boundary conditions are

$$\frac{\partial \Theta}{\partial \overline{y}}(x^+, 0) = -1 \text{ at the wall,} \qquad (F-3)$$

$$\frac{\partial \Theta}{\partial \overline{y}}(x^+, 1) = 0 \text{ at the centerline,}$$

and

$$\Theta(0, \overline{y}) = 0 \text{ at the start of heating} \qquad (F-4)$$

Use of Reynolds analogy, $\epsilon_H = \epsilon_m$, allows evaluation of $\beta(\overline{y})$ from the momentum eddy diffusivity distribution, equations 3-5 and 3-10. In terms of the present dimensionless variables this yields

$$\beta(\overline{y}) = \frac{\kappa}{6}\left[y_\epsilon^+ \overline{y} - y_1^+ \tanh\frac{y_\epsilon^+ \overline{y}}{y_1^+}\right]\left[2 - \overline{y}\right]\left[1 + 2(1 - \overline{y})^2\right] + \frac{1}{Pr} \quad (F-5)$$

where

$$y_1^+ = 11 + 9.1116 \exp(-0.27249 \text{ Re} \times 10^{-3})$$

$$+ \left[15.83 \exp(-0.9498 \text{ Re} \times 10^{-3})\right]^4$$

and $\kappa = 0.4225$.

The last term in the expression for y_1^+ is negligible for Reynolds numbers above 4000.

The velocity is determined directly from the defining equation for ϵ_m,

$$u^+(\overline{y}) = \int_0^{\overline{y}} \frac{1 - \overline{y}}{1 + \frac{\epsilon_m}{\nu}} y_\epsilon^+ \, d\overline{y} \qquad (F-6)$$

Since equation F-2 is linear, Θ can be separated into the sum of a solution for the fully developed region, Θ_∞, and the entrance region contribution, Θ_e,

$$\Theta \triangleq \Theta_e + \Theta_\infty \qquad (F-7)$$

For large values of x^+, Θ_e approaches zero. This separation of the dimensionless temperature is employed to obtain homogeneous boundary conditions for the entrance solution, as shown later. Caution must be used in the interpretation of the fully developed solution (Θ_∞). The term "fully developed temperature profile" refers to a profile generalized in terms of variables which make it invariant with axial position. Such a profile is normally used to obtain the fully developed heat transfer solution (2). While Θ_∞ describes the temperature for fully developed flow, it is not invariant with axial position and, thus, is not a fully developed temperature profile in the above sense.

Fully Developed Solution

At large x^+, $\Theta = \Theta_\infty$. The energy equation becomes

$$\frac{1}{y_Q^+(1 - \bar{y})} \frac{\partial}{\partial \bar{y}}\left[(1 - \bar{y})\beta(\bar{y}) \frac{\partial \Theta_\infty}{\partial \bar{y}}\right] = u^+(\bar{y}) \frac{\partial \Theta_\infty}{\partial x^+} \qquad (F-8)$$

with the boundary conditions

$$\frac{\partial \Theta_\infty}{\partial \bar{y}} (x^+,0) = -1, \quad \frac{\partial \Theta_\infty}{\partial \bar{y}} (x^+,1) = 0 \qquad (F-9)$$

The requirements for fully established thermal conditions are that the dimensionless temperature, $(T_w - T)/(T_w - T_b)$ or $(T_w - T)/(T_w - T_{\math4{L}})$, and the heat transfer coefficient h,

$$h \triangleq \frac{q''_w}{T_w - T_b} \qquad (F\text{-}10)$$

be invariant with the tube length (2). For a constant wall heat flux (q''_w) these two requirements yield, in terms of the present variables,

$$\frac{\partial \Theta_\infty}{\partial x^+} = \frac{d\Theta_b}{dx^+} \qquad (F\text{-}11)$$

where

$$\Theta_b \triangleq \frac{1}{AV_b^+} \int u^+ \Theta dA \qquad (F\text{-}12)$$

An energy balance on the fluid shows

$$\frac{d\Theta_b}{dx^+} = \frac{4}{RePr} = \text{constant.} \qquad (F\text{-}13)$$

Combination of equations F-11 and F-13 leads to

$$\frac{\partial \Theta_\infty}{\partial x^+} = \frac{4}{RePr} \qquad (F\text{-}14)$$

The dimensionless temperature, Θ_∞, could be obtained directly at this point from equation F-8, after substitution of F-14, by integration. However, the alternate approach of a further separation of Θ_∞ will be employed.

This approach will yield a more tractable form of Θ_∞ for use in the entrance solution.

The general solution of equation F-14 is

$$\Theta_\infty = \frac{4}{RePr}\, x^+ + F(\overline{y}) \qquad (F-15)$$

where $F(\overline{y})$ is an unknown function of $\overline{y}$ to be determined. Integration of equation F-13 yields

$$\Theta_b = \frac{4}{RePr}\, x^+ \qquad (F-16)$$

where the constant of integration is zero by virtue of the boundary condition $\Theta_b\big|_{x^+=0} = 0$. Combination with equation F-15 for Θ_∞ reveals that

$$F(\overline{y}) = \Theta_\infty - \Theta_b = \frac{T - T_b}{q''_{wk}\frac{r_w}{k}} \qquad (F-17)$$

Substitution of the equations for $\dfrac{\partial \Theta_\infty}{\partial x^+}$ and Θ_∞ into the energy equation (F-8) yields a second order, ordinary differential equation for $F(\overline{y})$,

$$\frac{1}{y_{\mathfrak{C}}^+(1-\overline{y})}\frac{d}{d\overline{y}}\left[(1-\overline{y})\beta(\overline{y})\frac{dF}{d\overline{y}}\right] = u^+(\overline{y})\frac{4}{RePr} \qquad (F-18)$$

with boundary conditions

$$\frac{dF(0)}{d\overline{y}} = -1, \quad \frac{dF(1)}{d\overline{y}} = 0 \qquad (F-19)$$

Integration from 0 to $\overline{y}$ leads to

$$(1 - \overline{y})\beta(\overline{y}) \frac{dF(\overline{y})}{d\overline{y}} = -\beta(0) + \frac{4y_{\xi}^{+}}{RePr} \int_{0}^{\overline{y}} u^{+}(\zeta)(1 - \zeta)d\zeta \quad (F-20)$$

The value of $\beta(0)$ is obtained from the above equation with $\overline{y} = 1$,

$$\beta(0) = \frac{4y_{\xi}^{+}}{RePr} \int_{0}^{1} u^{+}(\zeta)(1 - \zeta)d\zeta \quad (F-21)$$

The numerical result of this integration was used for $\beta(0)$, rather than $1/Pr$ (see equation F-5). The use of the former assured that the right-hand side of equation F-20 would approach zero as $\overline{y}$ approached one. If this criterion is not fulfilled, errors can result in $F(\overline{y})$ due to a non-zero value of the right-hand side of F-20. The integral expression for $\beta(0)$ will reduce to $1/Pr$ only if the numerical evaluation of the integral of the velocity, in F-21, identically equals the correct value of the bulk velocity.

A second integration of equation F-20 yields

$$F(\overline{y}) - F(0) = \int_{0}^{\overline{y}} \left[\frac{1}{(1 - \gamma)\beta(\gamma)} \right]$$

$$\left[-\beta(0) + \frac{4y_{\xi}^{+}}{RePr} \int_{0}^{\gamma} u^{+}(\zeta)(1 - \zeta)d\zeta \right] d\gamma \quad (F-22)$$

where it is observed, from equation F-17, that

$$F(\bar{y}) - F(0) = \frac{-(T_w - T)_\infty}{q''_w r_w / k} \qquad \text{(F-23)}$$

Thus, an axially invariant form of the fully developed temperature profile is given by

$$\frac{T_w - T}{T_w - T_{\mathcal{L}}} = \frac{F(0) - F(\bar{y})}{F(0) - F(1)} \qquad \text{(F-24)}$$

Equation F-17 shows that $F(0)$ can be obtained directly from the definition of bulk temperature,

$$F(0) = \frac{T_w - T_b}{q''_w \frac{r_w}{k}} = \frac{2 \int_0^1 -u^+(\bar{y}) \left[F(\bar{y}) - F(0) \right] (1 - \bar{y}) d\bar{y}}{\int_0^1 u^+(\bar{y})(1 - \bar{y}) d\bar{y}} \qquad \text{(F-25)}$$

The local Nusselt number is defined as

$$Nu = \frac{hD}{k} \qquad \text{(F-26)}$$

Substitution of F-10 for h and F-25 for $\frac{T_w - T_b}{q''_w r_w / k}$ yields

$$Nu_\infty = \frac{2}{F(0)} \qquad \text{(F-27)}$$

Thermal Entrance Region

The entrance region contribution is defined by

$$\Theta_e = \Theta - \Theta_\infty \qquad \text{(F-28)}$$

By the linearity of the energy equation, Θ_e also satisfies equation F-1,

$$\frac{1}{y_{\mathcal{L}}^+(1 - \overline{y})} \frac{\partial}{\partial \overline{y}} \left[(1 - \overline{y})\beta(\overline{y}) \frac{\partial \Theta_e}{\partial \overline{y}} \right] = u^+(\overline{y}) \frac{\partial \Theta_e}{\partial x^+} \qquad (F-29)$$

By virtue of equations F-3 and F-9, the boundary conditions are

$$\frac{\partial \Theta_e}{\partial \overline{y}} (x^+,0) = 0, \ \frac{\partial \Theta_e}{\partial \overline{y}} (x^+,1) = 0 \qquad (F-30)$$

Substitution of the expression for Θ_∞, F-15, into F-28 yields the initial condition

$$\Theta_e(0,\overline{y}) = -F(\overline{y}) \qquad (F-31)$$

A product solution is assumed

$$\Theta_e = R(\overline{y})X(x^+) \qquad (F-32)$$

Separation of variables leads to

$$X = Ce^{-\lambda^2 x^+} \qquad (F-33)$$

and

$$\frac{d}{d\overline{y}} \left[(1 - \overline{y})\beta(\overline{y}) \frac{dR}{d\overline{y}}(\overline{y}) \right] + \lambda^2 y_{\mathcal{L}}^+(1 - \overline{y})u^+(\overline{y})R(\overline{y}) = 0 \qquad (F-34)$$

$$\frac{dR(0)}{d\overline{y}} = 0, \ \frac{dR(1)}{d\overline{y}} = 0 \qquad (F-35)$$

The sep..ration constant is chosen so that Θ_e will approach zero for large x^+.

Equation F-34 and its boundary conditions form a Sturm-Liouville problem: λ_n^2 are the discrete eigenvalues (though infinite in number) for which a solution exists, and $y_{\mathcal{L}}^+(1 - \overline{y})u^+(\overline{y})$ is the weighting function. The solution for R is expressible in terms of an infinite series of functions, R_n, which are orthogonal with respect to the weighting function. R_n and λ_n^2 are the nth unique combination of a function and a constant multiplier which will satisfy the differential equation and boundary conditions.

Thus, the solution for Θ_e is given by

$$\Theta_e = \sum_n C_n R_n(\overline{y}) e^{-\lambda_n^2 x^+} \qquad (F-36)$$

Application of the initial condition, F-31, at $x^+ = 0$ yields

$$-F(\overline{y}) = \sum_n C_n R_n(\overline{y}) \qquad (F-37)$$

The orthogonality of R_n with respect to the weighting function, $y_{\mathcal{L}}^+(1 - \overline{y})u^+(\overline{y})$, allows evaluation of C_n, from equation F-37, by using the principle of orthogonality (60),

$$C_n = \frac{\displaystyle\int_0^1 -\left[y_{\mathcal{L}}^+(1 - \overline{y})u^+(\overline{y})\right] F(\overline{y})R_n(\overline{y})\,d\overline{y}}{\displaystyle\int_0^1 \left[y_{\mathcal{L}}^+(1 - \overline{y})u^+(\overline{y})\right] R_n^2(\overline{y})\,d\overline{y}} \qquad (F-38)$$

The dimensionless temperature at any position is given by the sum of Θ_∞ and Θ_e

$$\Theta = \frac{4}{\text{RePr}} x^+ + F(\overline{y}) + \sum_{n=1}^{\infty} C_n R_n(\overline{y}) e^{-\lambda_n^2 x^+} \qquad (F-39)$$

Substitution of equation F-16 for the first term of F-39 and $\overline{y} = 0$ yields the dimensionless wall--bulk temperature difference

$$\Theta_w - \Theta_b = \frac{T_w - T_b}{q_w'' r_w / k} = F(0) + \sum_{n=1}^{\infty} C_n R_n(0) e^{-\lambda_n^2 x^+} \qquad (F-40)$$

Heat Transfer Results

Combination of the definitions of the heat transfer coefficient and Nusselt number (equations F-10 and F-26, respectively) yields

$$\text{Nu}(x^+) = \frac{q_w'' D}{(T_w - T_b)k} \qquad (F-41)$$

In terms of the present variables

$$\text{Nu}(x^+) = \frac{2}{\Theta_w - \Theta_b}$$

Substitution of equation F-40 for $\Theta_w - \Theta_b$ yields

$$\text{Nu}(x^+) = \frac{2}{F(0) + \sum_{n=1}^{\infty} C_n R_n(0) e^{-\lambda_n^2 x^+}} \qquad (F-43)$$

The fully developed Nusselt number is obtained from the above expression by allowing x^+ to approach infinity. The result agrees with the fully developed value predicted earlier by equation F-27,

$$Nu_\infty = \frac{2}{F(0)} \qquad (F-27)$$

The normalized entry length Nusselt number, used for prediction purposes, is obtained by division of F-42 by F-27

$$\frac{Nu(x^+)}{Nu_\infty} = \frac{1}{1 + \sum_{n=1}^{\infty} A_n e^{-\lambda_n^2 x^+}} \qquad (F-44)$$

where

$$A_n \triangleq \frac{C_n R_n(0)}{F(0)} \qquad (F-45)$$

The equations presented above were solved numerically on an IBM 7072. The eigenvalue solution and other important numerical details are presented in Appendix G. A listing of the FORTRAN program is included.

APPENDIX G

DETAILS OF NUMERICAL HEAT TRANSFER SOLUTION

Fully Developed Solution

The fully developed solution follows in a straight forward fashion from equations F-22 and F-25, which were evaluated numerically using Simpson's rule. Prior to the integration, values of $\beta(\bar{y})$ and $u^+(\bar{y})$ were calculated for the velocity profile in use at fixed $\bar{y}$ intervals ($\Delta\bar{y} = 0.00125$) and stored in the computer memory. $\beta(0)$, the value of $\frac{\epsilon_m}{\nu} + \frac{1}{Pr}$ at $\bar{y} = 0$, was evaluated from the expression

$$\beta(0) = \frac{4y_c^+}{RePr} \int_0^1 u^+(\bar{y})(1 - \bar{y})d\bar{y} \qquad (G-1)$$

The reason for using this equation is discussed in Appendix F.

A comparison of the fully developed Nusselt numbers with existing formulations is presented in Table G-1.

Eigenvalue Solution

For the purpose of solution, equation F-34 was reduced to two first order equations,

$$R' = S \qquad (G-2)$$

149

Table G-1. Comparison of Fully Developed Predictions

Investigators	Pr	Fully Developed Nusselt Numbers, $\overline{Nu}_\infty$ Re					
		3000	6000	10000	20000	30000	50000
Present	0.71	11.06	19.57	29.46	50.27	68.38	100.81
McEligot, Ormand & Perkins (9)	0.71	11.69	19.07	29.04	50.26	--	106.7
Malina & Sparrow (42)[a]	0.70	--	--	32.28	52.31	70.02	101.9
Haberstroh & Baldwin (44)	0.70	10.55	--	28.18	--	66.00	99.84
Botje-Deissler (61)[b]	0.71	16.0	24.4	34.0	54.5	73	111
Dittus-Boelter, eq. 8-2	0.71	11.07	19.29	29.02	50.53	69.89	105.18

[a]Based on the eddy diffusivity distribution used by Sparrow, Hallman and Siegel (35).

[b]Values obtained from plot of tabular results at different Re.

and

$$S' = (\frac{1}{1 - \overline{y}} - \frac{\beta'(\overline{y})}{\beta(\overline{y})})S - \lambda_n^2 y_c^+ u^+(\overline{y})R \qquad (G-3)$$

with $R'(0) = 0$, $R'(1) = C$. The primes indicate differentiation with respect to $\overline{y}$. $\beta'(\overline{y})$ is obtained by differentiation of equation F-5.

The trial and error solution for pairs of λ_n^2 and R_n was initiated by evaluating the coefficients of S and R and storing them in the computer memory. Starting with the initial trial value of $\lambda^2 = 0$, the above set was solved simultaneously as an initial value problem. A fourth order predictor-corrector-technique with a Runge-Kutta method for starting was used (Hildebrand (59), equations 6.6.1 and 6.16.12). The process was continually repeated, incrementing λ^2 until a change in the sign of $R'(1)$ was observed. Since the value of $R'(1)$ varies in a damped periodic manner as λ^2 increases, the change in sign represents the bracketing of a value of λ^2 for which $R'(1) = 0$. Linear interpolation was then used to predict the value of λ^2 for $R'(1) = 0$. The equations were then solved with this value of λ^2 to find the corresponding value of $R'(1)$ predicted by the differential equation. Linear interpolation was again employed, with the two most recent values of λ^2 and $R'(1)$, and the process was continually repeated to converge to the eigenvalue. Values of C_n

were then determined from equation F-38, using integration by Simpson's rule. The entire process was repeated until the first seven eigenvalues were found.

Presented below is a listing of the FORTRAN program. It is divided into two main sections, the fully developed solution and the eigenvalue entrance solution. The choice is provided for a solution based on either the present velocity formulation or the velocity formulation used by Sparrow, Hallman and Siegel. Due to core limitations of the computer used, a separate program was employed for the McEligot, Ormand and Perkins solution.

In the fully developed section, the eddy diffusivity and velocity values (for the profile chosen) are computed and stored for the desired Reynolds and Prandtl number. The fully developed temperature profile, $(T_w - T)/(T_w - T_c)$; $F(\bar{y})$; and the fully developed Nusselt number, Nu_∞, are then calculated in the order indicated, from the expressions in Appendix F. Simpson's Rule integration is employed in all integrations.

In the entrance region, or eigenvalue solution section, the coefficients of equation G-3 are calculated and stored. Values of the velocity and eddy diffusivity calculated in the previous section are used where needed. The trial and error eigenvalue solution is then performed to obtain the first seven values of λ_n^2, C_n, and A_n. The entry Nusselt number is then calculated and normalized by

two different values, the fully developed Nusselt number and a Dittus-Boelter formulation. The normalized values are then printed and new values of Reynolds and Prandlt number read. The program terminates if no new values for these two quantities are provided.

FORTRAN LISTING OF COMPUTER PROGRAM

```
C       COMPUTER  PROGRAM  LOW REYNOLDS NUMBER TURBULENT HE
C    ***                                    AT TRANSFER
      DIMENSION YR(802), EDDY(402),DER(802),UPLUS(402),VA
     ***                                    R(402)
      DIMENSION X(206),EE(206),E(206),C(206),R(206),S(206
     ***                                    ),SP(206)
      DIMENSION FY(104),DMIT(104),DUMY(104),A(9),GEI(9),R
     ***                                    NU(30)
      DIMENSION XPLUS(30),ED(4),CD(4),YPLUS(802)
      DIMENSION RDB(30)
C       DOWNSTREAM, FULLY DEVELOPED FLOW SOLUTION
    4 READ 5,RE,CC,IEDDY
    5 FORMAT(2F10.0,I1)
C       CC=RATIO OF FRICTIONFACTOR (FRIT)/BLAUSIUS FRICTION
C    ***                                    FACTOR
C       CC SHOULD BE SET = TO 1. IF BLAUSIUS FRICTION FACTO
C    ***                                    R IS USED
C       EXPRESSION FOR FRICTION FACTOR AND THEORETICAL BULK
C    ***                                    VELOCITY
C       IEDDY DETERMINES VELOCITY PROFILE USED
C       IEDDY=1 MODIFIED REICHARDT,  2 SPARROW ET AL.
      READ 4000,PP
 4000 FORMAT(F10.0)
      FRIT=.0791/(RE**.25)
      FRIT=CC*FRIT
      YMAX=RE*SQRTF(FRIT/2.)/2.
      VBTH=SQRTF(2./FRIT)
      PRINT 300,RE,YMAX
  300 FORMAT(10X,16HREYNOLDS NUMBER=,F7.0,5X,10HYPLUS MAX
     ***                                    =,F10.2)
      PRINT 301,CC
  301 FORMAT(10X,41HFRICTION FACTOR/BLAUSIS FRICTION FACT
     ***                                    OR =, F7.4)
C       NNN=NUMBER OF Y/2W SPACES=IN MAGNITUDE TO DEL, USED
C    ***                                    IN INTEGRATION
C       OF U+.  NNN MUST= EVEN INTEGER MULTIPLE OF 80. THE
C    ***                                    RESULTING
C       SPACING USED IN SOLUTION OF  EIGEN VAL  PROBLEM  A
C    ***                                    ND IN OBTAINING
C       T-TW WILL BE 4DEL. AND WILL= 8DEL IN NUMERICAL INTE
C    ***                                    GRATION OF CN.
      NNN=800
      AA=NNN
      DEL=1./AA
      J=NNN+1
      JEND=J/4 +1
      YR(1)=0.0
C       INSERT  FORM FOR EDDY DIFFUSIVITY HERE
```

```
      GO TO(6,50,70),IEDDY
   7  CONTINUE
C     MODIFIED REICHARDT PROFILE
   6  PRINT 1
   1  FORMAT(10X,26HMODIFIED REICHARDT PROFILE)
C     EXPRESSION FOR YL
      RK=.4225
      REYN=RE*.001
      YL=11.+9.1116/EXPEF(.27249*REYN)
      IF(REYN-7.)11,12,12
  11  YL=YL+(15.83/EXPEF(.9448*REYN))**4.
  12  CONTINUE
C     END OF EXPRESSION FOR YL
  13  PRINT 14,RK,YL
  14  FORMAT(10X,2HK=,F7.4,9X,4HY+L=,F7.3)
      DO 100 I=1,J
      N=I+1
      YPLUS(I)=YR(I)*YMAX
      IF(YPLUS(I)/YL-10.)7,8,8
   7  B=EXPEF(YPLUS(I)/YL)
      TANH=(B-1./B)/(B+1./B)
      GO TO 9
   8  TANH=1.0
   9  AA=RK*(YPLUS(I)-YL*TANH)
      EDDY(I)=AA*(2.-YR(I))*(1.+2.*((1.-YR(I))**2.))/6.
      DER(I)=(1.-YR(I))/(1.+EDDY(I))
 100  YR(N)=YR(I)+DEL
C     INTEGRATION OF EDDY DIFFUSIVITY TO OBTAIN VELOCITY
      YPDEL=DEL*YMAX
      UPLUS(1)=0.0
      ARE=0.0
      NN=J-2
      K=2
      DO 200 I=1,NN,2
      UPLUS(K)=ARE+(DER(I)+4.*DER(I+1)+DER(I+2))*YPDEL/3.
      ARE=UPLUS(K)
 200  K=K+1
      GO TO 229
C     END OF MODIFIED REICHARDT PROFILE
C     SPARROW,ET AL. EDDY DIFFUSIVITY EXPRESSION
  50  DER(1)=1.
      PRINT 2
   2  FORMAT(10X,32HSPARROW, HALLMAN, SIEGEL PROFILE)
      YPLUS(1)=0.
      YR(1)=0.
      EDDY(1)=0.
      YPDEL=DEL*YMAX
      RK=.124**2.
      UPLUS(1)=0.
      UGES=2.*YPDEL
      ARE=0.0
```

```
      K=2
      I=1
      L=1
66    N=I+1
      M=I+2
      YR(N)=YR(I)+DEL
      YR(M)=YR(N)+DEL
      YPLUS(N)=YPLUS(I)+YPDEL
      YPLUS(M)=YPLUS(N)+YPDEL
77    U=UPLUS(L)+(UGES-UPLUS(L))/2.
      AA=RK*U*YPLUS(N)
      EDDY(N)=AA*(1.-1./EXPEF(AA))
      DER(N)=(1.-YR(N))/(1.+EDDY(N))
      AA=RK*UGES*YPLUS(M)
      EDDY(M)=AA*(1.-1./EXPEF(AA))
      DER(M)=(1.-YR(M))/(1.+EDDY(M))
      UPLUS(K)=ARE+(DER(I)+4.*DER(N)+DER(M))*YPDEL/3.
      D=UPLUS(K)-UGES
      IF(ABSF(D)-.005)15,15,99
99    IF(D)10,15,10
10    UGES=(UPLUS(K)-UGES)/2. +UGES
      GO TO 77
15    IF(YPLUS(M)-26.)16,17,17
16    UGES=UPLUS(K)+UPLUS(K)-UPLUS(L)
      ARE=UPLUS(K)
      K=K+1
      L=L+1
      I=I+2
      GO TO 66
17    BB=.36*YMAX
      NN=M+1
      YR(NN)=YR(M)+DEL
      YPLUS(NN)=YPLUS(M)+YPDEL
      DO 20 L=NN,J
      EDDY(L)=BB*YR(L)*(1.-YR(L))
      DER(L)=(1.-YR(L))/(1.+EDDY(L))
      N=L+1
      YPLUS(N)=YPLUS(L)+YPDEL
20    YR(N)=YR(L)+DEL
      NN=J-2
      ARE=UPLUS(K)
      I=K+1
      DO 30 L=M,NN,2
      UPLUS(I)=ARE+(DER(L)+4.*DER(L+1)+DER(L+2))*YPDEL/3.
      ARE=UPLUS(I)
30    I=I+1
      GO TO 229
C     END OF SPARROW,ET AL. EDDY DIFFUSIVITY EXPRESSION
C     CALCULATION OF F(Y)-F(0),CALLED TF(I)
229   DELZ=2.*DEL
      Z=0.0
```

```
      L=J/2 +1
      DO 230 K=1,L
      VAR(K)=UPLUS(K)*(1.-Z)
230   Z=Z+DELZ
      CONST=4.*YMAX/(RE*PR)
      WW=0.0
      DELZZ=2.*DELZ
      AA=1./PR
      Z=0.0
      I=2
      L=J/2-1
      DO 240 N=1,L,2
      W(I)= WW+(VAR(N)+4.*VAR(N+1)+VAR(N+2))*DELZ/3.
      WW=W(I)
240   I=I+1
      BO=W(JEND)
      VBR=2.*BO/VRTH
801   PRINT 900,VBR
900   FORMAT(10X,24HVBULK/VBULK THEORETICAL=,F10.4)
      Z=0.0
      W(1)=0.0
      L=JEND-1
      DO 241 I=1,L
      W(I)=-1.+W(I)/BO
      K=4*I-3
      EE(I)=W(I)/((1.-Z)*(EDDY(K)*PR +1.))
241   Z=Z+DELZZ
      EE(JEND)=0.0
      BT=0.0
      I=2
      L=JEND-2
      DO 250 N=1,L,2
      FY(I)=BT +(EE(N)+4.*EE(N+1)+EE(N+2))*DELZZ/3.
      BT=FY(I)
250   I=I+1
      FY(1)=0.0
C     CALCULATION OF  TW-T/TW-TC,CALLED DMIT(I),F(0),CALL
C     ***                              ED TFO,AND NU-
      Z=0.0
      ZZ=2.*DELZZ
      IEND=J/8+1
      DO 260 I=1,IEND
      DMIT(I)=FY(I)/FY(IEND)
      K=4*I-3
      DUMY(I)=-FY(I)*(1.-Z)*UPLUS(K)
260   Z=Z+ZZ
      L=J/8-1
      TFO=0.0
      DO 270 N=1,L,2
270   TFO=TFO+(DUMY(N)+4.*DUMY(N+1)+DUMY(N+2))*ZZ/3.
      TFO=TFO/BO
```

```
      FDNU=2./TED
C        CALCULATION OF F(Y), FY(I) NOW  IS EQUAL TO F(Y)
      DO 265 I=1,IEND
 285  FY(I)=FY(I)+TEO
C        OUTPUT FORMATS FOR FULLY DEVELOPED FLOW
      PRINT 290,FDNU,TEO
 290  FORMAT(1 X,19HNU  FULLY DEVELOPED=,F10.3,5X,5HF(C)=1
    ***                                       Pc12.4/)
      PRINT 291
 291  FORMAT(13X,4HY/RW,6X,9HTW-T/TW-TC,5X,7HF(Y/RW),9X,
    ***                                       2HY+,7X,2HU+,3X
    1,14HEDDY DIF./VIS./)
      K=NNA/8.
      DO 293 M=1,IEND,K
      I=8*M-7
      L=4*M-3
      PRINT 292,YR(I),DMIT(M),FY(M),YPLUS(I),UPLUS(L),EDD
    ***                                       Y(I)
 292  FORMAT(13X,0PF5.3,F12.2,5X,1PE12.4,0PF12.2,F10.2,F1
    ***                                       1.3)
 293  CONTINUE
C        END OF FULLY DEVELOPED FLOW SOLUTION-START OF
C        SOLUTION OF EIGEN VALUE  PROBLEM-
C        CALCULATION OF F(N) AND G(N) AND DERIVATIVE OF EDDY
C     ***                                       DIFFUSIVITY
      GO TO(299,3000,3001),IEDDY
 3001 CONTINUE
C        MODIFIED REICHARDT PROFILE
 299  L=2
      V=YMAX/YL
      Z=DELZ
      DO 400 K=2,6,2
      B=EXPEF(V*Z)
      DEN=B+1./B
      SECH=4./(DEN**2.)
      TANH=(B-1./B)/DEN
      YY= Z**2.
      YYY=Z**3.
      EDYP=(YMAX-YMAX*SECH)*(6.-11.*Z+6.*YY-2.*YYY)
      EDYP=(EDYP+(YMAX*Z-YL*TANH)*(-11.+16.*Z-6.*YY))*RK/
    ***                                       6.
      M=2*K-1
      DENO=(EDDY(M)+1./PR)
      ES(L)=-1./(1.-Z)+EDYP/DENO
      GS(L)=YMAX*UPLUS(K)/DENO
      L=L+1
 400  Z=Z+DELZZ
      N=2
      Z=DELZZ
      L=J/2+1
      DO410 K=3,L,2
```

```
      IF(V*Z-1..)401,4 2,402
  401 B=EXPEF(V*Z)
      DEN=B+1./B
      SECH=4./(DEN**2.)
      TANH=(B-1./B)/DEN
      GO TO 403
  402 SECH=0.
      TANH=1.
  403 YY=Z**2.
      YYY=Z**3.
      EDYP=(YMAX-YMAX*SECH)*(6.-11.*Z+3.*YY-2.*YYY)
      EDYP=(EDYP+(YMAX*Z-YL*TANH)*(-11.+16.*Z-6.*YY))*K/
     ***                                            6.
      M=2*K-1
      DENO=EDDY(M)+1./PR
      E(N)=EDYP/DENO
      G(N)=YMAX* UPLUS(K)/DENO
      Z=Z+DELZZ
  410 N=N+1
      GO TO 412
C         END OF MODIFIED REICHARDT PROFILE
C         CACULATION OF E(N) AND G(N) USING SPARROW.ET AL. EX
C    ***                                         PRESSIONS
 3000 AA=26./YMAX
      BB=(.124**2.)*YMAX
      L=2
      Z=DELZ
      DO 340 K=2,6,2
      M=2*K-1
      DENO=EDDY(M)+1./PR
      IF(Z-AA)310,310,320
  310 BBB=BB*UPLUS(K)*Z
      EDYP= ( (YMAX*Z*(1.-Z')/DENO +UPLUS(K))*BB
      EDYP=EDYP*(1.+(-1.+BBB)/EXPEF(BBB))
      GO TO 330
  320 EDYP=.36*YMAX*(1.-2.*Z)
  330 ES(L)=-1./(1.-Z) +EDYP/DENO
      GS(L)=YMAX*UPLUS(K)/DENO
      L=L+1
  340 Z=Z+DELZZ
      N=2
      Z=DELZZ
      L=J/2 +1
      DO 408 K=3,L,2
      M=2*K-1
      DENO=EDDY(M)+1./PR
      IF(Z-AA)350,350,405
  350 BBB=BB*UPLUS(K)*Z
      EDYP= ( (YMAX*Z*(1.-Z')/DENO +UPLUS(K))*BB
      EDYP=EDYP*(1.+(-1.+BBB)/EXPEF(BBB))
      GO TO 407
```

```
  4.5 DOYF=.36*YMAX*(1.-2.*Z)
  4.7 F(N)=DOYF/DENO
      G(N)=YMAX*UPLUS(N)/DENO
      Z=Z+DELZZ
  405 N=N+1
      GO TO 412
C     END OF SPARROW,ET AL.
  412 L=JEND-1
      Z=DELZZ
      DO 411 N=2,L
      F(N)=-1./(1.-Z)+F(N)
  411 Z=Z+DELZZ
      F(1)=-1
      G(1)=0.0
      INDEX=1
C     DELEG=STEP SIZE BY WHICH EIGEN VALUE IS ADVANCED.
C     TOL=ACCURACY TO WHICH BOUNDARY CONDITION AT Y/RW=1
C     ***                                      IS DESIRED
      EIG=0.0
      DELEG=.01
      TOL=.00001
      JEIG=0
C     CALCULATION OF COEFFICIENTS FOR PREDICTOR-CORRECTOR
C     ***                                      EQUATIONS
      WPAR=DELZZ/24.
      U=55.*WPAR
      X=59.*WPAR
      Y=37.*WPAR
      T=9.*WPAR
      WW=19.*WPAR
      XX=5.*WPAR
C     RUNGE KUTTA START OF SOLUTION
  420 S(1)=0.0
      R(1)=1.0
      SP(1)=-EIG*G(1)*R(1)
      DELH=DELZZ
      DO 430 I =1,3
      N=I+1
      Q=-DELH*(E(I)*S(I)+EIG*G(I)*R(I))
      QQ=-DELH*(ES(N)*(S(I)+.5*Q)+EIG*GS(N)*(R(I)+.5*DELZ
     ***                                  Z*S(I)))
      QQQ=(ES(N)*(S(I)+.5*QQ))
      QQQ=-DELH*(QQQ+EIG*GS(N)*(R(I)+.5*DELZZ*S(I)+.25*DE
     ***                                  LZZ*Q))
      QQQQ=(E(N)*(S(I)+QQQ))
      QQQQ=-DELH*(QQQQ+EIG*G(N)*(R(I)+DELZZ*S(I)+.5*DELZZ
     ***                                  *QQ))
      R(N)=R(I)+DELZZ*S(I)+DELZZ*(Q+QQ+QQQ)/6.
      S(N)=S(I)+(Q+2.*(QQ+QQQ)+QQQQ)/6.
  430 SP(N)=-(E(N)*S(N)+EIG*G(N)*R(N))
C     CONTINUATION OF SOLUTION BY 4TH ORDER PREDICTOR-COR
C     ***                                      RECTOR
```

```
        L=JEND-1
        DO440 N=5,L
C       PREDICTOR
        R(N)=R(N-1)+U*S(N-1)-X*S(N-2)+Y*S(N-3)-T*S(N-4)
        S(N)=S(N-1)+U*SP(N-1)-X*SP(N-2)+Y*SP(N-3)-T*SP(N-4)
        SP(N)=-(E(N)*S(N)+EIG*G(N)*R(N))
C       CORRECTOR
        R(N)=R(N-1)+T*S(N)+WW*S(N-1)-XX*S(N-2)+S(N-3)*WPAR
        S(N)=S(N-1)+T*SP(N)+WW*SP(N-1)-XX*SP(N-2)+SP(N-3)*W
   ***                                                   PAR
  440   SP(N)=-(E(N)*S(N)+EIG*G(N)*R(N))
        N=JEND
        R(N)=R(N-1)+U*S(N-1)-X*S(N-2)+Y*S(N-3)-T*S(N-4)
        S(N)=S(N-1)+U*SP(N-1)-X*SP(N-2)+Y*SP(N-3)-T*SP(N-4)
        GO TO(500,450,460,480),INDEX
  450   EIGP=EIG
        TEST=S(JEND)
        EIG=EIG+DELEG
        INDEX=3
        GO TO 420
  460   RATIO=S(JEND)/TEST
        IF(RATIO)480,500,450
  480   IF(ABSF(S(JEND))-TOL)500,500,490
  490   DOG=EIG
        CAT=S(JEND)
        TOP=S(JEND)*EIGP-TEST*EIG
        TBTM=S(JEND)-TEST
        SMALL=ABSF(EIG-EIGP)
        IF(SMALL-.0000005)500,500,491
  491   CONTINUE
        IF(ABSF(TBTM)-.0000002)500,494,494
  494   CONTINUE
        IF(ABSF(TOP)-.0000002)500,495,495
  495   EIG=TOP/TBTM
        EIGP=DOG
        TEST=CAT
        INDEX=4
        GO TO 420
C       CALCULATION OF CN. NOTE DUMY(I),DMIT(I) ASSUME NEW
C   ***                                               MEANINGS
  500   I=1
        JEIG=JEIG+1
        Z=0.0
        DO 510 M=1,JEND,2
        N=2*M-1
        DUM=R(M)*UPLUS(N)*(1.-Z)
        DUMY(I)=-FY(I)*DUM
        DMIT(I)=R(M)*DUM
        Z=Z+ZZ
  510   I=I+1
        DEN=0.0
```

```
      BTM=0.0
      L=J/8-1
      DO 520 I=1,L,2
      DEN=DEN+(DUMY(I)+4.*DUMY(I+1)+DUMY(I+2))*ZZ/3.
  520 BTM=BTM+(DMIT(I)+4.*DMIT(I+1)+DMIT(I+2))*ZZ/3.
      C=DEN/BTM
      A(JEIG)=C*R(1)/TFO
      GEI(JEIG)=EIG
      PRINT 525,EIG,C,S(JEND),A(JEIG)
  525 FORMAT(10X,12HEIGEN VALUE=,0PF10.5,3X,3HCN=,1PE12.4
     ***                                    ,5X,6HR'(1)=,PE
     112.4,5X,3HAN=,0PE13.6)
      PRINT 530
  530 FORMAT(13X,4HY/RW,3X,18HEIGEN FUNCTION (R))
      L=NNN/40
      DO 541 N=1,JEND,L
      I=4*N-3
      PRINT 540,YR(I),R(N)
  540 FORMAT(13X,F5.3,6X,1PE12.4)
  541 CONTINUE
      INDEX=2
      EIG=EIG+DELEG
      IF(JEIG-7)420,550,550
C        CALCULATION OF AN.NU/NU FULLY DEVELOPED.
  550 XYZ=0.
      K=0
      DB=FDNU/(.021*(RE**.8)*(PR**.4))
      DO 570 N=1,30
      K=K+1
      XPLUS(N)=XYZ+5.
      SUM=0.0
      DO 560 L=1,7
  560 SUM=SUM+A(L)/EXPEF(GEI(L)*XPLUS(N))
      RNU(N)=1./(1.+SUM)
      RDB(N)=RNU(N)*DB
      IF(RNU(N)-1.0025)585,585,570
  570 XYZ=XPLUS(N)
  585 PRINT 580
  580 FORMAT(15X,2HX+,3X,21HNU/NU FULLY DEVELOPED,1X,7HNU
     ***                                        /NUDB)
      DO 591 N=1,K
      PRINT 590,XPLUS(N),RNU(N),RDB(N)
  590 FORMAT(10X,0PF8.3,F13.4,F19.4)
  591 CONTINUE
      PRINT 592
  592 FORMAT(1H1)
      GO TO 4
      END
```

APPENDIX II

TABULATED HEAT TRANSFER DATA

Nomenclature:

T_b bulk static temperature, °F

T_w/T_b wall-to-bulk temperature ratio, °R/°R

Nu_{DB} normalized parameter from Dittus-Boelter correlation, $0.021\ Re^{0.8}\ Pr^{0.4}$

Re Reynolds number, $\dfrac{4\dot{m}}{\pi D \mu}$, properties based on local T_b

Pr Prandtl number, $\dfrac{c_p \mu}{k}$, properties based on local T_b

q^+ heat flux parameter, $\dfrac{q''_w}{\dfrac{\dot{m}}{A}\,H_{o,i}}$

Air, Nominal Reynolds Number = 3860, Prandtl Number = 0.7111

Run		4				5				6				7		
Re_i		3887				3876				3858				3844		
Pr_i		0.7111				0.7111				0.7111				0.7111		
T_{b_i} (°F)		76.24				76.80				76.86				76.95		
q^+		0.00416				0.00111				0.000283				0.00275		
x/D	T_w/T_b	T_b	Nu/Nu_{DB}	Nu	T_w/T_b	T_b	Nu/Nu_{DB}	Nu	T_w/T_b	T_b	Nu/Nu_{DB}	Nu	T_w/T_b	T_b	Nu/Nu_{DB}	Nu
1.21	1.043	87.41	1.961	26.38	1.012	79.73	1.945	26.37	1.003	77.51	2.056	27.85	1.029	84.63	1.947	26.06
4.08	1.073	87.41	1.337	17.99	1.020	79.63	1.342	18.20	1.005	77.56	1.354	18.34	1.048	84.19	1.344	18.01
8.14	1.085	94.64	1.137	15.16	1.023	81.58	1.169	15.82	1.006	78.05	1.189	16.10	1.056	88.95	1.147	15.28
16.09	1.090	111.38	1.020	13.35	1.025	86.08	1.083	14.56	1.006	79.21	1.199	16.21	1.060	99.94	1.044	13.72
25.92	1.089	132.59	0.987	12.61	1.025	91.80	1.083	14.47	1.006	80.69	1.098	14.81	1.059	113.90	1.022	13.22
34.61	1.086	151.47	0.977	12.22	1.024	96.90	1.078	14.31	1.006	81.98	1.086	14.63	1.058	126.35	1.020	13.02
52.01	1.076	188.75	0.983	11.85	1.022	107.02	1.109	14.56	1.007	84.57	1.039	13.95	1.053	151.06	1.028	12.77
86.74	1.061	257.47	1.044	11.82	1.020	126.42	1.170	15.03	1.006	89.57	1.178	15.72	1.046	197.21	1.043	12.37

Helium, Nominal Reynolds Number = 4180, Prandtl Number = 0.6644

Run	45				46				47				48			
Re_i	4180				4175				4157				4159			
Pr_i	0.6643				0.6644				0.6644				0.644			
T_f (°F)	73.34				74.27				74.36				74.02			
q^+	0.000291				0.000737				0.00267				0.000361			
x/D	T_w/T_b	T_b	Nu/Nu_{DB}	Nu	T_w/T_b	T_b	Nu/Nu_{DB}	Nu	T_w/T_b	T_b	Nu/Nu_{DB}	Nu	T_w/T_b	T_b	Nu/Nu_{DB}	Nu
1.21	1.006	73.49	1.507	.20	1.021	74.92	1.647	23.12	1.066	76.51	1.395	27.88	1.216	77.70	1.716	23.06
4.08	1.007	73.68	1.269	.84	1.028	75.74	1.276	17.90	1.105	79.56	1.273	17.73	1.176	83.29	1.248	17.61
8.14	1.007	74.05	1.245	17.50	1.031	77.30	1.177	16.21	1.117	85.71	1.134	15.71	1.196	93.09	1.217	15.37
16.09	1.008	74.80	1.128	15.84	1.034	80.42	1.067	14.91	1.123	97.39	1.053	14.43	1.208	112.59	1.016	13.73
25.92	1.008	75.72	1.072	15.04	1.034	84.28	1.056	14.70	1.128	111.90	0.990	13.39	1.213	136.85	0.944	12.48
34.61	1.007	76.53	1.172	16.43	1.034	87.71	1.049	14.56	1.127	124.73	0.972	12.99	1.203	158.34	0.953	12.36
52.01	1.008	78.15	1.115	15.61	1.033	94.56	1.058	14.58	1.116	150.42	1.006	13.13	1.183	201.38	0.971	12.15
86.74	1.003	81.39	2.578	35.99	1.031	108.16	1.106	15.05	1.106	201.35	1.001	12.52	1.155	286.41	0.999	11.17
95.68																

Run	49				60				61			
Re_i	4173				4190				4195			
Pr_i	0.6644				0.6644				0.6644			
T_f (°F)	74.36				75.47				75.79			
q^+	0.000115				0.00237				0.00351			
x/D	T_w/T_b	T_b	Nu/Nu_{DB}	Nu	T_w/T_b	T_b	Nu/Nu_{DB}	Nu	T_w/T_b	T_b	Nu/Nu_{DB}	Nu
1.21	1.003	74.35	2.045	28.72	1.068	77.50	1.638	23.04	1.101	78.71	1.641	23.09
4.08	1.005	74.58	1.273	17.88	1.092	80.23	1.261	17.69	1.136	82.85	1.260	17.65
8.14	1.005	74.82	1.178	16.53	1.103	85.27	1.118	15.62	1.153	90.31	1.106	15.38
16.09	1.006	75.32	1.021	14.32	1.109	95.37	1.035	14.31	1.161	105.21	1.014	13.92
25.92	1.008	75.93	0.727	10.20	1.108	107.85	1.022	13.97	1.160	123.75	0.989	13.34
34.61	1.007	76.47	0.836	11.72	1.106	118.94	1.014	13.72	1.156	140.17	0.980	13.03
52.01	1.006	77.55	1.006	14.09	1.101	141.11	1.014	13.45	1.146	173.00	0.984	12.71
86.74	1.005	79.71	1.134	15.85	1.092	185.12	1.022	13.05	1.128	238.11	0.998	12.25
95.68					1.091	196.42	1.016	12.86	1.125	254.80	0.991	12.01

Helium. Nominal, Reynolds Number = 6800, Prandtl Number = 0.6644

Run	52					53					54			
Re_i	6823					6930					6746			
Pr_i	0.6644					0.6644					0.6644			
Tb_i (°F)	73.81					73.96					76.13			
q^+	0.00291					0.00173					0.00592			
x/D	T_w/T_b	T_b	Nu/Nu_{DB}	Nu		T_w/T_b	T_b	Nu/Nu_{DB}	Nu		T_w/T_b	T_b	Nu/Nu_{DB}	Nu
1.21	1.100	75.86	1.525	31.68		1.064	75.19	1.426	29.67		1.204	79.98	1.511	31.07
4.08	1.128	79.48	1.217	25.23		1.080	77.31	1.172	24.34		1.236	87.83	1.197	24.42
8.14	1.141	85.67	1.095	22.53		1.088	81.01	1.057	21.88		1.290	100.55	1.062	21.42
16.09	1.145	97.97	1.037	21.10		1.091	88.32	1.007	20.69		1.296	125.83	0.990	19.49
25.92	1.144	113.24	1.019	20.45		1.090	97.46	0.994	20.26		1.284	157.26	0.975	18.66
34.61	1.141	126.76	1.011	20.03		1.090	105.44	0.979	19.80		1.272	185.11	0.970	18.14
52.01	1.135	153.81	1.003	19.40		1.088	121.52	0.968	19.30		1.244	240.85	0.977	17.51
86.74	1.126	207.66	0.975	18.04		1.084	153.54	0.961	18.61		1.201	351.50	1.002	16.61
95.68	1.121	221.51	0.988	18.08		1.083	161.77	0.947	18.21		1.192	379.85	1.007	16.40

Run	55					56					57			
Re_i	6781					6800					6812			
Pr_i	0.6644					0.6644					0.6644			
Tb_i (°F)	75.22					76.50					76.66			
q^+	0.00771					0.00416					0.00137			
x/D	T_w/T_b	T_b	Nu/Nu_{DB}	Nu		T_w/T_b	T_b	Nu/Nu_{DB}	Nu		T_w/T_b	T_b	Nu/Nu_{DB}	Nu
1.21	1.263	79.93	1.523	31.40		1.147	79.32	1.480	30.64		1.050	77.62	1.448	30.07
4.08	1.339	90.37	1.196	24.42		1.188	84.69	1.189	24.50		1.061	79.33	1.217	25.24
8.14	1.379	106.82	1.036	20.83		1.207	93.64	1.064	21.73		1.067	82.29	1.110	22.95
16.09	1.387	139.46	0.955	18.63		1.212	111.42	1.000	20.09		1.070	88.14	1.049	21.58
25.92	1.364	180.09	0.944	17.39		1.209	133.50	0.976	19.21		1.069	95.41	1.055	21.56
34.61	1.350	216.12	0.924	16.92		1.203	153.06	0.967	18.71		1.070	101.84	1.027	20.85
52.01	1.307	288.17	0.932	16.20		1.188	192.19	0.969	18.13		1.067	114.70	1.035	20.77
86.74	1.239	430.73	0.976	15.47		1.164	270.00	0.979	17.29		1.065	140.31	1.021	20.02
95.68	1.231	457.08	0.959	14.90		1.160	289.98	0.970	16.90		1.065	146.90	1.006	19.60

Helium, Nominal, Reynolds Number = 10,250, Prandtl Number = 0.6645

Run	64					65					66			
Re_i	10,266					10,206					10,229			
Pr_i	0.6644					0.6645					0.6645			
T_{bi} (°F)	75.04					77.19					77.34			
q^+	0.00193					0.00279					0.00389			
x/D	T_w/T_b	T_b	Nu/Nu_{DB}	Nu		T_w/T_b	T_b	Nu/Nu_{DB}	Nu		T_w/T_b	T_b	Nu/Nu_{DB}	Nu
1.21	1.076	76.06	1.455	41.94		1.110	78.90	1.457	41.78		1.155	79.64	1.437	41.27
4.08	1.095	78.58	1.198	34.46		1.137	82.60	1.195	34.15		1.191	84.89	1.190	34.00
8.14	1.103	82.73	1.089	31.21		1.149	88.62	1.087	30.88		1.207	93.31	1.081	30.65
16.09	1.105	90.92	1.053	29.93		1.153	100.54	1.033	29.04		1.211	109.95	1.024	28.59
25.92	1.105	101.09	1.037	29.21		1.151	115.33	1.019	28.25		1.207	130.61	1.004	27.51
34.61	1.103	110.09	1.032	28.83		1.148	128.41	1.012	27.71		1.202	148.90	0.995	26.82
52.01	1.100	128.10	1.026	28.18		1.142	154.62	1.003	26.85		1.188	185.52	1.000	26.12
86.74	1.094	164.02	1.019	27.11		1.130	206.88	0.996	25.53		1.164	258.57	1.016	25.10
95.68	1.094	173.26	1.006	26.57		1.129	220.33	0.981	24.89		1.160	277.38	1.010	24.62

Run	67					68				
Re_i	10,231					10,322				
Pr_i	0.6645					0.6644				
T_{bi} (°F)	77.49					76.42				
q^+	0.00534					0.00764				
x/D	T_w/T_b	T_b	Nu/Nu_{DB}	Nu		T_w/T_b	T_b	Nu/Nu_{DB}	Nu
1.21	1.213	80.51	1.427	40.97		1.305	80.44	1.435	41.43
4.08	1.264	87.86	1.167	33.28		1.376	91.26	1.165	33.30
8.14	1.286	99.37	1.058	29.83		1.406	107.72	1.049	29.53
16.09	1.289	122.17	1.000	27.60		1.404	140.31	0.990	27.05
25.92	1.278	150.49	0.986	26.55		1.384	180.82	0.970	25.60
34.61	1.268	175.57	0.981	25.84		1.362	216.71	0.968	24.82
52.01	1.243	225.81	0.988	25.02		1.318	288.64	0.982	23.90
86.74	1.206	325.95	1.002	23.62		1.253	431.64	1.011	22.45
95.68	1.201	351.69	0.986	22.84		1.243	468.29	1.000	21.76

NOMENCLATURE

English Symbols

A_n quantity used in calculating Nusselt numbers from equation 6-5

C_n coefficient in eigenvalue solution

C turbulence velocity correction, defined by equation A-6

c_p specific heat at constant pressure

D tube diameter

e emissivity

F_{in} radiation view factor from i to n

$F(\bar{y})$ function arising in fully developed solution, $\dfrac{T - T_b}{q''_w r_w / k}$

g_c dimensional constant, e.g., $32.174 (lbm)(ft)/(lbf)(sec^2)$

H_o stagnation enthalpy

h heat transfer coefficient, $h = \dfrac{q''_w}{T_w - T_b}$

k thermal conductivity

$\overset{\circ}{m}$ mass flow rate

P pressure

ΔP pressure drop

q heat transfer rate

q' lineal heat transfer rate, $\dfrac{dq}{dx}$

q'' heat flux

r	tube radius
R_n	eigenfunction used in the separation of variables
R	gas constant
S	function defined by equation G-3
T	temperature
u	velocity in axial direction
u'	turbulent velocity fluctuation in the axial direction
u^*	shear velocity, $\sqrt{\dfrac{\tau_w g_c}{\rho}}$
V_b	bulk velocity, $\dfrac{2}{r_w^2} \displaystyle\int_0^{r_w} u(r)r\,dr$ or $\dot{m}/\rho_b \pi r_w^2$
W_m	uncertainty interval of the quantity m
x	axial distance from the start of heating
y	radial distance from the tube wall
y_1^+	Reynolds number dependent coefficient in correlation of eddy diffusivity for momentum
Z	compressibility factor

Greek Symbols

$\beta(\bar{y})$	total thermal diffusivity, $\dfrac{\epsilon_m}{\nu} + \dfrac{1}{Pr}$
γ	intermittency factor
Δ	effective center displacement, equation A-10
ϵ	eddy diffusivity; ϵ_m for momentum; ϵ_H for heat
θ	dimensionless temperature, $\dfrac{T - T_i}{q_w'' r_w/k}$
κ	constant of velocity profile
λ_n^2	eigenvalue

μ absolute viscosity

ν kinematic viscosity

ρ density

τ shear stress

Dimensionless Groups

f   friction factor, $\dfrac{\tau_w g_c}{\dfrac{\rho v_b^2}{2}}$

Nu   Nusselt number, $\dfrac{hD}{k}$

Pr   Prandtl number, $\dfrac{\mu c_p}{k}$

q^+ heat flux parameter, $\dfrac{q_w''}{\dfrac{\dot{m}}{A} H_{o,i}}$

Re   Reynolds number, $\dfrac{\rho V_o D}{\mu}$ or $4\dot{m}/\pi D\mu$

u^+ velocity parameter, $\dfrac{u}{u^*}$

v_b^+ bulk velocity parameter, $\dfrac{V_b}{u^*}$

x^+ dimensionless axial distance, $\dfrac{x}{r_w}$

$\bar{y}$ dimensionless radial distance, $\dfrac{y}{r_w}$

y^+ radial distance parameter, $\dfrac{yu^*}{\nu} = \dfrac{y}{2} \dfrac{Re}{r_w}\sqrt{\dfrac{f}{2}}$

Subscripts

b   bulk, evaluated at bulk static temperature

cond   conduction

e	entrance
g	generated
i	inlet
w	wall
∞	fully developed
₵	centerline

REFERENCES

1. J. G. Knudson and D. L. Katz, Fluid Dynamics and Heat Transfer, McGraw-Hill. New York, 1958.

2. W. M. Kays, Convective Heat and Mass Transfer, McGraw-Hill, New York, 1966.

3. R. D. Cess, "A Survey on the Literature on Heat Transfer in Turbulent Tube Flow," Westinghouse Research Report 8-0529-R24, December 2, 1958.

4. V. E. Senecal, "Characteristics of Transition Flow in Smooth Tubes," Sc.D. Thesis, Carnegie Institute of Technology, 1951.

5. R. R. Rothfus and C. C. Monrad, "Correlation of Turbulent Velocities for Tubes and Parallel Plates," Eng. Design and Process Development, Vol. 47, No. 6, 1955, p. 1144.

6. F. Page, W. G. Schlinger, D. K. Breaux, and B. H. Sage, "Point Valves of Eddy Conductivity and Viscosity in Uniform Flow between Parallel Plates," Ind. Eng. Chem., Vol. 44, No. 2, 1952, p. 424.

7. W. N. Gill and M. Scher, "A Modification of the Momentum Transport Hypothesis," A.I.Ch.E. Journal, Vol. 7, No. 1, 1961, p. 61.

8. E. R. Van Driest, "On Turbulent Flow Near a Wall," Heat Transfer and Fluids Mechanics Institute Preprints, Paper XII, University of California, 1955.

9. D. M. McEligot, L. W. Ormand, and H. C. Perkins, Jr., "Internal Low Reynolds Number Turbulent and Transitional Gas Flow with Heat Transfer," J. Heat Transfer, Vol. 88, No. 2, 1966, p. 239.

10. S. I. Pai, "On Turbulent Flow in a Circular Pipe," J. of the Franklin Inst., Vol. 256, No. 4, 1953, p. 337.

11. T. J. Hanratty and R. E. Johnk, "Development of a Temperature Profile for Turbulent Heat Exchange in a Pipe," *Engineering Experimental Station*, University of Illinois, Tech. Report No. 10, 1961 (DDC AD 253 399).

12. R. G. Deissler, "Analysis of Turbulent Heat Transfer, Mass Transfer, and Friction in Smooth Tubes at High Schmidt Numbers," NACA Report 1210, 1955.

13. H. Schlicting, *Boundary Layer Theory*, 4th Ed., McGraw-Hill, New York, 1960.

14. L. M. Boelter, R. C. Martinelli, and F. Jonassen, "Remarks on the Analogy between Heat Transfer and Momentum Transfer," *Trans. ASME*, Vol. 63, 1941, p. 447.

15. R. R. Rothfus and R. S. Prengle, "Laminar-Turbulent Transition in Smooth Tubes," *Ind. Eng. Chem.*, Vol. 44, 1952, p. 1683.

16. R. C. Martinelli, "Heat Transfer to Molten Metals," *Trans. ASME*, Vol. 69, 1947, p. 947.

17. J. Rotta, "Experimenteller Beitrag zur Entstehung turbulenter Stromung im Rohr," *Ing. Arch.*, Vol. 24, 1956, p. 258.

18. J. H. Preston, "The Minimum Reynolds Number for a Turbulent Boundary Layer and the Selection of a Transition Device," *J. of Fluid Mech.*, Vol. 3, 1958, p. 373.

19. J. Nikuradse, "Gesetzmassigkeit der turbulenten Stromung in glatten Rohren," *Forschungsheft 356*, 1932. Project SQUID Report TM-Pur-11, 1949.

20. R. R. Rothfus, C. C. Monrad, and V. E. Senecal, "Velocity Distributions and Friction in Smooth Concentric Annuli," *Ind. Eng. Chem.*, Vol. 42, 1950, p. 2511.

21. R. A. Seban and T. T. Shimazaki, "Heat Transfer to a Fluid Flowing Turbulently in a Smooth Pipe with Walls at a Constant Temperature," *Trans. ASME*, Vol. 73, 1951, p. 803.

22. R. G. Deissler, "Analytical and Experimental Investigation of Adiabatic Turbulent Flow in Smooth Tubes," NACA TN 2138, 1950.

23. H. P. Bakewell, Jr.. "An Experimental Investigation of the Viscous Sublayer in Turbulent Flow," Technical Report, Aerospace Engineering Department, Pennsylvania State University, 1966 (DDC AD 639 804).

24. H. Reichardt, "Complete Representation of Turbulent Velocity Distribution in Smooth Pipes," Z. Angew. Math. Mech., Vol. 31, No. 7, 1951, p. 208.

25. J. L. Chance, "An Apparatus for Heat Transfer and Frictional Studies of Gas Flow in a Tube with Large Temperature Differences," Research Report, School of Engineering, Texas Technological College, 1964.

26. V. A. Sandborn and R. J. Slogar, "Study of the Momentum Distribution of the Turbulent Boundary Layers in Adverse Pressure Gradient," NACA TN 3264, 1955.

27. J. W. Daily and R. L. Hardison, "Rigid Particle Suspensions in Turbulent Shear Flow: Measurement of Total Head, Velocity and Turbulence with Impact Tubes," Hydrodynamics Laboratory, Massachusetts Institute of Technology, Report No. 67, 1964.

28. V. A. Sandborn, "Experimental Evaluation of Momentum Terms in Turbulent Pipe Flow," NASA TN 3266, 1955.

29. A. Fage, "The Estimation of Pipe Delivery From Pitot-Tube Measurements," Engineering, Vol. 145, 1938, p. 616.

30. S. J. Kline and F. A. McClintock, "The Description of Uncertainties in Single Sample Experiments," Mechanical Engineering, Vol. 75, 1953, p. 38.

31. R. L. Haugen and A. M. Dhanak, "Momentum Transfer in Turbulent Separated Flow Past a Rectangular Cavity," J. Applied Mech., Vol. 23, 1966, p. 641.

32. J. O. Hinze, Turbulence, McGraw-Hill, New York, 1959.

33. D. B. Spalding, Personal Communication, Third Annual Aerospace Heat Transfer Seminar, University of Arizona, Lecture 1, May 9, 1967.

34. H. G. Elrod, "Note on the Turbulent Shear Stress near a Wall," _J. Aero. Sci._, Vol. 24, 1957, p. 468.

35. E. M. Sparrow, T. M. Hallman, and R. Siegel, "Turbulent Heat Transfer in the Thermal Entrance Region of a Pipe with Uniform Heat Flux," _Appl. Sci. Res._, Section A, Vol. 7, 1957, p. 37.

36. R. G. Deissler, "Analytical Investigation of Turbulent Flow in the Entrance Regions of Smooth Passages," NACA TN 3016, 1953.

37. W. B. Hall and P. H. Price, "The Effect of Longitudinally Varying Wall Heat Flux on the Heat Transfer Coefficient for Turbulent Flow in a Pipe," _International Developments in Heat Transfer_, ASME, New York, 1961, p. 607.

38. H. Wolf, "Heating and Cooling Air and Carbon Dioxide in the Thermal Entrance Region of A Circular Duct with Large Gas to Wall Temperature Differences," _J. Heat Transfer_, Vol. 81, 1959, p. 267.

39. P. M. Magee and D. M. McEligot, "Effect of Property Variation on the Turbulent Flow of Gases in Tubes: The Thermal Entry," _Nuc. Sci. Eng._, to be published.

40. H. C. Perkins and P. M. Worsoe-Schmidt, "Turbulent Heat and Momentum Transfer for Gases in a Circular Tube at Wall-to-Bulk Temperature Ratios of Seven," _Int. J. Heat and Mass Transfer_, Vol. 8, No. 7, 1965, p. 1011.

41. D. M. McEligot, P. M. Magee, and G. Leppert, "Effect of Large Temperature Gradients on Convective Heat Transfer: The Downstream Region," _J. Heat Transfer_, Vol. 87, No. 1, 1965, p. 67.

42. J. A. Malina and E. M. Sparrow, "Variable-Property, Constant-Property, and Entrance Region Heat Transfer Results for Turbulent Flow of Water and Oil in a Circular Tube," _Chem. Eng. Sci._, Vol. 19, 1964, p. 953.

43. W. N. Gill and S. M. Lee, "An Analytical Study of Heat Transfer in Laminar-Turbulent Transition Flow Between Parallel Plates," _A.I.Ch.E. Journal_, Vol. 8, 1962, p. 303.

44. R. D. Haberstroh and L. V. Baldwin, "Application of a Simplified Velocity Profile to the Prediction of Pipe Flow Heat Transfer," ASME Paper No. 67-HT-25, Heat Transfer Conference, Seattle, Washington, August, 1967.

45. R. G. Deissler, "Analytical Investigation of Turbulent Flow in Smooth Tubes with Heat Transfer with Variable Fluid Properties for Prandtl Number of 1," NASA TN 2242, 1950.

46. R. Siegel, E. M. Sparrow, and T. M. Hallman, "Steady Laminar Heat Transfer in a Circular Tube with Prescribed Wall Heat Flux," Appl. Sci. Res., Series A, Vol. 7, 1958, p. 386.

47. P. M. Worsoe-Schmidt and G. Leppert, "Heat Transfer and Friction for Laminar Flow of Gases in a Circular Tube at High Heating Rates," Int. J. Heat and Mass Transfer, Vol. 8, 1965, p. 1281.

48. W. G. Hess, "Thermocouple Conduction Error with Radiation Heat Loss," M.S. Thesis, Department of Aerospace and Mechanical Engineering, University of Arizona, 1965.

49. D. M. McEligot, "Effect of Large Temperature Gradients on Turbulent Flow of Gases in the Downstream Region of Tubes," Ph.D. Dissertation, Stanford University, 1963 (TID-19446).

50. H. E. Ferrell, "An Experimental Investigation of the Disturbance to a Velocity Profile in an Internal Flow Stream Caused by Placing a Pilot Tube in the Stream," M.S. Thesis, Texas Technological College, 1963.

51. J. Hilsenrath et al., Tables of Thermodynamic and Transport Properties of Air, Argon, Carbon Dioxide, Carbon Monoxide, Hydrogen, Nitrogen, Oxygen, and Steam, Pergamon Press, New York, N. Y., 1960. Also NBS Circular 564, 1955.

52. J. Laufer, "The Structure of Turbulence in Fully Developed Pipe Flow," NACA Number 1174, 1954.

53. D. B. Spalding, "A Single Formula for the Law of the Wall," J. Applied Mech., Vol. 28, 1961, p. 455.

54. P. M. Magee, "The Effect of Large Temperature Gradients on Turbulent Flow of Gases in the Thermal Entrance Region of Tubes," Ph.D. Dissertation, Stanford University, 1964 (TID-22247).

55. Anon., Fluid Meters, 5th Ed., ASME, New York, 1959, p. 63.

56. F. Kreith, Principles of Heat Transfer, International, Scranton, 1958.

57. L. S. Mills, "Radiant Heat Transfer in a Non-Isothermal Annulus," M.S. Thesis, Department of Aerospace and Mechanical Engineering, University of Arizona, 1966.

58. R. W. Shumway, "Electrical Resistance Investigation," EMMTLab TM 2, Department of Aerospace and Mechanical Engineering, University of Arizona, 1967.

59. F. B. Hildebrand, Introduction to Numerical Methods, McGraw-Hill, New York, 1956.

60. F. B. Hildebrand, Advanced Calculus for Applications, Prentice-Hall, Englewood Cliffs, 1962.

61. J. M. Botje, "An Analytical Evaluation of the Coefficients of Heat Transfer and Friction for Air, Carbon Dioxide and Helium in Incompressible Turbulent Flow," Document II, Ph.D. Dissertation, Purdue University, 1955.